NASA CONTRACTOR REPORT

NASA CR-857

NASA CR-857



# ON THE PREDICTION OF THE NEAR FIELD NOISE OF SUPERSONIC JETS

*by J. B. Ollerhead*

*Prepared by*
WYLE LABORATORIES
Huntsville, Ala.
*for George C. Marshall Space Flight Center*



NATIONAL AERONAUTICS AND SPACE ADMINISTRATION • WASHINGTON, D. C. • AUGUST 1967

NASA CR-857

# ON THE PREDICTION OF THE NEAR FIELD NOISE OF SUPERSONIC JETS

By J. B. Ollerhead



Issued by Originator as Report No. WR 67-6

Prepared under Contract No. NAS 8-21060 by
WYLE LABORATORIES
Huntsville, Ala.

for George C. Marshall Space Flight Center

NATIONAL AERONAUTICS AND SPACE ADMINISTRATION

For sale by the Clearinghouse for Federal Scientific and Technical Information
Springfield, Virginia 22151 – CFSTI price $3.00

## SUMMARY

The phenomenon of noise generation by supersonic jets is reviewed in a comparison of previous theoretical and experimental investigations. It is shown that three fundamental mechanisms exist, which are defined as turbulence-shear noise, Mach wave radiation, and shock-noise. The significance of each type of noise is evaluated, with reference to the nature of the jet-flow structure and particular attention is paid to the acoustic near field.

At the present time there is no general method for the prediction of the near field noise of either subsonic or supersonic jets. An appropriate expression is presented, and a series of experiments proposed, by which its empirical coefficients can be determined. These experiments would eventually lead to the establishment of scaling laws, enabling the expression to be used to compute the near field sound pressure contours of any supersonic jet of known configuration.

PRECEDING PAGE BLANK NOT FILMED.

# TABLE OF CONTENTS



PRECEDING PAGE BLANK NOT FILMED.

TABLE OF CONTENTS (Continued)

## LIST OF FIGURES

LIST OF FIGURES (Continued)

LIST OF FIGURES (Continued)

# LIST OF SYMBOLS

Only those symbols which are widely used are listed below. Other symbols, or different meanings to those given below, are used only locally and are defined where they first occur.

## Roman Symbols

| | |
|---|---|
| $a$ | speed of sound |
| $a$ | radius of laminar core |
| $b$ | mixing width parameter |
| $B(\underset{\sim}{r}, t, \tau^*)$ | far field pressure autocovariance |
| $f$ | frequency, Hertz |
| $F_{ij}(\theta)$ | far field directivity function |
| $G_{ij}(\theta)$ | near field directivity function |
| $H_{ij}(\theta)$ | near field directivity function |
| $I$ | acoustic intensity |
| $k$ | wave number $= 2\pi/\lambda$ |
| $\ell$ | correlation length; typical eddy dimension |
| $M$ | flow Mach number |
| $\overline{M}$ | Mach number relative to ambient speed of sound |
| $\overline{M}_c$ | eddy convection Mach number |
| $p$ | mean static pressure |
| $p$ | pressure fluctuation (acoustic pressure) |
| $p_T$ | total pressure |
| $P$ | sound power |
| $r$ | radius from jet centerline |
| $\underset{\sim}{r}$ | displacement of field point from sound source $= \underset{\sim}{x} - \underset{\sim}{y}$ |
| $r$ | magnitude of $\underset{\sim}{r}$ |
| $r$ | radial coordinate measured from nozzle center (equation 4.10) |

| | |
|---|---|
| $r_i$ | component of $\underset{\sim}{r}$ along $x_1$ axis |
| $r_i$ | distance from i-th source to observer (equation 4.10) |
| $R_{ijk\ell}$ | turbulent stress correlation tensor |
| $t$ | time |
| $t$ | ratio of total temperature to ambient temperature $T_T/T_o$ |
| $\overline{t}$ | retarded time $(t - r/a_o)$ |
| $T$ | temperature |
| $T_{ij}$ | turbulent stress tensor |
| $\overline{T^2}$ | mean square of $T_{ij}$ |
| $u, u_i$ | velocity fluctuation |
| $U$ | mean velocity (in x-direction parallel to jet axis) |
| $v, v_i$ | velocity fluctuation |
| $V$ | mean velocity |
| $V$ | volume |
| $V_e$ | eddy volume |
| $w$ | length of primary cell in shock pattern |
| $w(f)$ | sound power spectral density |
| $x$ | axial distance from jet nozzle |
| $x_1$ | Cartesian axis |
| $\underset{\sim}{x}$ | position vector of point in acoustic field |
| $x_s$ | axial location of sonic point |
| $x_t$ | axial location of laminar core tip |
| $\underset{\sim}{y}$ | position vector of point in turbulent flow |

## Greek Symbols

| | |
|---|---|
| $\alpha(\theta)$ | far field directionality factor |
| $\beta(\theta)$ | near field directionality factor |
| $\gamma$ | ratio of specific heats |
| $\delta_{ij}$ | Kronecker delta |
| $\Delta$ | incremental factor (e.g., $\Delta t$, $\Delta r$) |
| $\underset{\sim}{\Delta}$ | separation vector |
| $\eta$ | mixing width parameter ($r - a/b$) |
| $\theta$ | angle to jet axis |
| $\theta_M$ | Mach angle |
| $\lambda$ | wavelength |
| $\underset{\sim}{\lambda}$ | moving axis separation vector |
| $\underset{\sim}{\lambda}_s$ | area vector normal to $\theta_M$ direction |
| $\rho$ | density |
| $\sigma$ | time variable |
| $\tau$, $\tau^*$ | time delay, retarded time increment |
| $\tau_r$ | turbulent shear stress |
| $\phi$ | polar coordinate, phase angle |
| $\psi$ | phase angle |
| $\omega$ | radian frequency |

## Subscripts

| | |
|---|---|
| c | pertaining to eddy convection |
| E | nozzle exit plane conditions |
| F | far field |
| i, j, k, $\ell$ | tensor and vector notation |
| m | maximum (jet centerline values) |

| | |
|---|---|
| N | near field |
| r | pertaining to radius r |
| T | total conditions |
| o | ambient conditions |
| 0.5 | at radius specified by $U_r = 0.5\ U_m$ |
| 1, 2, 3 | Cartesian subscripts. |

# 1.0 INTRODUCTION

The rocket engine has the unfortunate side-effect of being a singularly powerful continuous source of noise. Apart from being an obvious physiological problem, this noise is sufficiently intense to constitute a potential hazard to structural components in the close vicinity of the exhaust stream. For this reason, there is a clear need for both understanding and control of the noise generation process. The noise is aerodynamic in origin, and results from the powerful shearing actions which take place as the high velocity exhaust gases mix with the surrounding atmosphere. Although Lighthill (References 1 and 2) established an analytical description of the fundamentals of aerodynamic noise generation as far back as 1952, a theoretical quantitative evaluation of the noise produced by a jet with known nozzle flow conditions still remains beyond reach, in spite of very considerable efforts by many investigators. The primary reason for this is the lack of understanding of the turbulence generation mechanisms in a jet flow.

However, by judicious use of available experimental tools, much can and has been done to close the gap between theory and experiment. This report reviews previous work, with particular emphasis on the near-noise field, and indicates major problem areas which are apparent. A series of experiments are suggested which should fill some of the gaps in present knowledge and assist the continuing attempts to develop a method by which the sound field of a supersonic jet can be completely predicted with reasonable confidence.

The noise field of a jet can be divided into three fairly well defined regions. These are:

a) The far field (or radiation field) which encompasses points that are sufficiently far from the jet for the noise to be considered as being radiated from a single point;

b) The mid-field or (geometric near field) where the geometry of the jet flow becomes important because an observer hears sound arriving from an extended source region; and,

c) The near field (or induction near field) whose boundaries are essentially a function of frequency, being confined to within a wavelength or so of the jet boundary, where hydrodynamic, non-propagating pressure fluctuations amplify the sound levels.

The near field discussed in this report includes regions (b) and (c).

In general, to define the far field sound pressure levels of a jet, it is necessary to describe the noise source in terms of its overall sound power, its frequency spectrur and its directionality.

Lighthill (Reference 1) showed that at low exhaust Mach Numbers, the overall sound power is proportional to the eighth power of the velocity. Since the mechanical power of the jet is proportional to the cube of the velocity, this law represents a net acoustic efficiency which is proportional to the fifth power. It has been found that this relationship is true up to jet velocities approaching twice the ambient speed of sound and, numerically, the efficiency is about $10^{-4}\ \overline{M}_E^3$ where $\overline{M}_E$ is the exit velocity divided by the ambient sound speed. At velocities higher than $\overline{M}_E = 2$, which represents a typical value for turbojet engines, the efficiency begins to fall off rapidly and for $\overline{M}_E > 3$ it reaches a constant value of approximately 0.006. This reduction is clearly shown in Figure 22 in which some typical experimental data show the variation of overall acoustic power with jet velocity. Since the large rocket boosters of today generate power of the order of $10^{10}$ watts, this still represents a formidable amount of noise energy, despite its apparently low numerical value. The reduction in acoustic efficiency at high Mach Numbers is explained theoretically by an extension of Lighthill's analysis by Ffowcs Williams (Reference 3) although, as will be seen later, the explanations put forward still await experimental confirmation.

The manner in which the sound energy is distributed through the frequency spectrum is mainly influenced by the geometry of the mixing process. The thickness of the annular turbulent mixing layer wherein the sound is generated, increases almost linearly with distance downstream, from zero near the tip of the nozzle until the laminar flow core, which it surrounds, disappears. From this point, the flow is completely turbulent and the flow boundaries begin to expand more rapidly. As the geometry suggests, small, high velocity turbulent eddies are created near the nozzle which generate correspondingly high frequency sound. Further downstream, mean velocities are lower, eddies become larger and associated acoustic frequencies are typically lower. This fact has been confirmed for subsonic jets both by direct hot-wire measurements of the turbulent velocity fluctuations (References 4 and 5) and by sound pressure measurements near the jet boundary (for example, References 6, 7, and 8). Mainly due to the fact that the mean velocity varies little in the initial mixing region (adjacent to the core) the sound power generated per unit jet length is roughly constant, in that region, since the rms velocity fluctuations vary approximately as the mean velocity. Downstream of the core tip both mean velocity and the sound power per unit length decay rapidly. The net result of these variations in subsonic jets is to generate a power spectrum which exhibits a single peak around the Strouhal Number $f d_E/U_E = 0.25$, and falls away at approximately 6 dB per octave on either side of this peak.

The sound power spectra of highly supersonic rockets, on the other hand show no such tendency to collapse on the basis of this simple Strouhal Number. The peak frequency has been found experimentally (References 9 and 10) to be almost independent of velocity and to lie within the vicinity of $a_o/d_E$, which is much lower than would be given by the Strouhal Number relationship above. Also, practically all measurements of rocket noise (e.g., References 10, 11, and 12) strongly indicate

that the major sound producing region is well downstream of the nozzle, around the point where the flow becomes subsonic (i.e., the flow Mach Number, M, approaches unity; the acoustic Mach Number $\overline{M}$, the ratio of the flow velocity to the ambient speed of sound, still remains around 3). Now these two facts are in complete disagreement with the predictions of the theory which accounts for the constant acoustic efficiency at high Mach Numbers.

This theory suggests that supersonically convected eddies radiate intense sound in a highly directional peak, a condition which has become known as Mach wave emission. Theoretically, Mach wave frequencies certainly tend to become independent of velocity, but the frequency range would be expected to extend to much higher limits than those observed. Furthermore, they originate from regions of high velocity, that is, from the initial mixing region. This discrepancy represents the biggest dilemma in the study of rocket noise which must be solved before further progress can be made. To date, the existence of Mach waves has only been verified by shadow photography, and Figure 1 is a typical example. Such pictures reveal what appear to be high frequency wave trains emanating from the supersonic regions of the flow in an essentially uniform direction. These waves also seem to be of greater intensity than radiation from other parts of the flow. The reason why this high frequency energy does not dominate the measured spectra remains a mystery, unless indeed it is outside the range of microphone response.

Theoretical solutions for the directional characteristics of jet noise show good qualitative agreement with experiment, showing that sound is predominantly radiated at acute angles to the flow direction. This is primarily the result of eddy convection effects and the quadrupole nature of the sound sources. Attempts to quantify the directional properties, however, have so far been relatively unsuccessful. It is known that the higher frequencies radiate at greater angles to the flow direction, the total range being from $20^{\circ}$ to $70^{\circ}$, within the usual eight octave band frequency range, for turbojet engines. Rocket engines, however, exhibit peaks at considerably greater angles and once again this might be expected of Mach wave emission, a further point favoring this mecahnism.

The discussion so far has indicated that knowledge of the far field noise of subsonic and sonic jets is substantial, and indeed, current prediction techniques based on a combination of analytical and empirical techniques are adequate to define these noise fields with sufficient accuracy for engineering purposes. In the case of far field rocket noise it has not proved possible to coordinate theoretical and experimental results, and methods which have been developed for prediction purposes are completely empirical. Such prediction is made difficult because of the complex

nature of the exhaust flow, which unlike that of a turbojet, is composed of a very different gas to that of the atmosphere, is at a very high temperature, and is characterized by a complex standing structure of compression, expansion and shock waves. It has three basic noise generation processes, as opposed to one; turbulence noise, similar to that of turbojets, originating from subsonic flow regions, Mach Wave emission from the supersonic turbulent flow and shock noise caused by interactions between the turbulence and the standing shocks. Additional complications are caused by fuel combustion downstream of the nozzle. It is not surprising that the theories, derived for relatively well-behaved flows, do not meet the demands of such a grotesque flow phenomenon. Potter and Crocker (Reference 13) and Wilhem (Reference 14) have performed extensive surveys of available prediction methods and recommended particular expressions for overall sound power and frequency spectra. Directivity data from a number of sources are also presented for suggested use, but these exhibit so much scatter that it is doubtful whether they could be applied with any confidence at all. It is all too regrettable that these works give a fairly complete picture of the current state-of-the-art, showing, as they do, the large deficiencies in our understanding of the problem.

It comes as no further surprise that current knowledge of the acoustic near field of jet and rocket noise is even more sketchy. Because of the practical unimportance of this problem prior to the advent of high thrust engines and the consequent concern for the durability of structure and personnel exposed to their intense noise, relatively little attention has been given to the near field problem. Very few measurements of the near field noise characteristics are available and even those are generally fragmentary and poorly correlated with flow parameters and the associated far sound field. Franz (Reference 15) extended Lighthill's work to include terms of importance in the near field of turbulence and demonstrated the formidable complexity of a theoretical treatment. No attempt has yet been made to apply his results to the problem of near field noise prediction, except to demonstrate the specific problem of the acoustic loading of a missile structure (Reference 16), probably because of the lack of experimental data required both to verify it and to provide the necessary unknown constants. The information required for near field noise prediction represents at least an order of magnitude increase over that for the far field, since the distribution of noise power, spectra, and directionality must be specified along the length of the exhaust stream, together with the hydrodynamic induction effects at positions within a few wavelengths of the flow.

Eldred, et al. (Reference 17) made a detailed study of some extensive near field sound pressure level measurements for a particular jet engine and, by correlating these data with corresponding far field measurements, were able to deduce the axial distributions of the source properties. They found the rather surprising result that induction near field effects were negligibly small, in contrast to Franz's theoretical conclusions that such effects could account for amplifications of the sound pressure levels of 20 dB or more.

Potter and Crocker found the same results when they applied similar techniques to the rocket noise data from Reference 11 . However, to make this analysis they were forced to make some rather sweeping assumptions concerning the directionality of local sound sources, and this conclusion must be questioned. So too must any method which attempts to interpret near field sound pressures in terms of acoustic intensity since the dangers of doing so in the possible presence of the reciprocating modes of non-propagating standing waves are self-evident.

This introduction is intended to illustrate some of the problems which must be solved in order to achieve the understanding required for the prediction of near field noise of supersonic jets. At the present time very little is known of the basic noise generation mechanisms of supersonic flow and we do not yet have the ability to predict accurately the noise contours of a simple jet operating in a quiescent, free atmosphere. It seems unreasonable to hope, therefore, that we can tackle the real problems of the near noise environment of, for example, a large rocket vehicle during its initial launch phase, taking account of the additional problems of clustered nozzles, deflected flows, sound reflections and attenuation and flight velocity, with any substantial degree of confidence. This report, therefore, puts emphasis on the very basic problems, associated with a single, supersonic jet with a stationary nozzle.

There is a clear need for a great deal more experimental information on the sound field of supersonic jets, particularly in the exhaust velocity range intermediate between those high speed turbojets and rockets, a gap of some 5000 ft. per second or more. The main result of this work therefore is a recommendation for a series of well controlled experiments which it is hoped will provide some of this information.

Previous work, which is basic to the jet noise generation problem, is reviewed in some detail with emphasis on its relation to the near field problem. Attention is confined in the main to the case of axisymmetric jets exhausting into stationary air. Throughout the report, equations taken from previous work have been converted, where necessary, to a consistent notation in order to preserve some continuity.

## 2.0 THE STRUCTURE OF AXISYMMETRIC JET EXHAUSTS

### 2.1 Introduction

A subsonic jet, that is one in which the Mach number of the exhaust gas is less than unity at the nozzle exit, is characterized by two basically different regions. The first extends for approximately five nozzle diameters downstream and comprises a laminar potential core surrounded by a highly turbulent region which throughout the report is termed the "initial mixing region". If the flow upstream of the nozzle exit is free from disturbances, the flow immediately downstream of the exit is also laminar. However, a jet exhausting into quiescent air is subjected to an intense shearing action at its boundary and within about half a diameter of the nozzle the flow in this shear region is fully turbulent. There is a continuous exchange of momentum between the potential flow and the ambient air so that the mixing region continues to encroach upon the laminar region it surrounds, eventually consuming it entirely. At some point in the exhaust, the flow becomes completely turbulent, and the boundary of the laminar region is approximately conical, giving rise to the expressions laminar "core" or "cone".

Within the initial mixing region it has been shown experimentally that velocity profiles are self-similar, a condition which is also reached in the second basic flow zone, the fully developed mixing region downstream of some point in the flow. This point is approximately one core length downstream from the core tip, and in the intermediate distance, sometimes known as the "transition" region the flow passes through a period of adjustment.

Supersonic jets retain the features of subsonic flow with the main exception that they practically all contain shocks of some description. A perfectly expanded exhaust stream, i.e., one in which the static pressure is uniform, and equal to atmospheric, across the nozzle exit plane, will be completely shock free. The flow structure of such an ideal jet is shown in Figure 2. The flow bears a strong similarity to that of a subsonic jet although an additional, important region can be defined, the supersonic core. The stream velocity in the laminar core is essentially constant, and equal to the nozzle velocity, which is supersonic. This core is surrounded by a turbulent mixing zone where the mean stream velocity decays with distance from the core boundary, reaching some point at which the velocity becomes subsonic. This "sonic boundary" is approximately conical in shape and can be thought of as defining a second core region which has been termed the "supersonic core".

Such a jet is very difficult to achieve in practice. Boundary layer growth and the three dimensional flow within the nozzle expansion chamber make it practically impossible to achieve a completely shock-free flow. However, well designed nozzles have been manufactured where conditions closely approach the ideal, and

shock patterns have been reduced to extremely weak Mach lines in the close vicinity of the nozzle. The flow from a well expanded nozzle is shown in Figure 1 which is a shadowgraph of a cold $M = 2.2$ air jet. It can be seen that this flow is free of strong shocks, and a criss-cross pattern of very weak compression and expansion waves caused by minor irregularities in the nozzle surface are confined to a small region of the flow close to the nozzle. Figure 2 gives a diagrammatic representation of the structure of this shock-free flow, showing five basic regions:

1) A supersonic laminar core;
2) A supersonic turbulent cone;
3) A subsonic turbulent mixing region;
4) A fully turbulent transition region;
5) A fully developed turbulent region.

} Both completely subsonic

As yet, there is no completely theoretical solution for the geometry of even the simplest form of incompressible jet flow structure, and the supersonic turbulent jet represents a formidable problem which is unlikely to be solved for a long time.

However, a considerable amount of work has been done which forms a firm basis for coordination of experimental work, and the combination of theory and experiment has given reliable semi-empirical methods for the prediction of subsonic jet flow at least.

## 2.2 Jet Mixing

The foundations for the study of turbulence were laid down by G. I. Taylor who developed a successful statistical theory as early as 1920. Subsequent work by himself and Von Karman, among others, further developed this theory but being confined to isotropic turbulence, it cannot be applied to the study of highly sheared, non-isotropic jet flow with any degree of success. The basis for practically all successful studies of jet flow was formed by Prandtl in 1935, when he developed his semi-empirical mixing length theory. This theory has been critized on several grounds, but it provides some very useful insight into the mechanisms of jet flow. Prandtl's early work has been developed and extended by such workers as Tollmien, Keuthe, and Squire and Trouncer, to cover the case of subsonic, incompressible jet flow.

The equations governing turbulent, axisymmetric jet flow are the continuity equation

$$r \frac{\partial (\rho U)}{\partial x} + \frac{\partial (r \rho V)}{\partial r} = 0 \qquad (2.1)$$

where $U$ and $V$ are the mean axial and radial velocities respectively, and the simplified Navier-Stokes equation,

$$r \rho U \frac{\partial U}{\partial x} + r \rho V \frac{\partial U}{\partial r} = \frac{\partial \tau_r}{\partial r} \qquad (2.2)$$

where it is assumed that pressure gradients are negligible and viscous stresses can be ignored in comparison to the turbulent shear stress $\tau_r$. These equations are combined and integrated, giving the result

$$\frac{\partial}{\partial x} \int_0^R \rho U^2 r \, dr - U_R \frac{\partial}{\partial x} \int_0^R \rho U r \, dr = \tau_R R \qquad (2.3)$$

where $R$ is an effective radius defined by a mean velocity $U_R$.

The turbulent shear stress $\tau_R$ can be expressed in two ways. The first,

$$\tau_R = \rho E \left(\frac{d U}{d r}\right)_R \qquad (2.4)$$

includes the apparent eddy viscosity $E$ which is an exchange coefficient. The second uses Prandtl's mixing length concept which is that the turbulent velocity fluctuation

$$u \propto v \propto \ell \cdot \frac{d U}{d r}$$

i.e., the product of the mixing length and the local velocity gradient. Since $\tau$ is primarly the Reynold's Stress $\rho \overline{u v}$,

$$\tau \propto \rho \ell^2 \left|\frac{d U}{d r}\right| \frac{d U}{d r} \qquad (2.5)$$

An additional relationship governing the flow is that which expresses the conservation of momentum along the jet, namely,

$$\int_0^\infty \rho U^2 r \, dr = \text{constant}. \tag{2.6}$$

Equations (2.1) through (2.6) are the basic equations of motion. The differences in the work of the various investigators lie essentially in the nature of the assumptions made to facilitate their solution.

For subsonic, incompressible flow the variation of density in the expressions of Reynolds stresses can be neglected, thereby considerably simplifying the solution. The unknowns remaining are the velocity distribution and the form of the shear stresses. In the core region of the jet, experimental data show that mixing region velocity profiles are similar along the length of the care and in a fully developed region downstream. In the core region the velocity decays approximately exponentially and can be written

$$U = U_E \, e^{-\eta^2/2} \tag{2.7}$$

where $\eta = (r - a)/b$, $a$ is the potential core radius and $b$ is a width parameter. Using this velocity profile, and assuming $\ell/b$ to be constant in the core region, Eldred et al. (Reference 17) use the mixing length representation of the turbulent shear stress equation (2.5) to solve the equations for a constant density jet, obtaining the flow in that region as a function of $\ell/b$ only. This parameter can only be derived experimentally, either by direct velocity correlation measurements in the turbulent flow, or by measurement of the flow geometry.

Downstream from the core tip, there is a transition region, of a length approximately equal to that of the core, within which the velocity profile adjusts itself. Further downstream of this region the velocity profiles remain similar. Eldred et al. extended their solution to the downstream region by ignoring this transition region and assuming the same type of velocity profile

$$U = U_m \, e^{-\eta^2/2}$$

where this time $\eta$ is simply $r/b$, and $U_m$ is the centerline velocity, which now decays with axial distance. The parameter $\ell/b$ is assumed to remain constant and equal to its value in the initial mixing region. Figure 3, taken from Reference 17, shows the calculated flow contours for a constant density axisymmetric jet with an exit Mach number of 1.0 and zero external velocity.

However, the incompressible, constant density jet represents the simplest possible case, and jets of practical importance for flight propulsion purposes have very hot compressible flow. In an attempt to take some account of compressibility effects, Eldred et al. retained the assumption of constant mean density to derive effective values of $\ell/b$ from experimental data and examined the variation of this parameter with jet Mach number. At low speeds its value was calculated from the turbulence data of Laurence (Reference 4) and at high Mach numbers from estimates of the potential core dimensions. The variation of the core length is shown in Figure 4, in which are plotted experimental data from References 4, 18, 19, 20, 21, 22, and 23. It can be seen that core length increases rapidly with Mach number implying a reduction in mixing length and consequently turbulent shear stress. The calculated equivalent reduction in $\ell/b$ is given in Figure 5. The most significant feature of these curves is the remarkably small effect which temperature appears to have upon the core length. At the high Mach numbers, data from very cold jets ($-300^{\circ}F$) and very hot rocket exhaust flow ($2000^{\circ}F$) fall close to the same empirical curve $x_t/d_E = 3.45\ (1 + 0.38\ M_E)^2$.

Figure 6 presents a series of curves, calculated according to the downstream solution of Reference 17, and again assuming $\ell/b$ constant, which shows the axial velocity decay for exit Mach numbers ranging from $M = 0.5$ to 3.5. Superimposed on this figure are some experimental points which indicate the magnitude of the errors introduced by this simplified approach. The same error is also evident in Figure 7, where the corresponding jet spreading curves are shown as plots of $b$ against $r/d_E$. The measured rate is indicated by a curve of $r_{0.5}$, the radius at which the mean velocity falls to half its value on the centerline. Since $b$ is in fact, equal to the radius at which the velocity ratio is 0.606 (in the downstream region), this gives a slightly pessimistic impression of the discrepancies between the simple theory and experiment.

In Figure 8, the position of the "sonic point" $x_s/d_E$, taken from the curves of Figure 6, i.e., the axial location at which the flow becomes subsonic, assuming the jet temperature to be equal to ambient, is compared with an empirical curve obtained by Anderson and Johns (Reference 20).

The theoretical curve is seen to overpredict $x_s/d_E$ by a large margin. Possible reasons for this discrepancy are discussed in detail below, but if the experimental data are correct, then temperature obviously plays a much more important part in the downstream region than it does in the initial mixing region and the assumption that $\ell/b$ remains constant throughout the jet is open to question.

More realistic flow models have been analyzed by several workers, notably Szablewski (Reference 24), Abramovitch (Reference 25), Kleinstein (Reference 26), and Warren (Reference 27). In a compressible fluid flow the density fluctuations in the Reynold's stresses are no longer negligible. The same is true in flow characterized by large variations of temperature. Thus, velocity fields and temperature fields must be considered simultaneously. As in the case of incompressible jet studies, great reliance has to be placed on experiment to provide empirical constants. Unfortunately, experimental investigations of the turbulence properties of supersonic flow are extremely difficult, because the prime tool for turbulence measurements, the hot wire anemometer, is sensitive to fluctuations of temperature and density, as well as velocity. All three quantities fluctuate simultaneously in supersonic flow. However, a good deal can be inferred from the mixing characteristics of compressible jets and, by making a number of plausible assumptions, incompressible theory can be extended to derive mean compressible flow properties.

As a step towards consideration of a complete, compressible flow, Abramovich (Reference 25) retained Prandtl's assumption that the mixing length is constant across the mixing region section and made the further assumption that the velocity, density and temperature profiles in the mixing region are similar. These enabled him to show that the effect of compressibility on variable density, low subsonic flow properties is negligible, in fact, experimentally evidenced by the dynamic similarity of jets with widely differing temperatures. He also found that the effect of compressibility upon the fundamental properties of jet mixing due to velocity up to $M = 1.0$ is negligible. Both results have the same implication; a velocity increase or a temperature decrease reduces the shear stresses and the mixing zone narrows, an experimentally observed fact.

Abramovitch's results are restricted to the case of moderate temperature difference and high subsonic velocity. The basic objection to the use of these methods for high temperature, supersonic flow concerns the mixing length concept. In compressible flow the eddy viscosity of equation (2.4) is no longer a measure of the transfer phenomena. It must be replaced by a dynamic transfer coefficient $\overline{\rho\epsilon}$ which accounts for thermodynamic fluctuations. Kleinstein, (Reference 26), assumed constancy of this parameter across the mixing width and accounted for its axial variations by the relationships

$$\overline{\rho\epsilon} = \frac{k_1}{2} \, r_{0.5} \, \rho_m \, U_m \tag{2.8}$$

in the downstream region, where $r_{0.5}$ is the radius at which the mean velocity is half the centerline velocity

$$\text{and} \quad \overline{\rho\epsilon} = k_2 \, \frac{x}{d_E} \tag{2.9}$$

in the initial mixing region.

By linearizing the equations for conservation of mass, momentum, specie and energy into a form of heat conduction equation, he obtained a solution for the centerline decay of the jet properties. Kleinstein reached the conclusion that the centerline velocity can be nondimensionalized on the basis of the parameter $(\rho_o)^{-0.5} x/d_E$, independent of flow Mach numbers and jet fluid. However, Eggers (Reference 21) compared this result with available experiments and found poor correlation; the general trend was for a reduction in centerline decay with increasing Mach number, a finding substantiated by the data of Anderson and Johns (Reference 20).

Warren (Reference 27) derived a simpler solution by restricting the problem to the conservation of mass, momentum and energy, consequently his results are only valid for the mixing of similar gases. Eggers, (Reference 21) performed experiments with a cold Mach 2.22 jet and compared his measurements with the theoretical results of both Kleinstein and Warren. He found that Warren's results generally gave the better agreement.

As previously mentioned, development of successful theories for the analytical prediction has been hindered by the lack of experimental data. Currently, available data is sketchy and the present theories rely on experiment to provide empirical constants such as the eddy viscosity terms. Some success has been achieved in predicting velocity profiles but, in general, no theory can yet be relied upon to provide the details of flow geometry which are important in a definition of the near field noise characteristics of a given flow. Even if an adequate theory is developed which may be applied to the flow from an ideally expanded nozzle, the real situation is so grossly complicated by the formation of shock waves within the flow, which again are important from an acoustic standpoint, that it is doubtful whether such a theory would be of practical value.

However, it is believed that available experimental information can be utilized to construct a realistic flow model which can be used with some confidence in the task of noise prediction.

## 2.3 The Development of a Shock Pattern in Supersonic Flow

Practically all supersonic exhaust flows are characterized by a standing shock pattern. Careful nozzle design and subsequent design-point operation can result in flow which is shock free for all practical purposes, but in practice, rocket nozzles normally encounter design operation at one particular ambient pressure only, i.e., at one particular altitude. On the launch pad and in the early stages of flight where acoustic problems are significant, the ambient pressure is higher and the nozzle is operating in an "overexpanded" condition.

However, it is appropriate to consider both over and underexpanded cases, and Figure 9 shows the development of shocks as the chamber pressure is increased from a low value through and above the design condition. The diagrams depict an idealized axisymmetric jet which, although influenced by the ambient air, does not mix with it. The shock patterns represent the first few cycles of an infinite series. Figure 9 (e) is the perfectly expanded, parallel, shock-free flow, (a) through (d) are overexpanded and (f) through (i) are underexpanded.

Starting at Figure 9 (f) the nozzle pressure ratio is slightly above its design value. The static pressure at the nozzle is therefore slightly above ambient and the flow expands slightly. At the same time the flow accelerates in an axial direction. The inertia of the fluid causes an overexpansion and the static pressure becomes less than atmospheric at a point downstream. Consequently, the jet boundary is compressed inwards again and at some point the pressure inequality gives rise to a shock wave where the flow attempts to correct matters. In doing so, however, the static pressure is increased to a value above ambient and the nozzle conditions are effectively regenerated so that the cycle is infinitely repeated. This cycle property of the shock structure is always found; it results merely because the fluid has inertia.

As the pressure ratio is increased, the shocks increase in both extent and strength and eventually meet at the jet axis, forming a cone. This state is shown in( g). At around the same pressure ratios, a fan of expansion waves emerge near the nozzle lip as the flow expands very rapidly. A further increase in pressure causes the shocks to reflect at the axis as illustrated in (b), and the flow near the axis now undergoes a double compression and expansion during each cycle.

As the pressure ratio is increased still further, conditions exceed those for which a reflection is possible and the intersection is split by a further shock which is normal to the axis. Since the flow is axially symmetric, this shock front takes the form of a disc which is known alternatively as the Mach disc or Riemann Wave. At greater pressure ratios no further change in the basic shock pattern occurs. The Mach disc increases in diameter and the flow boundaries exhibit increased curvature.

As Figure 9 indicates,an increasing pressure ratio also increases the basic length of each cycle of the periodic cellular structure. As the pressure is decreased below the design point, the reverse occurs, and the cell length decreases. Otherwise the shock patterns pass through a very similar series of changes, with the main exception that the excess ambient pressure causes a basic depression of the jet boundary and the mean flow diameter is significantly reduced. Figure 9 clearly demonstrates the general increase in the flow dimensions as the pressure ratio is increased from its lowest value which gives an increased thrust by increasing mass

flow. Another difference in the overexpanded flow structure is that between the nozzle and the first shock interaction or Mach disc, the pattern is not characteristic of the regular periodic flow which is established downstream of that intersection. In the underexpanded cases the structure is approximately periodic from the nozzle outwards. As the chamber pressure is reduced to the critical pressure ratio of 1.89 the shock pattern degenerates to a normal shock across the exit plane of the nozzle, eventually disappearing as the exhaust becomes subsonic.

The foregoing discussion of the flow properties relates only to an "idealized" jet which does not mix with the ambient atmosphere and which retains its momentum. In practice, neither of these stipulations is true. The flow interacts with the ambient medium forming a turbulent mixing region which eats into the laminar core, eventually consuming it entirely, and the shock structure itself extracts energy from the flow in the form of heat, a process which slightly reduces the mean velocity with increased axial distance. A more realistic representation of a typical flow structure is shown in Figure 10. Comparing this with Figure 2, which shows an equivalent shock-free flow, it can be seen that the main difference, in addition to the presence of the shocks themselves, lies in the deformation of the boundaries of the various flow regions. In contrast to the idealized jet of Figure 9 the supersonic region of the flow is now finite and the shock pattern deforms as the mean flow velocity decreases and eventually disappears at some point downstream where the velocity becomes subsonic. It is important to note that downstream of the laminar core tip the mean axial velocity decays rapidly and the disintegration of the shock structure proceeds at an equally rapid rate. Figure 11 shows a series of shadowgraphs from Reference 50 which clearly show the described development of the shock pattern as the pressure ratio is increased from sub-critical to supercritical as well as its downstream degeneration due to energy and momentum losses.

## 2.4 Definition of Shock Geometry

Compression, expansion and shock waves in jets were noted and experimentally studied by many noted scientists including Mach, Prandtl, Von Karman and Lord Rayleigh around the turn of the century. In later years, since 1920, attempts have been made to calculate flow patterns for various supersonic jets using the method of characteristics. Among many others, Pai (Reference 28) notes the work of Prandtl and Busemann, and Pack, who applied the method to two dimensional flows. Sauer (Reference 29) and Pai (Reference 30) calculated the flow pattern for a stationary, axisymmetric jet exhausting into quiescent air.

However, despite the extensive analytical studies that have been conducted, theory as yet, only provides understanding of the mechanisms which give rise to the shock patterns in a supersonic exhaust. The problem of calculating shock locations and shapes in a uniform flow is difficult enough, but the added complication of the highly sheared velocity profiles, which exist in a real jet, practically obviate all chance of developing a practical prediction method. We must therefore turn to experiment.

Probably the most comprehensive experimental study of supersonic jets has been performed by Love et al. (Reference 31). Although they were mainly interested in the flow in the immediate vicinity of the nozzle, they present valuable data from which it is possible to estimate the general form of the shock pattern by making some reasonable assumptions. Love et al. studied the effects upon the shock pattern of design Mach number (nozzle area ratio), nozzle divergence angle and the ratio of the specific heats of the jet gas. Unfortunately, their observations were restricted to the first cell of the shock pattern and it is well known that the pattern is not exactly periodic, non-periodicity generally increasing with departure of the pressure ratio from the design value. However, at pressure ratios in the vicinity of the design point the departure is sufficiently small to justify the assumption that the first cell is typical.

Figure 12, compiled from the results of Love et al. shows the variation of the ratio of primary cell length to nozzle diameter with pressure ratio for a number of nozzle design Mach numbers. The pressure ratio here is $p_E/p_o$, the ratio of the static pressure at the exit plane to the ambient pressure. At the design point ($p_E/p_o = 1$) the cellular pattern theoretically disappears but in practice weak shocks still remain due to imperfect flow conditions, and continue to define a cell length. The curves presented are in fact the empirical relations, derived by Love et al:

$$\frac{w}{d_E} = 1.55 \sqrt{M_E^2 \left(\frac{p_E}{p_o}\right)^2 - 1} - 0.55 \sqrt{M_E^2 - 1} \qquad (2.10a)$$

for

$$\frac{p_E}{p_o} \lessapprox 2$$

and

$$\frac{w}{d_E} = 1.52 \left(\frac{p_E}{p_o}\right)^{0.437} + 1.55 \left(\sqrt{2 M_E - 1} - 1\right) - 0.55 \sqrt{M_E^2 - 1} + 0.5 \left[\frac{1}{1.55} \sqrt{\left(\frac{p_E}{p_0} - 2\right) \sqrt{M_E^2 - 1}} - 1\right] \qquad (2.10b)$$

for

$$\frac{p_E}{p_o} \gtrapprox 2$$

The abrupt change in the variation of $w/d_E$ with $p_E/p_o$ at $p_E/p_c \approx 2$ is connected with the reappearance of the Mach disc around that pressure ratio.

These curves give a fair prediction of the experimental results throughout the range of $p_E/p_o$ and $M_E$ studied; although, there is some tendency at the higher pressure ratios to overpredict the wavelength at low Mach numbers and underpredict at the higher Mach numbers. It was found that varying the nozzle divergence angle had no significant effect on the primary wavelength.

Figure 13 shows the faired curves of the measured location of the shock intersection point or the Mach disc, whichever occurs at the given combination of $p_E/p_o$ and $M_E$. Superimposed upon these curves are the boundaries marking the ranges of $p_E/p_o$ and $M_E$ within which no Mach disc exists. As in the case of the primary wavelength it was found that the nozzle divergence angle had a negligible effect on the dimension. Figure 14, again derived from Reference 31, shows the effect of pressure ratio and Mach number on the diameter of the Mach disc, non-dimensionalized with respect to the nozzle diameter. The curves shown were faired through the data for an ideally-expanded nozzle design. This time it was found that the dimension was extremely sensitive to the nozzle divergence angle. The other results for conical nozzles have been omitted for clarity and because most rocket nozzles are designed to give good expansion contours. For a fuller description the reader is referred to Reference 31.

In order to use this data to estimate the shock pattern for a particular rocket flow it is necessary to make the following assumptions:-

(i) That the shock pattern is a function of pressure ratio and design Mach number only. Temperature effects were not studied, and it is not likely that they will have any significant effect upon shock geometry. However, temperature does have some effect upon the jet mixing process and governs to some extent the boundaries of the supersonic flow.

(ii) That the cells defined by the shock patterns are exactly periodic, i.e., that the cell wavelength is constant throughout the supersonic flow. This is known to be incorrect and a mere consideration of the variation of mean velocity throughout the supersonic region suggests that there will be significant distortion of the cells downstream of the potential cone at least.

(iii) That the pattern is independent of the ratio of specific heats, $\gamma$, of the jet. The validity of this assumption is unknown although calculations by Love et al. suggest that $\gamma$ has a negligible effect on the shape of the initial part of the jet boundary.

With these assumptions, and knowing the boundary of the supersonic flow, a reasonable estimate of the shock configuration can be established.

## 2.5 Mach Number Contours in Exhaust Flow

This section presents a method by which the mean flow properties of an ideally expanded supersonic axisymmetric jet can be estimated. It relies heavily on the experimental data of Anderson and Johns (Reference 20) which, although obtained twelve years ago, still remains the most comprehensive set of supersonic exhaust flow data generally available. Some inconsistencies in this work have been noted, however, and additional data have been sought to substantiate the material used. The following analysis applies to the particular case of identical jet and ambient gases although additional experimental data provided by Reference 20 could be used to extend the results, at the expense of additional complexity, to the more general case of dissimilar gases.

Figure 4 shows the variation of the length of the potential core (relative to the nozzle exit diameter) with Mach number. Eldred et al. (Reference 4) noted the collapse of the core length data on a basis of exit Mach number and derived the empirical relationship:

$$\frac{x_t}{d_E} = 3.45\ (1 + 0.38\ M_E)^2 \qquad (2.11)$$

This is the curve of Figure 4 and available experimental data for a variety of jet parameters is superimposed for comparison. It is seen that temperature and gas composition have remarkably little effect upon the core length.

As discussed above, analysis of the radial spreading characteristics of a large variety of jet flows has shown that the mean velocity decays approximately in an exponential manner with distance from the axis and can be represented by an expression of the form,

$$U = U_m\ e^{-\eta^2/2} \qquad (2.12)$$

A comparison of this relationship with some experimental results is shown in Figure 15. The error is seen to be small and of the same order as the differences in the experimental data. Unfortunately, the bulk of the measured data is for subsonic flow or for the fully turbulent flow downstream of the laminar core in supersonic jets. However, the one profile measured along side the core of a Mach 2.22 jet by Eggers (Reference 21) shows good agreement and provides justification for assuming velocity profile similarity throughout the entire jet.

Anderson and Johns (Reference 20) also found similarity of the total temperature profiles in the fully turbulent zones of a large variety of supersonic jets and rockets. The non-dimensional profile is shown in Figure 16 plotted against the same parameter $\eta$. Fitting a similar relationship to that for the velocity decay gives

$$\Delta T_T = \Delta T_{m_T} \; e^{-\eta^2/2.5}$$

where (2.13)

$$\Delta T_T = T_{m_T} - T_o$$

$T_{m_T}$ is the centerline (maximum) value of the temperature and the suffix T denotes total conditions. No temperature measurements were made in the core region but in their absence it will be assumed that temperature profile similarity is maintained right back to the nozzle.

Both Anderson and Johns (Reference 20) and Frauenberger and Forbister (Reference 32) found that the pressure downstream of the core tip decayed logarithmically according to the proportionality relationship,

$$\frac{p_{m_T} - p_o}{p_{E_T} - p_o} \propto \left( \frac{x}{d_E} \right)^{-n} \qquad (2.14)$$

where $p_T$ is the total pressure and $p_o$ is the ambient pressure.

The variation of n with Mach number is shown in Figure 17. The mean line through this data is

$$n = 1.4 + 0.43 \; M_E$$

The proportionality constant in equation (2.14) can then be derived from the boundary condition that, at the core tip position given by equation (2.11)

$$\frac{p_{m_T} - p_o}{p_{E_T} - p_o} = 1.0$$

Assuming that the static pressure throughout the jet is equal to ambient, the axial Mach number can be calculated from the isentropic flow relationship:

$$M_m = \left[ \frac{2}{\gamma - 1} \left( \frac{p_o}{p_T}^{-\left(\frac{\gamma - 1}{\gamma}\right)} - 1 \right) \right]^{1/2} \tag{2.15}$$

The decay of Mach number $M_m$ on the jet axis calculated according to equations (2.14) and (2.15) is shown for various exit Mach numbers in Figure 19.

The total temperature increment has also been found experimentally to decay in a similar fashion. The decay exponent measurements of References 20 and 32 are plotted in Figure 18 and use of the mean line leads to the expression

$$\frac{T_{m_T} - T_o}{T_{E_T} - T_o} = \text{constant} \times \left( \frac{x}{d_e} \right)^{-(1 + 0.23\, M_E)} \tag{2.16}$$

Assuming that velocity and temperature profiles in the initial mixing region also obey equations (2.12) and (2.13), Appendix A shows that the total momentum in the mixing region is given by

$$m_M = 2\pi \rho_o U_m^2 \int_{r=a r_E}^{\infty} \left[ 1 + \frac{\gamma - 1}{2} \left\{ \frac{t\, M_m^2\, e^{-\eta^2}}{\left(1 + \frac{\gamma - 1}{2} M_c^2\right)\left(1 - (t-1)\, e^{-\eta^2/2.5}\right)} \right\} \right]^{\frac{1}{\gamma - 1}} \times$$

$$\times \frac{e^{-\eta^2} \cdot r}{1 + (t-1)\, e^{-\eta^2/2.5}}\, dr \tag{2.17}$$

where $\rho_o$ is the ambient density, $U_m$ is the centerline velocity, $t$ is the ratio of centerline total temperature to the ambient temperature, $T_{m_T}$, and $\gamma$ is the ratio of the specific heats of the jet.

Further, it can be shown (see Appendix A) that

$$\frac{U_m}{U_E} = \frac{M_m}{M_E} \sqrt{\frac{1 + \frac{\gamma - 1}{2} M_E^2}{1 + \frac{\gamma - 1}{2} M_m^2} \cdot \frac{t}{t_E}} \tag{2.18}$$

Thus, assuming that the total axial momentum in the jet is constant, and that the laminar core is conical, such at

$$a = 1 - \left(\frac{x}{d_E}\right) \cdot \frac{1}{x_t}$$

the expression given by equation (2.17) can be equated to the relationship, given by nozzle exit conditions;

$$m_M = \rho_E U_E^2 \pi r_E^2 \tag{2.19}$$

From this equality and equations (2.15) and (2.16) the mixing width parameter $b$ can be derived as a function of axial distance. This has been calculated for an air jet ($\gamma = 1.4$) with $M_E = 2.0$, and $t = 5$ and is shown in Figure 20.

The axial variations of $M$, $t_m$, and $b$ are sufficient to define a complete Mach number distribution throughout the jet. Appendix A shows that at any axial station,

$$M^2(\eta) = \frac{t\, M_m\, e^{-\eta^2}}{\left(1 + \frac{\gamma-1}{2} M_m^2\right)\left(1 + (t-1)\, e^{-\eta^2/2.5}\right)} \times$$

$$\times \left[1 + \frac{\gamma-1}{2}\left\{\frac{t\, M_m^2 \left(1 + \frac{\gamma-1}{2} M_m^2\right)^{-1} e^{-\eta^2}}{1 + (t-1)\, e^{-\eta^2/2.5}}\right\}\right]^{-1} \qquad (2.20)$$

Using this result and the previously derived values of b, M, and $t_m$, the Mach number contours for the $M = 2$, $t = 5$ air jet have been calculated, by numerically integrating equation (2.17), and are presented in Figure 20.

A most important parameter in the acoustic definition of a supersonic jet is the axial position, $x_s$, of the point at which the axial velocity becomes subsonic, the "sonic point". Figure 8 shows three curves of $x_s/d_E$ as a function of exit Mach number. The first is calculated by the simple theory of Reference 17 described above and the second is taken from the curves of Figure 19, which were calculated according to equations (2.14) and (2.15). In both cases it was necessary to assume that the jet temperature is equal to ambient. The third curve fits the experimental data of Anderson and Johns (Reference 20). Both calculated curves are seen to overestimate the supersonic core length although equation (2.5) is nearer to the experimental results. The latter are based upon total pressure measurements on the axis of supersonic jets and rockets, assuming the static pressure at the same point to be equal to ambient. However, the results are susceptible to error, particularly at the high velocities where the measurements were taken in badly expanded rocket exhaust flow, where the presence of shock waves could invalidate the static pressure assumption. More important, the shock structure is likely to modify significantly the flow dimensions. Johannesen (Reference 18) suggests that the rate of spreading increases rapidly with shock strength causing a consequent reduction in the length of the supersonic cone. Another reason to suspect the experimental data is that around $M_E = 1.4$, Anderson and Johns results indicate that the sonic point lies within the laminar core as defined by the well substantiated empirical relationship given by equation (2.11). The Mach number in this region should, of course, remain equal to the nozzle value. Finally, since equation (2.15) utilizes the pressure data of Reference 20 it will seem strange that the calculated and experimental curves do not coincide. This is basically because the pressure decay exponents presented as Figures 17 and 18 are not established until a short distance downstream of the laminar core tip, although there does appear to be some discrepancy between the given locations of the sonic point and the actual total pressure measurements presented elsewhere in the same report. However, the decay rates show agreement with those measured by Frauenberger and Forbister (Reference 32) and the $(x_s/d_E)$ curve calculated by equations (2.14) and (2.15) is substantiated by two additional experimental points taken from References 18 and 21.

It is evident that there is considerable doubt attached to available experimental data on which the foregoing analysis is based. Although it has been utilized in the absence of positive confirmation, it demonstrates the clear need for further valid and comprehensive measurements of supersonic flow parameters if accurate estimates of the properties of the complex rocket exhaust structures are to be made.

## 3.0 GENERATION OF SOUND BY TURBULENT JETS

Before proceeding to the more complex problem of the noise of supersonic jets, it is as well to consider the noise generation mechanisms of low speed, subsonic jets, in the light of previous work, both theoretical and experimental.

### 3.1 The Noise of Subsonic Jets

#### 3.1.1 Lighthill's Theory

The foundations for the theoretical study of aerodynamic noise generation were laid by Lighthill in 1952 (Reference 1). Although the results of his work are applicable to the far-field sound of turbulence, its consideration is appropriate since it formed the basis for most subsequent work and for the coordination of early experiments.

The starting point is the general equation for the generation of aerodynamic noise in a uniform medium at rest due to externally applied fluctuating stresses which Lighthill showed to be, in tensor notation,

$$\frac{\partial^2 \rho}{\partial t^2} - a_o^2 \nabla^2 \rho = \frac{\partial^2 T_{ij}}{\partial x_i \partial x_j} \qquad (3.1)$$

$T_{ij}$ is the magnitude of the externally applied stress system. Since the right hand term is a second derivative, the sound field can be regarded as that due to a continuous distribution of acoustic quadrupoles of strength $T_{ij}$ per unit volume. Elements like $T_{11}$ represent "longitudinal" quadrupoles and those like $T_{12}$ "lateral" quadrupoles. A quadrupole can be simply thought of as a close combination of four simple sources fluctuating in phases pairs and whose sound field is therefore dominated by cancellation effects. $T_{ij}$ in equation 3.1 is, in fact, the difference between the effective stresses in the medium at rest.

$$T_{ij} = \rho v_i v_j + p_{ij} - a_o^2 \rho \delta_{ij}$$

where $\rho v_i v_j$ is the momentum flux tensor, $p_{ij}$ is the real stress, both static and viscous and $a^2 \rho \delta_{ij}$ is the acoustic stress. It is important to note that equation 3.1 is exact. $T_{ij}$ incorporates the generation of sound, its convection within the flow and its gradual dissipation by conduction and viscosity.

The quadrupole nature of aerodynamic noise is important both because of the directionality and the pressure decay within its sound field. The pressure field of a simple source falls off inversely as the distance from it. However, differences between the distances from the "simple source components" of a quadrupole are negligible at points in its far field and complete cancellation of the transmitted

pressures is only avoided because those arriving simultaneously at a given point were emitted at different times. The far field acoustic amplitude therefore depends entirely upon the manner in which the quadrupole strength changes with time, and is proportional to the second time derivative of $T_{ij}$.

The general solution to equation 3.1 for the sound pressure at the point $\underset{\sim}{r}$ is

$$p(\underset{\sim}{r}) = \frac{1}{4\pi} \int_V \frac{\partial^2}{\partial x_i \partial x_j} \left\langle \frac{T_{ij}}{r} \right\rangle \, dy \tag{3.3}$$

where the brackets $\langle\ \rangle$ denote evaluation at the retarded time $\overline{T} = t - r/a_o$, which defines the instant of emission of the sound arriving at $\underset{\sim}{r}$ at time $t$. The integration should strictly be carried out over all space, but for practical purposes, fluctuations outside the flow field $V$, can be ignored. The vector $\underset{\sim}{r}$ defines the position of the field point $\underset{\sim}{x}$ relative to the source position $\underset{\sim}{y}$ so that $\underset{\sim}{r} = \underset{\sim}{x} - \underset{\sim}{y}$ and $r = |\underset{\sim}{x} - \underset{\sim}{y}|$.

If the double differentiation in equation 3.3 is performed, the general expression for instantaneous sound pressure due to the distribution of quadrupoles becomes (Franz - Reference 15),

$$p(\underset{\sim}{r}) = \frac{1}{4\pi} \int_V \left\{ \frac{r_i r_j}{r^2} \left\langle \frac{\ddot{T}_{ij}}{r a_o^2} + \frac{3\dot{T}_{ij}}{r^2 a_o} + \frac{3T_{ij}}{r^3} \right\rangle - \right. \tag{3.4}$$

$$\left. - \delta_{ij} \left\langle \frac{\dot{T}_{ij}}{r^2 a_o} + \frac{T_{ij}}{r^3} \right\rangle \right\} \, d\underset{\sim}{y}$$

Here $r_i = x_i - y_i$, $\delta_{ij}$ is the Kronecker delta and a dot denotes differentiation with respect to time. The terms in $\ddot{T}_{ij}$ represent the radiated or far field sound pressure and the terms in $\dot{T}_{ij}$ and $T_{ij}$ represent the induction near field pressure. Geometric near field effects are manifested in the dependence upon $r$ and in the factor $r_i r_j / r^2$. If $r_i$ can be approximated by $x_i$, geometric near field effects are negligible. Lighthill ignored the second order near field terms to obtain the result for the far field:

$$p(\underset{\sim}{r}) = \frac{1}{4\pi} \int_V \frac{r_i r_j}{r^2} \left\langle \frac{\ddot{T}_{ij}}{r a_o^2} \right\rangle \, d\underset{\sim}{y} \tag{3.5}$$

In order to estimate this integral contribution from the extended flow field V, it is necessary to take into account the statistical randomness of turbulence flow. It is a general rule that for well correlated sources, acoustic pressure amplitudes combine linearly and for uncorrelated sources, intensities add linearly. Turbulent flow measurements show that the correlation between the flow properties at two separate points decreases with separation. As a simplified concept, we can consider turbulence to consist of numerous regions such that, within each, the quadrupole strength is perfectly correlated, whereas between different regions there is no correlation. This is the basic concept of an energy bearing eddy which can therefore be defined as a region of correlated momentum flux. The acoustic field of an eddy of volume $V_e$ can thus be written,

$$p(\underset{\sim}{r}) = \frac{1}{4\pi} \frac{r_i r_j}{r^3} \cdot V_e \left\langle \ddot{T}_{ij} \right\rangle \tag{3.6}$$

where the variations of both retarded times and quadrupole strength throughout the eddy are ignored. This leads to the approximation that the acoustic power output per unit volume of turbulence is proportional to

$$\frac{V_e \; f^4 \; \overline{T^2}}{\rho_o \; a_o^5} \tag{3.7}$$

The parameter $f$ is a typical fluctuation frequency and $\overline{T^2}$ is a typical mean square value of the quadrupole strength.

Lighthill applied this result to a crude dimensional analysis of the sound output from a low speed jet. He assumed firstly that $T_{ij}$ is predominantly dependent upon the term $\rho v_i v_j$ which in turn is proportional to $\rho_E U_E^2$. Secondly, it is known that the Strouhal number, $f d_E / U_E$, varies only slowly with Reynolds number so that $f$ is proportional to $U_E / d_E$. Eddy volume $V_e$ will increase typically as the jet dimensions, i.e., as $d_E^3$ and therefore from 3.7 the overall sound power, is proportional to

$$\frac{\rho_E^2 \; U_E^8 \; d_E^2}{\rho_o \; a_o^5} \tag{3.8}$$

which is the well known eighth power law.

Now, although the derivation of this result is strictly valid for low Mach numbers only, it has been experimentally observed to hold good for jet exhaust velocities up to twice the ambient speed of sound. Lighthill suggests that this remarkable finding is in fact due to the cancelling of two corrections which must be made to the theory at high Mach numbers, as follows.

An essential assumption in the derivation of equation 3.7 is that differences in retarded times within the region defined as an eddy can be ignored. This is only justified if the parameter $\omega \ell / a_o$ is small, where $\ell$ is a typical eddy dimension (or correlation length), and $\omega$ is a typical radian frequency. This is only true at low Mach numbers but Lighthill extended the valid range of Mach numbers to at least $M = 1$ by confining frequency considerations to a frame of reference which moves with the eddies. The existence of this frame of reference has been verified by the experimental work of Davies, Fisher and Barratt (Reference 5) who performed extensive hot-wire measurements in the mixing region of a subsonic jet, and showed that typical eddy velocities range from 0.2 to 0.7 times the mean centerline velocity with 0.5 as a reasonable average. This step significantly reduces the turbulent frequency range since $\omega \ell$ now becomes proportional to a velocity fluctuation rather than a mean velocity. It also means that the eddies may now be thought of as moving quadrupole sources and theory (References 33 and 34) shows that equation 3.6 becomes

$$p(\underset{\sim}{r}) = \frac{1}{4\pi a_o} \frac{r_i r_j}{r^3} \frac{V_e \left\langle \ddot{T}_{ij} \right\rangle}{(1 - \overline{M}_c \cos\theta)^3} \tag{3.9}$$

where $\overline{M}_c$ is the convection velocity, $U_c$, divided by the ambient speed of sound. The directional effect of the convection velocity is apparent.

Inclusion of equation 3.9 in an expression for acoustic intensity must be accompanied by an additional factor $(1 - \overline{M}_c \cos\theta)$ to account for the increased number of eddies whose sound arrives at the field point simultaneously (Reference 35). Applying these convection effects, the sound intensity due to a unit volume of turbulence becomes (c.f. equation 3.7),

$$I(\theta) \propto \frac{V_e f^4 \overline{T^2}}{\rho_o a_o^5} (1 - \overline{M}_c \cos\theta)^{-5} \tag{3.10a}$$

and extending this result to the case of a jet, after the manner of equation 3.8 gives:

$$I(\theta) \propto \frac{\rho_E^2 U_E^8}{\rho_o a_o^5} \left(\frac{d_E}{r}\right)^2 (1 - \overline{M}_c \cos\theta)^{-5} \tag{3.10b}$$

which at low values of $\overline{M}_c$ retains the original $U^8$ dependence. Now turbulence measurements at higher subsonic Mach numbers (see Section 2.0) indicate a definite reduction in the ratio of rms fluctuating velocity to mean velocity. If, in fact, the rms velocity is proportional to $U^{3/4}$, a rule which appears to be approached at the high subsonic Mach numbers, then $V_e f^4 \overline{T^2}$ will be proportional to $U^6$ rather than $U^8$. Lighthill (Reference 36) points out that intensity-measurements at $\theta = 90^\circ$, where the directionality factor is unity, verify this for Mach numbers between 0.5 and 1.0.

Simultaneous with this modification to the velocity power law, the directionality factor $(1 - \overline{M}_c \cos\theta)^{-5}$ increases the net acoustic power output of the jet by increasing the power radiated at acute angles to the flow direction by a greater amount than the reduction in sound power radiated backwards. In fact the integral of $(1 - \overline{M}_c \cos\theta)^{-5}$ over a sphere varies roughly as $U^2$, which, when combined with the $U^6$ dependence shown above, restores the original $U^8$ law.

Thus, Lighthill's theory retains its validity up to exhaust velocities which yield mean eddy convection velocities approaching $\overline{M}_c = 1.0$. Not only does it account for the observed dependence of acoustic power output on the eighth power of the velocity but it also demonstrates the directional properties of jet noise, i.e., that the bulk of the sound is radiated at acute angles to the jet.

3.1.2 Extension of Lighthill's Analysis to the Near Field

Franz (Reference 15) extended Lighthill's work by retaining the near field terms of equation 3.4 which is

$$p(\underset{\sim}{r}) = \frac{1}{4\pi} \int_V \left\{ \frac{r_i r_j}{r^2} \left\langle \frac{\ddot{T}_{ij}}{r a_o^2} + \frac{3\dot{T}_{ij}}{r^2 a_o} + \frac{3T_{ij}}{r^3} \right\rangle - \right. \tag{3.11}$$

$$\left. - \delta_{ij} \left\langle \frac{\dot{T}_{ij}}{r^2 a_o} + \frac{T_{ij}}{r^3} \right\rangle \right\} d\underset{\sim}{y}$$

where all but the first term on the right hand side express the near field complications of a quadrupole field. The sound intensity, defined as the average product of the particle velocity and sound pressure at a point can no longer be approximated in the near field by the far field relationship, $I = p^2/2\rho_o a_o$.

The velocity equation is even more complicated than the pressure relationship 3.4 with the consequence that the intensity equation, as well as that for the mean square pressure, becomes extremely formidable (see Reference 15).

For this reason, neither will be repeated here. However, by making the assumptions that $r$ is large compared with an eddy dimension and that eddy decay is a slow process, Franz reduced the mean square pressure equation to

$$\overline{p^2}(\underset{\sim}{r}) = \frac{1}{16\pi^2 a_o^4} \iint_{V\,V'} \frac{1}{r^2} \left\langle \frac{r_i\, r_j\, r'_k\, r'_\ell}{r^4} \quad \overline{\ddot{T}_{ij}\ \ddot{T}'_{k\ell}} \right. \tag{3.12}$$

$$+ \frac{a_o^2}{r^2} \left( \frac{3 r_i\, r_j\, r'_k\, r'_\ell}{r^4} - 4\delta_{ij}\, \frac{r'_k\, r'_\ell}{r^2} + \delta_{ij}\, \delta_{k\ell} \right) \overline{\dot{T}_{ij}\, \dot{T}'_k}$$

$$\left. + \frac{a_o^4}{r^4} \left( \frac{9\, r_i\, r_j\, r'_k\, r'_\ell}{r^4} - 6\,\delta_{ij}\, \frac{r'_k\, r'_\ell}{r^2} + \delta_{ij}\, \delta_{k\ell} \right) \overline{T_{ij}\, T'_{k\ell}} \right\rangle \underset{\sim}{y}\, d\underset{\sim}{y}'$$

where the primes denote conditions at the independent position $\underset{\sim}{y}'$ in the turbulent region. From this equation the near sound pressure field of a lateral quadrupole, oriented along the $x_1$ and $x_3$ axes, was derived as, in a polar coordinates, (see Figure 21a)·

$$\overline{p^2}(\underset{\sim}{r}) = \frac{4}{16\pi^2 a_o^4} \iint_{V\,V'} \frac{1}{r^2} \sin^2\theta \cos^2\theta \cos^2\phi \left\langle \overline{\ddot{T}_{13}\ \ddot{T}'_{13}} \right. \tag{3.13}$$

$$\left. + \frac{3\, a_o^2}{r^2}\, \overline{\dot{T}_{13}\, \dot{T}'_{13}} + \frac{9\, a_o^4}{r^4}\, \overline{T_{13}\, T'_{13}} \right\rangle d\underset{\sim}{y}\, d\underset{\sim}{y}'$$

Making the same assumptions regarding the nature of eddies which were made in the derivation of equation 3.6, and confining attention to the narrow band of frequencies centered on $\omega$, equation 3.13 can be written

$$\overline{p^2}(\underset{\sim}{r}) = \frac{4}{16\pi^2 a_o^4} \iint \frac{1}{r^2} \left\langle \overline{\ddot{T}_{13}\ddot{T}'_{13}} \right\rangle \sin^2\theta \cos^2\theta \cos^2\phi \quad \times$$

$$\times \left[ 1 + \frac{3a_o^2}{r^2\omega^2} + \frac{9a_o^4}{r^4\omega^4} \right] d\underset{\sim}{y}\, d\underset{\sim}{y}' \tag{3.14}$$

The equivalent expression for the radiation from a distribution of longitudinal quadrupoles oriented with their axes along the $x_3$ axis is given as

$$\overline{p^2}(\underset{\sim}{r}) = \frac{1}{16\pi^2 a_o^4} \iint \frac{1}{r^2} \left\langle \overline{\ddot{T}_{33}\ddot{T}'_{33}} \right\rangle \left[ \cos^4\theta + \frac{a_o^2}{r^2\omega^2} (3\cos^4\theta - 4\cos^2\theta + 1) \right.$$

$$\left. + \frac{a_o^4}{r^4\omega^4} (9\cos^4\theta - 6\cos^2\theta + 1) \right] d\underset{\sim}{y}\, d\underset{\sim}{y}' \tag{3.15}$$

It should be noted that the far field terms of equations 3.14 and 3.15 (namely the first) can be derived directly from equation 3.6. Also the sound field of the longitudinal quadrupole is independent of $\phi$ by virtue of its symmetry about the $x_3$ axis.

For a single correlated eddy composed of like oriented quadrupoles of a single type, lateral or longitudinal, the terms enclosed by square brackets in the relevant equation 3.14 or 3.15 give the relation between the near and far sound fields (as a function of $\theta$ in the case of longitudinal quadrupoles). However, before these equations are used, to perform a dimensional analysis of the near sound field, following Lighthill, it must be remembered that the equations are subject to the same restrictions which apply to the far field $U^8$ law, namely that their derivation is strictly valid for low subsonic Mach numbers only.

Franz examined the effects of eddy convection upon these equations using the same transformations employed by Lighthill (Reference 1) and found that the near field terms contained factors which are extremely involved functions of $\overline{M}_c$, $\theta$, $(1 - \overline{M}_c \cos\theta)$ and $(1 - \overline{M}_c^2)$. The complete expressions are much too lengthy to repeat here, but as an example, Appendix B shows the derivation from Franz's equations of the mean square pressure field of an eddy containing correlated lateral quadrupoles oriented along the $x_1$, $x_3$ axes and convected along the $x_3$ axes at the Mach

number $\overline{M}_c$. This is, for a narrow-band of frequencies around $\omega$ (here measured in the moving frame of reference)

$$\overline{p^2}(\omega) = \frac{15\,\rho_o a_o P(\omega)}{2\pi r^2} \frac{(1-\overline{M}_c^2)^4}{(1+5\overline{M}_c^2)} \frac{\sin^2\theta\cos^2\phi}{(1-\overline{M}_c\cos\theta)^5}\left[\cos^2\theta + \right.$$

$$+\frac{a_o^2}{r^2\omega^2}\left\{\frac{3(1-\overline{M}_c^2)^2\cos^2\theta}{(1-\overline{M}_c\cos\theta)^2} - \frac{6\overline{M}_c(1-\overline{M}_c^2)\cos\theta}{(1-\overline{M}_c\cos\theta)} + 4\overline{M}_c^2\right\}$$

$$\left.+\frac{a_o^4}{r^4\omega^4}\left\{\frac{9(1-\overline{M}_c^2)^4\cos^2\theta}{(1-\overline{M}_c\cos\theta)^4} - \frac{18\overline{M}_c(1-\overline{M}_c^2)^3\cos\theta}{(1-\overline{M}_c\cos\theta)^3} + \frac{9\overline{M}_c^2(1-\overline{M}_c^2)^2}{(1-\overline{M}_c\cos\theta)^2}\right\}\right] \tag{3.16}$$

where $P(\omega)$ is the total radiated sound power in the narrow frequency band. The first term on the right hand side is as usual, the radiated, far field component in a form which can be derived from Lighthill's solution (Reference 1). Throughout the righthand side, the factors like $\sin^2\theta$, $\cos^2\phi$, $\cos^n\theta$ define the directionality of the particular lateral quadrupole chosen. The mean effect of eddy convection upon arbitrarily oriented quadrupoles, of either type is expressed by the factors $(1-\overline{M}_c\cos\theta)^m$ where $m$ is seen to take values between 5 and 9. The generality of this result can clearly be seen in equation (90) of Reference 15.

The terms of equation 3.16 express the relationship between the near and far field sound pressure level, which is seen to be dependent upon both $\theta$ and $\overline{M}_c$. For these lateral quadrupoles, writing the wave number $k = \omega/a_o$,

$$\frac{\overline{p_N^2}}{\overline{p_F^2}} = \frac{1}{(kr)^2}\left\{\frac{3(1-\overline{M}_c^2)^2}{(1-\overline{M}_c\cos\theta)^2} - \frac{6\overline{M}_c(1-\overline{M}_c^2)}{(1-\overline{M}_c\cos\theta)\cos\theta} + \frac{4\overline{M}_c^2}{\cos^2\theta}\right\}$$

$$+\frac{1}{(kr)^4}\left\{\frac{9(1-\overline{M}_c^2)^4}{(1-\overline{M}_c\cos\theta)^4} - \frac{18\overline{M}_c(1-\overline{M}_c^2)^3}{(1-\overline{M}_c\cos\theta)^3\cos\theta} + \frac{9\overline{M}_c^2(1-\overline{M}_c^2)^2}{(1-\overline{M}_c\cos\theta)^2\cos^2\theta}\right\}$$

(3.17)

Where the subscripts N and F denote near and far field components respectively. It can also be shown that for longitudinal (Reference 15) quadrupoles with their axes along the $x_3$ axis.

$$\frac{\overline{p_N^2}}{\overline{p_F^2}} = \frac{1}{(kr)^2}\left\{\frac{3(1-\overline{M}_c^{\,2})^2}{(1-\overline{M}_c\cos\theta)^2} - \frac{12\,\overline{M}_c(1-\overline{M}_c^{\,2})}{(1-\overline{M}_c\cos\theta)\cos\theta} - \frac{(4-9\,\overline{M}_c^2)}{\cos^2\theta}\right.$$

$$\left. + \frac{6\,\overline{M}_c}{\cos^3\theta} + \frac{1}{\cos^4\theta}\right\} + \frac{1}{(kr)^4}\left\{\frac{9(1-\overline{M}_c^{\,2})^4}{(1-\overline{M}_c\cos\theta)^4} - \frac{36\,\overline{M}_c(1-\overline{M}_c^{\,2})^3}{(1-\overline{M}_c\cos\theta)^3\cos\theta}\right.$$

$$\left. - \frac{6(1-9\,\overline{M}_c^2)(1-\overline{M}_c^2)^2}{\cos^2\theta(1-\overline{M}_c\cos\theta)^2} + \frac{12(1-3\,\overline{M}_c^2)(1-\overline{M}_c^2)\,\overline{M}_c}{\cos^3\theta(1-\overline{M}_c\cos\theta)} + \frac{(1-3\,\overline{M}_c^2)^2}{\cos^4\theta}\right\} \tag{3.18}$$

The variation of $\overline{p_N^2}/\overline{p_F^2}$ with convection Mach number $\overline{M}_c$, for the lateral quadrupole case calculated according to equation 3.17 for $kr = 0.25$, is shown in Figure 21b. Equation 3.18, for the longitudinal quadrupole, on the other hand, shows some inconsistencies, in particular, becoming negative through a considerable range of $\overline{M}_c$, $kr$, $\theta$. The same is true of equation 3.15 for the unconvected case. For this reason the validity of the quadrupole expressions is suspected although no errors have yet been found.

As discussed in paragraph 3.1.3, lateral quadrupole radiation as defined by equation 3.17 with the $x_3$ axis corresponding to the jet axis, is typical of the initial mixing region of a jet. Figure 21b, therefore, gives some idea of the magnitude of the near field amplifications which may be expected due to hydrodynamic fluctuations near the jet boundary, i.e., of the order of 30 dB. The particular profiles of these amplifications are the result of the complicated lobed patterns associated with the different terms in the equation. In reality, a somewhat random source orientation and disposition will obscure these patterns, although the amplifications would be expected to remain of the same order.

### 3.1.3 Correlation of Theory and Experiment for Subsonic Jet Noise

As previously discussed in Sections 1.0 and paragraph 3.1.1, Lighthill's $U^8$ law for law for the noise power of subsonic jets is now well substantiated experimentally

(see Figure 22 taken from Reference 37). Further, the directionality factor $(1 - \overline{M}_c \cos\theta)^{-5}$ explains to some extent the observed increase with nozzle velocity of the sound radiated at acute angles to the exhaust flow direction.

This factor taken no account of quadrupole type or orientation, it merely defines the effects of source motion. However, Lighthill points out that in the region of high shear alongside the laminar core, lateral quadrupoles will show preferred orientation with their axes normal and parallel to the jet axis. This is due to the effect of the mean rate of strain. Such quadrupoles exhibit directionality peaks at 45° and 135° to the jet axis, and convection emphasizes the peak at the acute angle (Figure 23a). However, in addition to these particular predominant sources, quadrupoles of different types and orientations will exist as a result of the fluctuating rates of strain and the other terms in $T_{ij}$. This causes a general smoothing of the directionality pattern due to the dominant lateral quadrupoles. A sketch of this effect is included in Figure 23a. Experimental corroboration for this result is to be found in the model jet results of Lee et al. (Reference 38) which are presented in Figure 23b. Directionality curves at the higher frequencies clearly show the two "humps" and it is the higher frequencies which are generated in the core region. Further downstream in the fully developed mixing region the mean shear is much reduced with the result that quadrupoles of both types will exist in more random orientation, thus, explaining the disappearance of the first "hump" in the low frequency curve of Figure 23b.

The convection effects included in the factor $(1 - \overline{M}_c \cos\theta)^{-5}$ will vary with radial positions in the flow. Davies, Fisher and Barratt (Reference 5) have measured in the high shear region, by hot wire anemometer correlation techniques, eddy convection velocities varying between 0.2 and 0.7 times the exhaust velocity. This variation will obviously have further effects upon directionality, although these are closely related to the notion that sound rays are refracted in "wind gradients", which of course, are very high in the shear region.

Jet temperature gradients also affect directionality through variations of the local speed of sound which again causes sound refraction. An increase in the speed of sound in the jet increases refraction causing directionality peaks to rotate outwards from the jet axis. This effect has been shown experimentally by Atvars et al. (Reference 39) who investigated the radiation from a point source inserted in a jet flow. Also, Lee et al. (Reference 38) collapsed experimental directivity data on a basis of a temperature-modified Strouhal number, suggesting the angle of peak directivity to be given as

$$\theta_{max} = 17 \log_{10} \left[ \frac{f\, d_E}{V_E} \cdot \frac{T_E}{T_o} + 2.1 \right] \text{ degrees}$$

The scatter of the data is considerable but the equation clearly expresses the trend.

Ribner (Reference 40) and Lighthill (Reference 36) use equation 3.7 to examine the axial distribution of sound power generation in a subsonic jet, basing their arguments on the experimental measurements of turbulence intensities in the various flow regions (References 4, 5, and 41). It has been shown that in the core region, typical root mean square velocities are constant and proportional to the jet exit velocity. Eddy dimensions (correlation length) increase with axial distance from the nozzle and in direct proportion to it. Downstream of the transition region, both the axial velocity and rms velocity fluctuations vary approximately inversely as axial distance.

Now the sound power per unit volume is given by the proportionality

$$\frac{dP}{dV} \propto \frac{V_e f^4 \overline{T^2}}{\rho_o a_o^5} \tag{3.7}$$

and in the core region,

$$T_{ij} \propto \rho v_i v_j \propto \rho U_E^2 ; \quad f \propto \frac{U}{\ell} \propto \frac{U}{x} ;$$

$$V_e \propto \ell^3 \propto x^3$$

so that

$$\frac{dP}{dV} \propto \frac{\rho_o U_E^8}{a_o^5 x}$$

but the volume is proportional to $x$ (for an annular section) and therefore,

$$\frac{dP}{dx} \propto \frac{\rho_o U_E^8}{a_o^5} \tag{3.19}$$

i.e., a constant along the core region.

In the fully developed mixing zone the mean centerline velocity $U$ is roughly proportional to $1/x$. Therefore,

$$\frac{dP}{dV} \propto \ell^3 \left(\frac{1}{x\ell}\right)^4 \left(\frac{1}{x}\right)^4$$

i.e., to $x^{-8} \ell^{-1}$

but the volume is proportional to $x^2$ (for a circular section) so that

$$\frac{dP}{dx} \propto x^{-6} \ell^{-1} \tag{3.20}$$

Although $\ell$ varies little until well downstream, around 20 diameters, it varies approximately as $1/x$ again beyond that point and

$$\frac{dP}{dx} \propto x^{-7} \tag{3.21}$$

This theoretical prediction, that in the core region the sound power per unit length is constant, and, in the fully developed downstream region, proportional to $x^{-7}$ is difficult to verify experimentally. Certainly the power does fall off rapidly downstream of the core tip, but sound pressure measurements near to the jet boundary suggest that the decay is less rapid than $x^{-7}$. Eldred et al. for example, (Reference 17) performed an extensive analysis of measurements of the near field noise of a turbojet exhaust taken by Howes and Callaghan (Reference 42). From considerations of source distributions and directionality they determined that the sound power distribution increases slightly with distance up to the core tip and beyond there decays more nearly as $x^{-3}$. This disagreement with the theory is explained as a result of the convection of turbulence downstream from the core region, but an alternative explanation, and one which is corroborated by other observations discussed below, is that induction near field effects increase the sound pressures close to the jet, giving rise to overestimations of sound power. Since near field effects increase with a decrease in frequency, at a given distance, the near field sound pressure increment will increase with distance from the nozzle. The near field amplifications are in fact proportional to $f^{-2}$ and $f^{-4}$ (see equations 3.17 and 3.18) and the frequency, f, varies approximately as either $1/x$ or $1/x^2$. Thus, the axial error in sound power could vary as powers of x between 2 and 8. This could easily explain the $x^{-4}$ discrepancy described above.

Based on the same measured turbulence properties, it is also possible to use equations 3.19 and 3.21 to estimate the form of the noise spectrum. It is assumed that each axial location of the jet is associated with a unique frequency, an assumption which although incorrect, is a reasonable approximation, since the frequency at which the peak level occurs changes with axial distance, in the core region at least. The assumptions that $f(x) \propto 1/x$ in the core region, and $f(x) \propto 1/x^2$ downstream, are retained and the spectrum is given by

$$\frac{d P}{d f} = \frac{d P}{d x} \cdot \frac{d x}{d f} \qquad (3.22)$$

Thus, from 3.19, 3.21, and 3.22, in the core region, $d P/d f \propto f^{-2}$ and downstream, $d P/d f \propto f^{2}$. In other words, at low frequencies the spectrum increases by 6 dB per octave and at high frequencies it decreases by 6 dB per octave. Figure 24 shows the envelope by many measured far field noise spectra, taken from Reference 49, plotted against the non-dimensional Strouhal number, compared with these theoretical slopes. The agreement is seen to be good in the light of the crude assumptions made.

Contrary to the assumptions made above, sound of a given frequency is generated throughout an extended region of the jet, although an axial position can be defined at which the power per unit length (in a given frequency band) reaches a maximum. Alternatively, a given "slice" of jet generates a finite spectrum of sound.

Support for the validity of the assumed relationships for the dependence of frequency on axial distance is illustrated in Figure 25, taken from Reference 17. This shows the frequency of the peak spectrum level, taken from the turbojet boundary sound pressure measurements of Reference 42 as a function of axial distance. A sharp change from the $1/x$ law is clearly seen to occur at the core tip although the exponent of the downstream decay is nearer to 2.5 than 2.0.

Since frequency is inversely proportional to distance, in the core region, it might be expected that the spectrum per unit slice would scale as a function of an "axial" Strouhal number with the constant length parameter $d_E$ replaced by $x$. Eldred, et al. (Reference 17) verify this, showing that the measured sound pressure level spectra measured at various points along the 10 degree jet boundary collapse when plotted against a modified Strouhal number $f x \ a_E/U_E \ a_o$.

Now, in the downstream region where $f \propto 1/x^2$ it might similarly be expected that an $x^2$ factor results, since the peaks of downstream spectra should occur at lower frequencies than those near the nozzle, but this is not the case, and Eldred, et al. found the puzzling result that, downstream, the spectrum is independent of axial distance. This could again be explained by near field effects. As axial distance is increased, boundary measurements are made at greater radial displacements from the probable source locations because of the expanding flow contours. This means that augmentation of the low frequency levels (small kr) will be greater at points nearer to the nozzle, effectively shifting the measured spectral peaks to lower frequencies. This will tend to oppose or nullify the shift in the radiated component predicted from the variations in turbulence frequencies. Such an effect is illustrated in Figure 26.

More difficult to explain is the excellent agreement found in Reference 17 between the sound power spectra calculated from sound pressure measurements taken either

at the jet boundary or in the far field of a turbojet engine. Near field effects would be expected to amplify low frequency sound pressure levels by increments in the order of 15 dB or more, at positions close to the jet. The technique for evaluation of the near field measurements was rather laborious, involving an equation to calculate the variation of the directionality of the radiated sound with both frequency and axial location. Briefly, initial estimates of the variations of angles of peak radiation were made from the correlations of the filtered outputs of two microphones spaced on a line parallel to the jet boundary. These angles were utilized, in combination with the measured sound pressure levels, to estimate the sound power radiated from each of a number of truncated conical segments of the exhaust stream. On the assumption that the axial variation of directivity is a function of $x/\lambda$, an iteration was performed, equating measured far field directivity indices to the integrated effects of successive approximations to the directivity functions for each segment, using a relationship of the form

$$\frac{\sum P_i \; D_i \; (f,\theta)}{\sum P_i} = F\,(f,\theta) \qquad (3.23)$$

Here, $P_i$ is the calculated power of the i-th segment, $D_i\,(f,\theta)$ is the directivity for the i-th segment, of the sound in the frequency band defined by f, and $F\,(f,\theta)$ is the far field directivity in the same band. Since this method includes no requirement to equate near and far field sound power, a comparison of the far field spectrum with that calculated from the boundary measurements in conjunction with the derived directivity functions, affords a check on the accuracy of the latter. Very close agreement was obtained, a finding which implies a complete absence of near field effects. This seems unlikely, and it is admitted that there are many possible sources of error. Among these, the fundamental assumption regarding the parameter $x/\lambda$ could be incorrect. Also, the iteration was performed using the individual segment power estimates based on the mean directionalities derived from space correlation measurements. The dangers of utilizing, for this purpose, the correlation coefficients measured in a sound field containing near field reciprocations and eddy convection effects are apparent.

## 3.2 The Noise of Supersonic Jets

When the pressure ratio across a jet nozzle exceeds the critical value of approximately 1.89, the jet can be classified as supersonic, because in some region of the exhaust, the flow Mach number will exceed 1.0. From an acoustic point of view a better definition of a "supersonic" jet would be one in which eddy convection velocities exceed the ambient speed of sound, for it is when this condition is reached that Lighthill's fundamental theories break down completely. Thus, aerodynamically subsonic jets whose exhaust gases are at high temperatures or are composed of gases which have a high speed of sound (e.g., helium) may be classified as "acoustically supersonic". For supercritical flows (i.e., jets with

$p_T/p_o > 1.89$) which are aerodynamically supersonic, additional complications are caused by the generation of shock waves within the flow which both modify the flow geometry and generate additional sound by independent mechanisms.

The flow characteristics of supersonic jets have been discussed in Section 2.0. It is apparent that downstream of the sonic point, the flow is essentially similar to the fully developed mixing region of subsonic jets, and will therefore retain similar acoustic properties. Upstream of this point however, the flow is characteristically different, and additional theory is required to explain its sound generation mechanisms. It is shown in Section 2.0 that the flow upstream of the sonic point can be divided into three distinct regions which are important in defining the exhaust structure. They are:

a) A supersonic laminar core;

b) A supersonic, turbulent annular core;

c) A subsonic turbulent annular mixing region.

For an ideally expanded jet these regions can be reasonably well defined and mean velocity contours can be mapped with a fair degree of accuracy. For an improperly expanded jet, compression, expansion and shock waves appear in the flow, producing distortions of the regional boundaries, which are difficult to predict.

Supersonic flow introduces many complications to the problem of analyzing sound generation, both theoretically and experimentally, and the majority of these are unsolved. These problems, together with the general properties of the noise field of supersonic jets, form the subject of this section.

### 3.2.1 Ffowcs Williams' Extension of Lighthill's Theory to Supersonic Flow

Before discussion the practical problem of noise prediction for a supersonic exhaust, it is necessary to examine the basic mechanisms of aerodynamic noise generation by supersonic flow. It is clear from a consideration of acoustic efficiency that some fundamental change takes place as its value falls from a $U^5$ dependency to a constant at very high speeds. Also, as discussed in Section 1.0, the general noise field of a rocket exhaust differs appreciably from that of a turbojet (see Figure 27) with the major noise producing region apparently located at some large distance downstream. Some of the observations are explained to some extent by an extension of Lighthill's basic theory due to Ffowcs Williams (Reference 3), which gives an exact solution for the peak noise radiation given by the singularity in Lighthill's equation 3.10 when $\cos\theta = 1/\overline{M}_c$.

Ffowcs Williams recognized that the limitation to Lighthill's solution was imposed by the assumption that the variation of retarded time within an eddy can be neglected. This assumption leads to the result that both the "emission time" and "emission volume"

of an eddy increase as the factor $(1 - \bar{M}_c \cos\theta)^{-1}$ It will be remembered that the emission time is the period during which a particular eddy generates sound which arrives at a field point simultaneously, and the emission volume is the source volume associated with this time period). Thus, when $\cos\theta = 1/\bar{M}_c$ the amplification due to eddy convection becomes infinite, clearly an impossible situation. The fault with Lighthill's assumption, of which he was aware, is that an eddy has a finite coherent lifetime and the decay of its character prevents an indefinite increase of the emission properties with $(1 - \bar{M}_c \cos\theta)^{-1}$.

Instead of expressing the mean square sound pressure as a function of the mean turbulence stress tensor within a correlated eddy, Ffowcs Williams (Reference 3) derived a relationship for the far field pressure autocorrelation in terms of the space-time turbulent stress-tensor correlation function. Thus, the square of equation 3.5 is replaced by an equation of the form*

$$B(\underset{\sim}{r}, t, \tau^*) \propto \frac{1}{a_o^4} \iint \frac{r_i r_j r_k r_\ell}{r^6} \frac{\partial^4}{\partial \tau^4} R_{ijk\ell}(\underset{\sim}{\eta}, \underset{\sim}{\Delta}, \tau)\, d\underset{\sim}{y}\, d\underset{\sim}{\Delta} \tag{3.24}$$

where

$$B(\underset{\sim}{r}, t, \tau^*) = \overline{p(\underset{\sim}{r}, t)\, p(\underset{\sim}{r}, t + \tau^*)}$$

$\underset{\sim}{y}$ is the turbulence position vector, $\underset{\sim}{\Delta}$ is a displacement vector such that

$$R_{ijk\ell} = \overline{T_{ij}(\underset{\sim}{y}, \bar{t})\, T_{k\ell}(\underset{\sim}{y} + \underset{\sim}{\Delta}, \bar{t} + \tau)}$$

where $\bar{t}$ is the value of the retarded time at station $\underset{\sim}{y}$ and $\tau$ is the difference in the retarded times between stations $\underset{\sim}{y}$ and $\underset{\sim}{y} + \underset{\sim}{\Delta}$.

The effects of eddy convection are studied by transforming the separation vector $\underset{\sim}{\Delta}$ of equation 3.24 to one which moves with the eddy, $\underset{\sim}{\lambda}$ where $\underset{\sim}{\Delta} = \underset{\sim}{\lambda} + a_o \underset{\sim}{\bar{M}}_c \tau$ ($\underset{\sim}{\bar{M}}_c$ is the eddy convection Mach number relative to $\underset{\sim}{y}$). Specifying a moving axis correlation tensor,

$$P_{ijk\ell}(\underset{\sim}{y}, \underset{\sim}{\lambda}, \tau) = R_{ijk\ell}(\underset{\sim}{y}, \underset{\sim}{\Delta}, \tau)$$

it is then shown that equation 3.24 can be written in the form

* In fact, reference 3 includes consideration of an aircraft flight Mach number, but the equations presented here have been simplified to the static case.

(3.25)

$$B(\underset{\sim}{r}, t, \tau^*) \propto \frac{1}{a_o^4} \iint \frac{r_i r_j r_k r_\ell}{r\left|r - \underset{\sim}{\overline{M}}_c \cdot \underset{\sim}{r}\right|^5} \frac{\partial}{\partial \tau^4} P_{ijk\ell}(\underset{\sim}{y}, \underset{\sim}{\lambda}, \tau)\, d\underset{\sim}{\lambda}\, d\underset{\sim}{y}$$

which is evaluated with

$$\tau = \frac{a_o \tau^* r + \underset{\sim}{\lambda} \cdot \underset{\sim}{r}}{a_o (r - \underset{\sim}{\overline{M}}_c \cdot \underset{\sim}{r})}$$

The factor $\left|r - \underset{\sim}{\overline{M}}_c \cdot \underset{\sim}{r}\right|^{-5}$ in equation 3.25 is synonymous with $(1 - \overline{M}_c \cos\theta)^{-5}$ in Lighthill's equation 3.10 which causes the singular condition at supersonic eddy convection velocities, namely when r approaches $\underset{\sim}{\overline{M}}_c \cdot \underset{\sim}{r}$. However, in this case the correlation function time derivative also approaches zero and the solution remains finite. The radiation emitted in this case takes the form of eddy Mach waves which are analogous to the Mach waves generated by thin supersonic airfoils.

This type of sound generation mechanism was first described, and so named by Phillips, (Reference 43). It has already been explained (Section 3.1.1) how at low speeds quadrupole acoustic efficiencies are low due to the near-cancellation of the opposing source elements. As the component of the convection velocity in the direction of the observer increases, cancellation becomes less complete, enhancing the radiation in that direction. This process is obviously subject to the limitation that the efficiency cannot increase beyond that of simple sources, where there is no cancellation. This is the situation which arises when the convection Mach number is unity in the direction of the observer who then "hears" the quadrupole as four simple sources. At convection Mach numbers higher than unity, the constitutent sources are heard in reverse time, (i.e., the sound from "aft" components reaches the observer before that from the "forward" components) and there is once again some cancellation. This cancellation increases with further increases in velocity with a consequent decrease in acoustic efficiency.

Thus, the noise from a supersonic turbulent stream is highly directional, having a strong peak in the direction of greatest acoustic efficiency which is the Mach Angle, $\theta_M = \cos^{-1}(1/\overline{M}_c)$.

The simplified physical description of Mach waves accounts for the theoretical findings of Reference 3. Ffowcs Williams was able to show that, near the singularity in equation 3.25, the volume integral can be reduced to a surface integral by integrating in the direction of $\underset{\sim}{r}$ giving

$$\int \frac{\partial^4}{\partial \tau^4} P_{ijk\ell}\,(\underset{\sim}{y}, \underset{\sim}{\lambda}, \tau)\, d\underset{\sim}{\lambda}$$

$$\propto \left(\frac{r - \underset{\sim}{\overline{M}}_c \cdot \underset{\sim}{r}}{r}\right)^5 \iint_s \frac{\partial^4}{\partial \lambda_r^4} P_{ijk\ell}\,(\underset{\sim}{y}, \underset{\sim}{\lambda}_s, \sigma)\, d\sigma\, d\underset{\sim}{\lambda}_s \tag{3.26}$$

where the suffix $r$ denotes differentiation with respect to the component of $\underset{\sim}{\lambda}$ in the $\underset{\sim}{r}$ direction, $\sigma$ is the time variable of integration, and $d\underset{\sim}{\lambda}_s$ is an area element in the plane normal to the direction of Mach wave emission defined by

$$a_o\, \tau^* r + \underset{\sim}{r} \cdot \underset{\sim}{\lambda}_s$$

Combining equations 3.25 and 3.26 leads to

$$B(\underset{\sim}{r}, t, \tau^*) \propto a_o \iint_s \frac{r_i r_j r_k r_\ell}{r^6} \cdot \frac{\partial^4}{\partial \lambda_r^4} P_{ijk\ell}\,(\underset{\sim}{y}, \underset{\sim}{\lambda}_s, \sigma)\, d\sigma\, d\underset{\sim}{\lambda}_s \cdot d\underset{\sim}{y} \tag{3.27}$$

Immediately apparent in this equation for Mach wave emission is that it does not involve the infinity at points where $r - \underset{\sim}{\overline{M}}_c \cdot r = 0$, and it can therefore be used to define acoustic intensity at those points. It should also be noted that the solution is independent of retarded time differences.

Turbulence correlation functions have not, of course, been measured in supersonic flow, but by assuming a hypothetical, but realistic form for the correlation tensor in equation 3.25, (i.e., one where turbulent scales are constant while frequency varies directly with velocity) Ffowcs Williams (Reference 3) was able to demonstrate that the effect of eddy convection on the radiated sound intensity is accounted for by a factor which is proportional to

$$\left\{(1 - \overline{M}_c \cos\theta)^2 + \left(\frac{\omega \ell}{a_o}\right)^2\right\}^{-5/2} \tag{3.28}$$

In particular, the acoustic intensity of unit volume of turbulence, the low-speed form of which, due to Lighthill, is given as equation 3.10 is proportional to

$$\frac{V_e f^4 \overline{T^2}}{\rho_o a_o^5} \left\{ (1 - \overline{M}_c \cos\theta)^2 + \left( \frac{\omega \ell}{a_o} \right)^2 \right\}^{-5/2} \qquad (3.29)$$

Lighthill (Reference 36) gives a particularly illuminating physical explanation for the presence of the additional term inside the brackets at positions associated with the directional peak.

Figure 28a represents the progression of a non-decaying eddy with time for various convection velocities and it can be seen that both emitting volume and emission time increase to infinity as $\overline{M}_c \cos\theta$ approaches 1 (i.e., as the slope of the lines representing eddy motion approach the slope of the second signal). However, as discussed previously, this notion of a moving eddy is unrealistic and account must be taken of the finite lifetime of the eddy. This is done in Figure 28b which is similar to Figure 28a but represents the real eddy by curves of constant correlation. This clearly shows that for low convection velocities, when $\overline{M}_c \cos\theta << 1$ the emission volume and time differences are still increased approximately by the factor $(1 - \overline{M}_c \cos\theta)^{-1}$. However, now, when the previous singular condition is reached, both remain finite. In fact, both are increased by the factor $a_o/\omega\ell$.

Using equations 3.25 and 3.27 it is possible to perform a crude dimensional analysis of the sound radiation by supersonic jets. This must be based upon the assumption that the stress tensor $T_{ij}$ remains proportional to $\rho_E U^2_E$, in the lack of any experimental evidence.

In equation 3.25 the correlation tensor $P_{ijk\ell}$ is dimensionally similar to $\rho_E^2 U_E^4$ and the time derivative can be obtained by dividing by a typical time scale $d_E/U_E$ giving

$$\frac{\partial^4}{\partial \tau^4} P_{ijk\ell}(\underset{\sim}{y}, \underset{\sim}{\lambda}, \tau) \quad \propto \quad \frac{\rho_E^2 U_E^8}{d_E^4}$$

The integrations over $\underset{\sim}{\lambda}$ and $\underset{\sim}{y}$ are both represented by multiplying by the volume scale, $d_E^3$. Thus, from equation 3.25, the acoustic intensity, which is proportional to $B(\underset{\sim}{r}, t, 0)/\rho_o a_o$ is given by the proportionality

$$I \quad \propto \quad \frac{\rho_E^2}{\rho_o} \frac{U_E^8}{a_o^5} \frac{d_E^2}{r^2} (1 - \overline{M}_c \cos\theta)^{-5} \qquad (3.30)$$

which is the previously derived result (equation 3.10) for low speed flows.

At very high velocities, where $\overline{M}_c \cos\theta >> 1$, this approaches the asymptotic form

$$I \propto \frac{\rho_E^2}{\rho_o}\left(\frac{d_E}{r}\right)^2 U_E^3 \cos^{-5}\theta \qquad (3.31)$$

where it is clear that the sound generation efficiency is much reduced and the eighth power law has been replaced by a cube law.

At and near the singularity inherent in equation 3.30, when Mach wave emission is predominant, the dimensional analysis is applied to equation 3.27. In this case the differentiation with respect to $\lambda$ is effected by dividing by the typical dimension $d_E$; the integration with respect to time, $\sigma$, by multiplying by the time scale $d_E/U_E$; and over $\lambda_s$ by multiplying by a typical area $d_E^2$. Thus, from equation 3.27 the peak intensity at the Mach angle $\theta_M$ is

$$I_{peak} \propto \frac{\rho_E^2}{\rho_o}\left(\frac{d_E}{r}\right)^2 U_E^3 \qquad (3.32)$$

which is very similar to equation 3.31 for quadrupole radiation at high speeds, again showing dependence on the cube of velocity. Since the mechanical power of a jet is also proportional to the third power of its velocity, both equations 3.31 and 3.32 imply that the sound generation efficiency of a jet is constant in the regions where convection velocities approach and exceed the ambient speed of sound.

The dimensional relationship 3.32 can also be derived from equation 3.29 and this description is probably more meaningful, physically. At the Mach wave condition, $1 - \overline{M}_c \cos\theta = 0$ and equation 3.29 becomes

$$\frac{V_e\, f^4 \overline{T^2}}{\rho_o\, a_o^5} \cdot \frac{a_o^5}{(\omega \ell)^5} \qquad (3.33)$$

Again extending subsonic results to the supersonic regime, assuming the basic property of turbulence, which Davies, Fisher, and Barratt (Reference 5) found experimentally, that the product of frequency and length scale, $\omega \ell$, measured in the moving frame, is roughly proportional to the rms turbulent velocity, 3.33 gives the same result as 3.32.

### 3.2.2 The Near Field of Supersonic Jets

Section 3.1.2 describes an extension of Lighthill's subsonic flow analysis which takes account of the acoustic near-field effects which are characteristic of multipole sources. Figure 21b gives some indication of the magnitude of the near-field sound pressure amplification as the eddy convection velocity increases to the value 0.9. However, equations 3.17 and 3.18, from which these curves were derived suffer the same limitations as Lighthill's basic result (equation 3.10) for convected eddies, in that the neglect of retarded time variations leads to the singularity at the Mach angle, $\theta_M = \cos^{-1}(1/\bar{M}_c)$, for supersonic flow. It has been found experimentally that the simple $U^8$ law for total acoustic power (equation 3.8) maintains its accuracy up to sonic convection velocities, and Lighthill has suggested (see paragraph 3.1.1) that this is because the sound power amplification caused by the integrated effect of the directionality term $(1 - \bar{M}_c \cos\theta)^{-5}$ is offset by the reductions in the rate of growth of turbulent velocity fluctuations with mean velocity. However, whether or not a similar argument would apply to the near field sound pressures is open to question. Equations 3.17 and 3.18 show that pressure amplifications in the near field are elaborate functions of $\bar{M}_c$ and $\theta$, whereas Lighthill's compensating mechanism would only seem to hold if these corrections were independent of velocity.

At very high velocities, at angles where $\bar{M}_c \cos\theta \gg 1$, equation 3.17, which defines the ratio of near field induction sound pressure level to the radiated component, for the $x_1$, $x_3$ lateral quadrupoles, approaches the asymptotic form

$$\frac{\overline{p_N^2}}{\overline{p_F^2}} \rightarrow \frac{1}{(kr)^2} \quad \frac{\bar{M}_c^2}{\cos^2\theta} \tag{3.34}$$

and so again assuming $k \propto f \propto U/\ell$, and $M_c \propto U$

$$\frac{\overline{p_N^2}}{\overline{p_F^2}} \propto \left(\frac{\ell}{r}\right)^2 \tag{3.35}$$

It is interesting to note that the term in $(kr)^{-4}$ disappears and that the remainder is independent of velocity. The equivalent asymptotic proportionality for the $x_3$ longitudinal quadrupole, on the other hand, retains both terms and

$$\frac{\overline{p_N^2}}{\overline{p_F^2}} \rightarrow \frac{6\,\bar{M}_c^2}{(kr)^2\cos^3\theta} + \frac{60\,\bar{M}_c^4}{(kr)^4\cos^4\theta} \tag{3.36}$$

However, at distances from the flow which are small enough for either term to have any significance, the second of these will dominate and therefore, with the previous assumption,

$$\frac{\overline{p_N^2}}{\overline{p_F^2}} \propto \left(\frac{\ell}{r}\right)^4 \qquad (3.37)$$

From these two results, equations 3.35 and 3.37, we can make the following observations, bearing in mind that the result given in equation 3.36 can only be tentative in view of the possible errors mentioned in paragraph 3.1.3.

For the case of a supersonic jet, the $x_1$, $x_3$ lateral quadrupoles are those sources which may be expected to predominate in the highly sheared mixing layer adjacent to the core, as discussed in paragraph 3.1.1, whereas longitudinal quadrupoles will mainly be confined to the downstream regions. Thus, in the sound field adjacent to the initial mixing region of a highly supersonic jet, at angles less than the Mach angle, where $\overline{M}_c \cos >> 1$, the induction near field effects may be expected to decay as $(\ell/r)^2$. Extending the assumptions made in the dimensional analysis of paragraph 3.1.3 for subsonic jets, namely that $\ell \propto x$ in the initial mixing region, the decay is proportional $(x/r)^2$. Thus, the decay rate obviously decreases with distance from the nozzle. Downstream, equation 3.37 for longitudinal quadrupoles would be more appropriate and the near field decay is apparently more rapid, being proportional to the fourth power of $\ell/d$. However, in this region, making the crude approximation that $\ell \propto x^2$ (see paragraph 3.1.3) the near field increment will vary as $(x^2/r)^4$ and since $x$ is large in this area the near field is likely to be important over an extended area. But it is important to note that the eddy convection velocities in this region will be much less than in the initial shear layer, and thus the range of $\theta$ in which $\overline{M}_c \cos\theta$ will be significantly greater than unity, i.e., the range for which the dimensional reasoning which resulted in equation 3.37 is valid, is much reduced. In fact, since the mean velocity decays roughly as $x^{-1}$ beyond the tip of the laminar core the region of application is probably very limited.

In the region of the singularity, when $\overline{M}_c \cos\theta$ approaches unity, the near field relationship of equations 3.18 and 3.17 break down completely. A correlation analysis similar to that of Reference 3 which takes account of the important retarded time differences would be formidable indeed, if not intractable. However, in the immediate vicinity of the singularity, which corresponds to Mach wave emission, the concept that quadrupoles degenerate into their component simple sources, implies a large reduction in near field effects. Since this condition is believed to be associated with a large intensity peak in the radiated sound, it seems likely that aggregate near field effects in the vicinity of the core region are small.

### 3.2.3 Correlation of Theory and Experiment for Supersonic Jet Noise

The majority of noise problems encountered during the operation of turbojet engines and rockets have been concerned with subjective and community response to noise, and for this reason there exists, at the present time, considerable quantities of experimental data on the far field sound pressures, overall power and spectra generated by the exhausts of the two types of propulsion engines. The acoustic near field, on the other hand, is normally only of interest to structural designers, both of the flight hardware and support facilities, and has only relatively recently become a practical problem with the advent of very high power engines. Consequently, there is a noticeable lack of near field acoustic measurements for both turbojet and rocket exhausts. The limited data that exist, are fragmentary and generally poorly correlated with important exhaust parameters and the associated far field. More importantly, there is a large gap in acoustic measurements, both near and far field, for the intermediate range of supersonic exhaust velocities existing between the sonic velocities of the turbojet, which normally lie around 2,000 feet per second, and those of the rocket engine which reach values as high as 10,000 feet per second at nozzle Mach numbers in excess of 3.

So little is known about the noise generation mechanisms of a supersonic exhaust, that the very basic problem of which region of the exhaust stream is the predominant noise source remains unresolved. The immediate noise field of a rocket differs appreciably from that of a turbojet as Figure 27, taken from Reference 13, clearly shows. Sound pressure contours such as this are typical of rocket measurements and strongly suggest that the bulk of the sound is generated in some region well downstream of the nozzle, as much as 20 or 30 diameters away. This observation would seem contrary to the well established fact that noise radiation increases rapidly with velocity, whereas typical mean velocities in this downstream region are considerably less than those in the initial mixing region. Ffowcs Williams' basic theoretical result, expressed in dimensional form as equation 3.32 suggests that the condition of Mach wave emission, which will predominate in the region adjacent to the core where eddy convection velocities are high, forms a particularly intense and highly directional source of sound. Shadowgraph pictures of the acoustic radiation from this part of the jet, of which Figure 1 is a particular example, support the view, if the intensity of the projected wave image is any guide to acoustic intensity. The acoustic Mach number $\overline{M}_E$ of this jet is approximately 2.9 and the Mach wave inclination corresponds to eddy convection velocities of $M_c = 2.2$ which are, therefore, 0.76 times the jet exit velocity. Similar shadowgraphs in References 23 and 50 show intense radiation from a region near the nozzle lip, which it is tempting to associate with Mach wave emission. However, in both these instances the corresponding eddy convection velocities implied are almost equal to the nozzle velocity and it is difficult to believe that significant eddies will move at such high speeds. Also the fact that the radiation is confined to such a small extent of the flow tends to lessen the likelihood that it is in fact Mach wave emission. In this event, the source of this noise is a further puzzle. However, in every case, the shadowgraphs give the impression that the highly directional

sound from the supersonic region is more intense than the radiation from other regions of the exhaust stream. The reason why this sound field is not evidenced in the acoustic measurements is obscure. One possibility is that their energy is confined to frequencies which are highly ultrasonic and outside the range of the microphones. Such frequencies would be rapidly attenuated within a short distance of the jet. Some evidence that this may be the case can be found in the shadowgraphs of Reference 50, which show an increase in the spacing of the Mach waves with distance from the jet.

Since the evidence, which leads to the supposition that the major noise is created downstream, is based upon sound pressure measurements made close to the flow boundaries, it is quite conceivable that the discrepancy between theory and practice is entirely due to induction near field effects. As in the case of the turbojet results which show some anomalies (see paragraph 3.1.3), sound pressure augmentation due to near field effects will increase with distance from the nozzle. However, in the case of a rocket the variation of these effects along the jet boundary is likely to be much greater. The peak intensity adjacent to the core is associated with the Mach wave radiation which, as discussed in paragraph 3.2.2 has reduced near field complications. At radiation angles other than the Mach angle the quadrupole near field effects apply, decaying as $(kr)^{-2}$ and $(kr)^{-4}$ at angles greater than $\cos^{-1}(1/\overline{M}_c)$ and as $(d_E/r)^{-2}$ where $\overline{M}_c \cos\theta$ is significantly greater than unity. However, the radiation component at these other angles is small compared to the peak emission, and the corresponding near field effects may also be expected to be relatively small. In contrast, at large distances downstream, both typical frequencies and eddy convection velocities become much lower and the quadrupole near field terms are undoubtedly large. Figure 21b shows that near field sound pressures can exceed their associated radiation components by as much as 20 to 30 dB, at moderate distances from the flow boundaries. Such effects could obviously account for a very large increase in the apparent intensity measured at such points.

Unfortunately, although some support for such near field effects can be found in the correlation measurements of Reference 51, it is difficult to justify crude reasoning of this kind. A complete lack of information on the characteristics of the turbulence in a supersonic jet, together with the unknown effects of the complex shock structure which is inevitably present in rocket flow, make the foregoing arguments highly speculative. Nevertheless, the theory does facilitate an understanding of some of the experimental observations and, in its light, the basic properties of the acoustic field, namely its overall power, frequency spectrum and directionality, each of which has an important bearing on the near field pressures, can now be discussed.

Figure 22 shows an experimental curve of sound power per unit nozzle area for exhaust velocities ranging from low subsonic Mach numbers for small model jets to values in excess of 3, for rockets. The obvious reduction in the exponent of the velocity dependence at velocities above 2,000 feet per second is apparent,

and both the $U^8$ law and $U^3$ laws, predicted by theory below about 2,000 feet per second and above approximately 3,000 feet per second respectively, are included for comparison. Experiment has shown that the acoustic efficiency of rocket exhausts is approximately constant and equal to 0.006 times the mechanical power of the jet stream. Since the latter is proportional to $U^3$, so also must be the acoustic power.

Since the theory suggests that acoustic efficiency is constant for eddy convection velocities in excess of approximately 1.5 times the ambient sound speed, and if the eddy convection velocities are assumed to be approximately half the jet center line mean velocity, then a considerable length of the exhaust, as much as 50 diameters in the case of rockets, should be predicted to generate sound at constant efficiency. This result is in good agreement with observation (Reference 10). The simple Strouhal number frequency parameter $fU_E/d_E$ which gives an excellent collapse of sound power spectra for subsonic jets is found to be completely invalid for rocket noise. It is found that the spectrum peak in fact occurs near a frequency given by $a_o/d_E$, i.e., independent of velocity. Potter and Crocker (Reference 13) collapsed various sets of rocket data against a modified Strouhal number,

$$S = \frac{f D_c}{a_o}$$

where $D_c = D_t p_s/p_o$, $D_t$ is the nozzle throat diameter, $p_s$ is the static pressure at the throat and $p_o$ is the ambient pressure. This parameter obviously changes more slowly than $fV_E/d_E$. This observation is explained to some extent by the Mach wave theory of Reference 3, where Ffowcs Williams shows that at the Mach wave emission condition, all frequencies in the turbulence contribute to the acoustic radiation. In the case of subsonic flow, or at angles well removed from the Mach angle in supersonic flow, only a limited range of small wave number components of the turbulence generate the sound. Thus, Mach wave radiation can be expected to exhibit a much wider frequency spectrum which would tend to become independent of speed. However, the typical frequencies of this sound, which come mainly from the high velocity initial mixing region, should be relatively high, whereas the observed approximate peak frequency value, $a_o/d_E$, is considerably lower than would be estimated by turbojet prediction methods which give a spectrum peak around $f = 0.25\ V_E/d_E$.

The comparison of the noise contours of jet and rocket engines in Figure 27 demonstrates the increased angles between the jet axis and the direction of peak radiation in the rocket case. This angle further increases with velocity, and could be the result of two factors. The first is that rocket exhausts are very hot, and consequently radiation angles will be increased by refraction. The second is that the Mach angle increases with increased velocity, so that a predominance of Mach wave radiation would explain the observed directionality.

## 3.3 Shock Noise

As discussed in Section 1.0 there are three basic noise producing mechanisms in a supersonic jet. Sections 3.1 and 3.2 dealt with two of these, namely turbulence noise and Mach waves, the latter being a special case of turbulence noise. The third arises in the presence of the standing shock pattern, which is very difficult to avoid in a high velocity jet, and is here loosely termed "Shock Noise". The generation of the shock patterns is discussed in detail in Section 2.3. These shock waves react with the turbulence in the jet mixing region to generate noise.

Under certain circumstances this shock noise becomes particularly intense and is known as "screech". When it occurs, "screech" is the most efficient sound generating process encountered in jet flow, as much as 10 percent of the flow energy being converted to sound. It is caused by a resonant coupling between oscillations in the cellular shock structure and the generation of fluid disturbances at the nozzle lip. The interaction between the oscillating compression shock and the disturbance radiates pressure waves which reach the nozzle and there generate further disturbances. This phenomenon has been extensively studied (see for example References 44 and 45, but since it only arises for very high supercritical pressure ratios it is not likely to occur during the flight phases of rocket vehicle operation which are critical from an acoustic standpoint, i.e., at low velocities, on or near to the ground. For this reason, attention will be confined here to the actual process by which sound is generated due to the convection of turbulent eddies through stationary shock waves.

It is a well known fact that the passage of turbulence through the shocks in a jet generates sound. Shadowgraph pictures of supersonic jet flow clearly show what appear to be strong, highly localized acoustic sources associated with the standing shock pattern. Reference 23 presents such shadowgraphs of a small $M = 2.5$ jet and includes a crude analysis which demonstrates, by a consideration of sound propagation and refraction effects, that the origin of each of a number of apparently omnidirectional sound fields is most probably the precise point where a standing compression shock penetrates the turbulent mixing region.

Theoretical studies of shock interaction noise have been made by Ribner (References 46 and 47). Kovasznay (Reference 48) demonstrated that disturbances in supersonic flow fall into three categories, identified as three fundamental modes, vorticity, entropy, and sound. Input of any one of these modes into a shock generally gives rise to all three modes behind the shock. Turbulence, of course, is represented by the vorticity mode.

Now, if the phase velocity of the input disturbances along the shock is greater than some critical value, then the pressure disturbances created behind the shock can propagate as acoustic radiation. If the phase velocity, however, is less than this value, then no sound is radiated and a decaying pressure field is generated.

Ribner, Reference 47 indicates that the near field mean square pressure at distance r from the interaction can be written in the form

$$\frac{\overline{p^2(r)}}{p_o^2(r)} \propto \frac{1}{m^2} \cdot e^{-f(M)kr} \cdot \frac{\overline{u^2}}{U^2} \qquad (3.38)$$

where m is the ratio of the mean velocities upstream and downstream of the shock (and also $m = (\gamma + 1) M^2 \{ 2 + (\gamma - 1) M^2 \}^{-1}$) where M is the upstream Mach number, $\overline{u^2}/U^2$ is the turbulence intensity, and $p_o$ is the static pressure at r. The sound pressure decays exponentially with kr, and f (M) is given as

$$\sqrt{\frac{|1 - M_N^2|}{1 - M^2}}$$

where $M_N$ is the Mach number component normal to the shock.

Ribner's theory is based upon a very simplified model of a single frequency inclined shear wave impinging upon an infinite plane shock and it is not claimed that equation 3.38 which is a crude approximation to Ribner's result gives any more than a guide to parameters which are important. The real situation in a supersonic jet is extremely complicated. The shock front forms a complex curved surface (see Figure 10) and since it exists in a region of high velocity shear, is of variable strength. In addition, the shock is subjected to all three disturbance modes, each of which can be expected to be of a particularly high level. However, Section 2.0 outlines methods by which the shock pattern can be estimated, which can at least provide information as to the location of shock noise sources and to coordinate experimental work which will help resolve this problem.

# 4.0 EXPERIMENTS TO ESTABLISH METHODS FOR THE PREDICTION OF THE NEAR NOISE FIELD OF SUPERSONIC JETS.

The preceding sections of this report have described what is known about supersonic jet flow and the various processes of noise generation which occur within it. It has been made fairly clear that we know very little about either, or at least, that our knowledge is inadequate for the purposes of predicting all but the very broadest details of the noise field. It has been shown that the noise generation mechanisms are very complex, particularly for the case of a typical rocket exhaust with its highly elaborate flow structure, and although current theory explains some of the observed features of the noise field, they are of limited application to the practical problem of near-field noise prediction.

A useful prediction method should be able to specify the sound pressure level contours around the exhaust stream from details of the nozzle exit flow conditions and the ambient atmosphere. As stated in Section 1.0 the problems associated with actual operational complications such as clustered nozzles and exhaust deflection are considerable, and, in the light of the current state-of-the-art, it is recommended that attention be confined, for the present, to those of a free jet exhausting into a quiescent atmosphere.

Assuming normal atmospheric conditions, the nozzle flow variables, which are likely to exercise influence on the turbulent mixing processes, and thus the noise, of a supersonic jet, are its velocity, Mach number, temperature, density, static pressure distribution, ratio of specific heats and molecular weight. Of these, the velocity is the most important since it has been conclusively shown that the sound power varies as a high power of the velocity. Given these quantities, it might be expected that the entire exhaust flow could be calculated. However this is not so, and it has been explained that the main reason for this inability is the almost complete lack of knowledge of the turbulence generating processes in supersonic flow, which stems from the lack of measuring tools. Fortunately this problem is not too serious because rocket engines, for which the prediction methods are desirable, are basically similar in their exhaust gas composition, so that flow dimensions can be interpolated or extrapolated from available data with reasonable confidence. Section 2.0 of this report presents evidence of flow similarity and shows an empirical method by which the mean flow properties of an air jet can be estimated.

Once flow similarity relationships have been established, then it is a relatively straightforward matter to apply these to the problem of scaling the acoustic characteristics, as has been convincingly demonstrated for subsonic jets (Paragraph 3.1).

The immediate task, to which attention whould first be turned, is to achieve the ability to predict the near noise environment of a jet of known flow properties.

Towards this end, this section outlines a comprehensive experimental program, suitable for execution in the Marshall Space Flight Center jet flow facilities, which is aimed to provide the vital data which is lacking at the present time. The initial phase of this program is described in detail in Appendix C.

Previous theoretical and experimental work, which has been reviewed in Section 3.0, gives insight into the nature of the near sound field. Based on this knowledge the following assumptions are made.

a) That the jet stream can be represented by an acoustic model consisting of a finite number of uncorrelated, discrete, sound sources distributed along its axis.

b) That each source can be ascribed a spectrum, a near field function, and a directivity.

In order to use this model to predict near field noise contours we must determine the location of the N sources, and their properties as defined in (b). This can be done experimentally for a particular jet, by making some further assumptions and by correlating the sound pressures in the vicinity of the jet by a method which is developed below.

Consider the far field radiation from a simple source of power P, frequency f. At a radius r from the source, the pressure amplitude is $(\rho_o a_o P/2\pi r^2)^{1/2}$, and the instantaneous sound pressure can be written

$$p(r) = \sqrt{\frac{\rho_o a_o P}{2\pi r^2}} \cdot \cos 2\pi f t \qquad (4.1)$$

and at radius $r + \Delta r$ as

$$p(r+\Delta r) = \sqrt{\frac{\rho_o a_o P}{2\pi (r+\Delta r)^2}} \cdot \cos 2\pi f \left(t - \frac{\Delta r}{a_o}\right) \qquad (4.2)$$

Thus the covariance of the two pressures is

$$\overline{p(r)\,p(r+\Delta r)} = \lim_{T\to\infty} \frac{1}{T}\int_0^T \frac{\rho_o a_o P}{2\pi r (r+\Delta r)} \cdot \cos 2\pi f t \cdot \cos 2\pi f \left(\frac{t-\Delta r}{a_o}\right) dt =$$

$$= \frac{\rho_o a_o P}{4\pi r (r+\Delta r)} \cdot \cos k\Delta r \qquad (4.3)$$

where the wave number $k = 2\pi f/a_o$ .

Now if the point source radiates random frequency sound of constant power spectral density $w(f)$, within the bandwidth $\Delta f$, equation (4.3) becomes

$$\overline{p(r)\,p(r+\Delta r)} = \frac{\rho_o a_o w(f)}{4\pi r (r+\Delta r)} \int_{f-\frac{\Delta f}{2}}^{f+\frac{\Delta f}{2}} \cos \frac{2\pi f}{a_o}\, \Delta r\, df =$$

$$= \frac{\rho_o a_o w(f)}{4\pi r (r+\Delta r)} \left(\frac{a_o}{\pi \Delta r}\right) \cos\left(\frac{2\pi f \Delta r}{a_o}\right) \sin\left(\frac{\pi \Delta f \Delta r}{a_o}\right) \qquad (4.4)$$

Introducing a time delay $\Delta t$ into the cross correlation it can further be shown that the space-time covariance is

$$\overline{p(r,t)\,p(r+\Delta r,\, t+\Delta t)} = \qquad (4.5)$$

$$= \frac{\rho_o a_o w(f)}{4\pi r (r+\Delta r)} \cdot \frac{1}{\pi\left(\frac{\Delta r}{a_o} - \Delta t\right)} \cos 2\pi f\left(\frac{\Delta r}{a_o} - \Delta t\right) \sin \pi \Delta f \left(\frac{\Delta r}{a_o} - \Delta t\right)$$

When $\Delta t = \Delta r/a_o$, i.e., the time increment taken for sound to travel the distance $\Delta r$, equation 4.5 reduces to

$$\overline{p(r,t)\,p(r+\Delta r,\, t+\Delta t)}_{(\Delta t = \Delta r/a_o)} = \frac{\rho_o a_o w(f)\,\Delta f}{4\pi\, r (r+\Delta r)} \qquad (4.6)$$

which is also the maximum value of the cross-covariance. Thus, if the signals from two microphones at $r$ and $r+\Delta r$ are cross correlated with a variable time

delay, a curve similar to that sketched in Figure 29 will be obtained. From its peak value, at $\Delta t = \Delta r/a_o$, given by equation 4.6, the source power, $w(f)\Delta r$, is easily derived.

Alternatively, if the sound source has a broadband spectrum, its power in a given narrow frequency band, assuming it to be constant within that band, may be measured similarly by filtering the microphone signals before correlating them.

Before this technique can be used to determine the strength of a "source" within a jet exhaust, we must consider not a uniform point source but one which has both near and far sound fields, each with different directional characteristics. The sound pressure of such a source for a single frequency whose radiation is axially symmetric, can be written

$$p(r,\theta) = \frac{A}{r}\left[\alpha(\theta)\cos 2\pi f t + q(r)\beta(\theta)\cos(2\pi f t + \phi)\right] \qquad (4.7)$$

Where $A/r$ is the amplitude of the radiative component, $A \cdot q(r)$ is the amplitude of the non-propagating component (an unknown function of r), $\alpha(\theta)$ and $\beta(\theta)/r$ are the respective directivity factors, and $\phi$ is a random phase angle which decorrelates the two terms. At the point $(r + \Delta r, \theta)$ the pressure is

$$p(r+\Delta r,\theta) = \frac{A}{(r+\Delta r)}\left[\alpha(\theta)\cos 2\pi f\left(t - \frac{\Delta r}{a_o}\right) + q(r)\beta(\theta)\cos(2\pi f + \phi + \psi)\right] \qquad (4.8)$$

where $\psi$ is some unknown phase angle.

Following equation 4.5, considering now a random source and introducing a time delay $\Delta t$, it is found that the cross-covariance of the two pressures becomes

$$\overline{p(r,\theta,t)\,p(r+\Delta r,\theta,t+\Delta t)} \qquad (4.9)$$

$$= \frac{\rho_o a_o \omega(f)}{4\pi r(r+\Delta r)}\left[\alpha^2(\theta)\,\frac{1}{\pi\left(\frac{\Delta r}{a_o} - \Delta t\right)}\cos 2\pi f\left(\frac{\Delta r}{a_o} - \Delta t\right)\sin\pi\Delta f\left(\frac{\Delta r}{a_o} - \Delta t\right)\right.$$

$$\left. + q(r)\,q(r+\Delta r)\,\beta^2(\theta)\,\frac{1}{\pi\left(\frac{\Delta r}{a_o} - \Delta t\right)}\cos 2\pi f(\tau - \Delta t)\sin\pi\Delta f(\tau - \Delta t)\right]$$

where $\tau$ is an unknown time increment relating to the non-propagating wave phase angle $2\pi f\tau$. The cross terms in the integration disappear becuase of their decorrelation.

Now if the point $(r + \Delta r, \theta)$ is outside the near field of the source, $q(r + \Delta r)$ is zero and the second term of equation 4.9 disappears. The remaining term is exactly equivalent to equation 4.5 for the case of spherical radiation. Thus, if the filtered sound pressure levels at the two points are cross correlated, the source power, $w(f)\,\alpha^2(\theta)$, can be determined from the peak value of the correlation curve (equation 4.6) even though one microphone is in the close near field.

If $w(f)\,\alpha^2(\theta)$ is determined in this way and the second microphone is then moved into the near field to measure the cross covariance as given by equation 4.9, the remaining unknowns are $q(r)\,q(r + \Delta r)\,\beta^2(\theta)$ and $\tau$. The maximum value of the second term occurs when $\Delta t = \tau$ and is equal to

$$\frac{\rho_o a_o w(f)\,\Delta f}{4\pi r (r + \Delta r)}\; q(r)\, q(r + \Delta r)\, \beta^2(\theta)$$

Knowing the variation of the first term, the second can be obtained by subtraction, as a function of $\Delta t$, and its peak value yields the near field cross product $q(r)\,q(r + \Delta r)\,\beta^2(\theta)$. Therefore, starting from the auto covariance ($\Delta r = 0$) and subsequently cross-correlating the signals at a number of microphone separations, $\Delta r$, the near field sound pressure increment $q^2(r)\,\beta^2(\theta)$ can be determined along the line given by $\theta$.

By making two further assumptions, this technique can now be used to determine the power spectrum, directivity and near field complications of each "source" in the acoustic model of the jet. The first assumption is that a microphone can be placed sufficiently near to the jet boundary to assure that it measures the sound field of one source alone, i.e., that there is no interference from adjacent sources. The validity of this premise is closely linked to that of the point source representation of the jet. In reality, sound is generated throughout a continuous volume of the jet and the question of interference is really one of source spacing. The second assumption is identical to that made in the derivation of equation 4.9; that the near and far sound fields are uncorrelated. The validity of this assumption is unknown, although it can be checked by performing the far field correlation (equation 4.5) at two or more microphone separations to ensure that the radiative sound pressure varies inversely as distance from the source. If not, then this, and subsequent correlations, at further spacings, can be used to establish the correct source power.

The remaining problem is to allocate the source positions. It would seem that this can only be achieved satisfactorily by a process of trial and error. However, an initial attempt can be made from the examination of the sound pressures and their space correlations along the length of the jet boundary. An analysis of the SPL distribution in each frequency band will suggest locations for the dominant sources in that band, and space correlations, using two microphones spaced parallel to the jet boundary in these regions will define a minimum separation for consistency with the assumption of uncorrelated sources.

For an ideally expanded, shock-free flow, the sources can be located with an arbitrary reference, although for convenience and simplicity of calculation, it is recommended that a regular spacing, or one based upon a mathematical progression, be used and referenced to the nozzle position. The source spacings indicated by the boundary SPL measurements can then be adjusted to coincide with these locations. Having fixed the source position, the correlation measurements, described above, can then be carried out to define the characteristics of each source.

Current theories which have been reviewed in Section 3.0 will serve as a useful guide in the analysis of the results. Equation 3.16 suggests that for a finite bandwidth analysis based upon the chosen model, the j-th frequency band sound pressure level at the point $(r,\theta)$ relative to the nozzle of an axisymmetric jet (see Figure 30) can be expressed in the form

$$p_j^2(r,\theta) = \sum_i^N \frac{\rho_o a_o P_{ij}}{4\pi r_i^2}\left[F_{ij}(\theta_i) + \frac{G_{ij}(\theta_i)}{(k_j r_i)^2} + \frac{H_{ij}(\theta_i)}{(k_j r_i)^4}\right] \qquad (4.10)$$

Where $P_{ij}$ is the sound power in the j-th frequency band of the i-th of N sources, f, G, and H are far and near field directivity functions and $r_i$, $\theta_i$ are the coordinates of the point $(r,\theta)$ relative to the i-th source. Comparing equations 4.8 and 4.10 it can be seen that

$$P_{ij} = w_i(f_j)\,\Delta f$$

$$F_{ij}(\theta_i) = a_i^2(\theta_i)$$

and

$$\frac{G_{ij}(\theta_i)}{(k_j r_i)^2} + \frac{H_{ij}(\theta_i)}{(k_j r_i)^4} = q_i^2(r_i)\,\beta_i^2(\theta_i) \qquad (4.11)$$

Thus $P_{ij}$ and $F_{ij}(\theta_i)$ are defined directly and $G_{ij}(\theta_i)$ and $H_{ij}(\theta_i)$ can be derived by an appropriate curve fitting process.

It is apparent that the program of data acquisition and analysis for this experiment is extensive and a high degree of automation is highly desirable. At the same time, it may prove profitable to optimize the allocation of source spectra, i.e., to minimize the number of sources per frequency band. This optimization should be included as part of an iterative cycle to establish satisfactory source spacings. Upon determination of all the parameters in equation 4.10 as functions of i, j, and $\theta_i$, the

equation can be used to compute the frequency band sound pressure contours. A comparison of the measured and calculated contours will indicate the accuracy of the model. Any deficiencies may be accounted for by a poor source distribution and an improved distribution can be sought. The cycle may then be repeated until agreement is optimized.

The preceding paragraphs describe how the constants in a general near field sound level prediction equation 4.10 may be experimentally determined. For these results to be of any value, they must be correlated with appropriate flow measurements, such as those described for use in the MSFC facilities in Reference 52. The most important details of the flow, from an acoustic standpoint, are the dimensions of the laminar core, the supersonic cone, the jet boundary and the axial velocity decay beyond the core tip. From this information, details of the turbulent mixing process can be estimated for later use in the establishment of scaling parameters.

One of the most important conclusions which should stem from these experiments at an early stage is the resolution of the Mach wave controversy. As discussed in Section 3.2.2, substantial Mach wave radiation whould have a negligible near field. The values of $G_{ij}(\theta_i)$ and $H_{ij}(\theta_i)$ calculated for the sources in the supersonic flow region will clearly show whether or not this is the case. Also the corresponding far field directivity functions $F_{ij}(\theta_i)$ should exhibit a large peak at the Mach angle.

If scaling laws are to be established, the experiments must be conducted with a large variety of jet configurations, covering a wide range of nozzle size, exhaust Mach number and temperature, exhaust gas composition, and including the effects of over and under expansion. The following sequence of configurations is recommended.

1) $M_E = 3$, air jet, ideal expansion, moderate temperature.

2) $M_E = 3$, air jet, conical nozzle, correct area ratio, moderate temperature.

These cases have several objectives:

a) To verify the proposed methods of analysis and subsequent prediction.

b) To investigate the general noise characteristics of shock-free supersonic jets, in particular to resolve the Mach wave problem. The moderate temperature should be chosen to give an "Acoustic" Mach number $\overline{M}_E$ of around 4.

c) To examine shock-turbulence noise. Cases (1) and (2) are run at the same conditions, except for the nozzle contours. This should maintain a reasonable flow similarity between the two cases except for the presence of a shock pattern in the latter, and this should be verified by flow measurements and shadow photography. The differences in the two noise fields should then be almost entirely due to shock noise. In the presence of shocks it may be necessary to change the source location to coincide with the shock patterns, or to introduce new ones. Full details of the experiments proposed to conduct cases (1) and (2) are given in Appendix C.

Further configurations are:

3) M = 3 air jet, over and under expansion.

4) M = 3 air jet, ambient and high temperatures.

5) M = 2, M = 2.5, M = 3.5 air jets, moderate temperatures.

6) M = 2, 2.5, 3 helium jets, ambient, moderate and high temperatures.

7) M = 3 helium jets over and under expanded.

8) Rockets.

## 5.0 CONCLUDING REMARKS

The basic mechanisms of noise generation by supersonic jets and rockets have been examined in a review of previous work, both theoretical and experimental. The general complexity of the problem has been clearly illustrated and it has been shown that although the theories of aerodynamic noise generation certainly provide insight into this problem, they cannot be used to predict more than the broadest features of the noise field of a given jet. Semi-empirical methods, based on these theories, do yield reasonable estimates of the far field noise, but the prediction of near field sound pressures is more difficult by an order of magnitude. At present, there is no reliable technique for the prediction of the near field noise of either turbojet or rocket engines, operating in even the most ideal conditions; that is exhausting into free, quiescent air.

This investigation has indicated an almost complete lack of good experimental data on the near field characteristics of supersonic jets. Previous near field prediction methods have relied on sound pressure measurements made close to the jet boundary to provide information regarding the sound power distribution in the jet. The dangers of doing so in the presence of unknown near field complications have been illustrated.

A semi-empirical prediction method is proposed, based on the conception that a jet exhaust can be adequately represented acoustically by a finite number of discrete sound sources. In addition, a suitable experimental program is outlined, which is designed to provide the necessary data for this technique. The first phase of this program, planned specifically for the Marshall Space Flight Center jet flow facilities, is described in detail in Appendix C. It must be emphasized that it is vital that these experiments are performed under extremely well controlled conditions if the results are to be of any value, since the problems of extracting accurately the described information from the statistical analytical processes are severe.

It is expected that such experiments will make a significant contribution towards the advancement of present knowledge of jet noise generation mechanisms. In particular, the basic question of where and how the predominant noise of a rocket exhaust is generated should be answered at an early stage in the program. Once the viability of the near field noise prediction technique is proved, and scaling laws have been established, the program can be logically extended to determine the effects of practical complications which include multi-nozzle configurations, deflected jets and the effects of sound reflection and refraction due to the ground, vehicle structure and supporting facilities.

## REFERENCES


1. Lighthill, M.J., "On Sound Generated Aerodynamically. I General Theory", Proc. Roy. Soc. A211, pp. 564-587, 1952.

2. Lighthill, M.J., "On Sound Generated Aerodynamically. II Turbulence as a Source of Sound", Proc. Roy. Soc. A222, pp. 1-32, 1954.

3. Ffowcs Williams, J.E., "The Noise from Turbulence Convected at High Speed", Proc. Roy. Soc. A255, pp. 469-503, 1963.

4. Laurence, J. E., "Intensity, Scale and Spectra of Turbulence in Mixing Region of Free Subsonic Jet", NACA Rpt. 1292, 1956.

5. Davies, P.O.A.L., Fisher, M.J., and Barratt, M.J., "The Characteristics of the Turbulence in the Mixing Region of a Round Jet", J. Fluid Mechanics, Vol. 15, pp. 337-367, 1963.

6. Howes, W.L., "Distribution of Time Averaged Pressure Fluctuations Along the Boundary of a Round Subsonic Jet", NASA TN D-468, 1960.

7. Franklin, R. E. and Foxwell, J.A., "Correlation in the Random Pressure Field Close to a Jet", British A.R.C. 20, 264, June 1958.

8. Mollo-Christensen, E., "Measurement of Near Field Pressure of Subsonic Jets", AGARD Rpt. 449, April 1963.

9. Cole, J.N., et al, "Noise Radiation from Fourteen Types of Rockets in the 1000 to 130,000 Pounds Thrust Range", WADC TR 57-354, December 1957.

10. Mayes, W.H. Lanford, W.E., and Hubbard, H.H., "Near Field and Far Field Noise Surveys of Solid Fuel Rocket Engines for a Range of Nozzle Exit Pressures", NASA TN D-21, August 1959.

11. Morgan, W.J. and Young, K.J., "Studies of Rocket Noise Simulation with Substitute Gas Jets and the Effect of Vehicle Motion on Jet Noise", ASD - TDR 62-787, March 1963.

12. Mull, H.R. and Erickson, J.C.Jr., "Survey of the Acoustic Near Field of Three Nozzles at a Pressure Ratio of 30", NACA TN 3978, April 1957.

13. Potter, R.C. and Crocker, M.J., "Acoustic Prediction Methods for Rocket Engines, Including the Effects of Clustered Engines and Deflected Exhaust Flow", NASA CR-566, October 1966.

14. Wilhem, D.P., "State-of-the-Art of Solid Rocket Engine Acoustic and Vibration Prediction", Northrop Report NOR 64-77, November 1964.

15. Franz, G.J., "The Near Sound-Field of Turbulence", DTMB Report 982, October 1959.

16. Dyer, I., "Estimation of Sound Induced Missile Vibrations", Random Vibration, (Ed. Crandall) MIT, Press, 1963.

17. Eldred, K.M., et al., "Suppression of Jet Noise with Emphasis on the Near Field", ASD-TDR-62-578, February 1963.

18. Johannesen, N.H., "The Mixing of Free Axially Symmetrical Jets of Mach Number 1.40", British A.R.C. 18,967, January 1957.

19. Pitkin, E.T. and Glassman, I., "Experimental Mixing Profiles of a Mach 2.6 Free Jet", J. Aerospace Sciences, pp. 791-793, December 1958.

20. Anderson, A.R. and Johns, F.R., "Nondimensional Characteristics of Free and Deflected Supersonic Jets Exhausting into Quiescent Air", NADC-ED- 5401, March 1954.

21. Eggers, J.M., "Velocity Profiles and Eddy Viscosity Distributions Downstream of a Mach 2.22 Nozzle Exhausting into Quiescent Air", NASA TN D-3601, September 1966.

22. Faris, G.N., "Some Entrainment Properties of a Turbulent Axi-Symmetric Jet", Mississippi State University Aerophysics Department Research Report No. 39, January 1963.

23. Ollerhead, J.B., "Some Shadowgraph Experiments with a Cold Supersonic Jet", Wyle Research Report WR 66-44, October 1966.

24. Szablewski, W., "The diffusion of a Hot Air Jet in Motion", NACA TM 1288, December 1950.

25. Abramovich, G.N., "The Theory of a Free Jet of a Compressible Gas", NACA TN 1058, 1944.

26. Kleinstein, G., "Mixing in Turbulent Axially Symmetric Free Jets", J. Spacecraft and Rockets, Vol. I, No. 4, pp. 403-409, July-August 1964.

27. Warren, W.R., "An Analytical and Experimental Study of Compressible Free Jets", Publ. No. 23, 885, University Microfilms, Inc., 1957.

28. Pai, S.I., Fluid Dynamics of Jets. Van Nostrand, New York, 1954.

29. Sauer, R., Theoretical Gas Dynamics, Edwards, Ann Arbor, 1947.

30. Pai, S.I., "On Two-Dimensional Flow of Jet in Uniform Stream", J. Aeronautical Sci., Vol. 19, No. 1, pp. 61-65, January 1952.

31. Love, E.S. et al., "Experimental and Theoretical Studies of Axisymmetric Free Jets", NASA TR - R6, 1959.

32. Frauenberger, J.H. and Forbister, J.G., "The Axial Decay and Radial Spread of a Supersonic Jet Exhausting into Air at Rest", The Aeronautical Quarterly, Vol. 12, pp. 131-149, May 1961.

33. Lighthill, M.J., "Sound Generated Aerodynamically", The Bakerian Lecture 1961, Proc. Roy. Soc., A267, pp. 147-182, 1962.

34. Lowson, M.V., "The Sound Field for Singularities in Motion", Proc. Roy. Soc., A286, pp. 559-572, 1965.

35. Ffowcs Williams, J.E., "Some Thoughts on the Effect of Aircraft Motion and Eddy Convection on the Noise from Air Jets", Univ. Southampton Aero. Astro. Rep. No. 155, 1960.

36. Lighthill, M.J., "Jet Noise", Wright Brothers Memorial Lecture, AIAA Journal, Vol. I, Part 7, 1963.

37. Eldred, K.M., "Review of Noise Generation of Rockets and Jets", JASA Vol. 32, p. 1502, 1960.

38. Lee, R., et al., "Research Investigations of the Generation and Suppression of Jet Noise", General Electric Report under U.S. Navy Contract No. ar 59-6160-c, January 1961.

39. Atvars, J. et al., "Refraction of Sound by Jet Flows or Jet Temperature", NASA CR-494, 1965.

40. Ribner, H.S., "The Generation of Sound by Turbulent Jets", Advances in Applied Mechanics, Academic Press, N.Y., Vol. 8, 1964.

41. Lassiter, L.W., "Turbulence in Small Air Jets at Exit Velocities up to 705 feet per Second", J. Appl. Mech., Vol. 24, pp. 349-354, 1957.

42. Howes, W.L. and Callaghan, E.E. et al., "Near Noise Field of a Jet Engine Exhaust", NACA Report 1338, 1957.

43. Phillips, O.M., "On the Generation of Sound by Turbulent Shear Layers", J. Fluid Mech., Vol. 9, Part 1, pp. 1-28, 1960.

44. Powell, A., "The Noise of Choked Jets", JASA, Vol. 25, pp. 385-389, 1953.

45. Davies, M.G. and Oldfield, D.E.S., "Tones from a Choked Axi-Symmetric Jet", Acustica, Vol. 12, pp. 257-277, 1962.

46. Ribner, H.S., "Convection of a Pattern of Vorticity Through a Shock Wave", NACA Rep. 1164, 1954.

47. Ribner, H.S., "Shock Turbulence Interaction and the Generation of Noise", NACA Rep. 1233, 1955.

48. Kovasznay, L.S.G., "Turbulence in Supersonic Flow", J. Aero. Sci., Vol. 20, pp. 657-674, 1953.

49. Howes, W.L., "Similarity of the Far Noise Fields of Jets", NASA TR R-52, 1960.

50. Lowson, M. V., "Shadowgraph Visualization of Noise from Cold Supersonic Jets," Wyle Research Report, WR 67-3, 1967.

51. Keast, D. N., and Maidanik, G., "Studies of the Near Field Noise Properties of a Small Air Jet", Bolt, Beranek and Newman, Report 1272, February 1966.

52 Potter, R. C., "Experimental Program for Helium Jet", Wyle Research TM 65-3, May 1965.

# APPENDIX A

## SUPERSONIC JET FLOW EQUATIONS

The total axial momentum in the jet mixing region is given by

$$m_M = 2\pi \int_{r_o}^{\infty} \rho U^2 r \, dr \tag{A1}$$

where $\rho$ and $U$ are the local free stream mean density and velocity respectively, $r$ is the radius and $r_o$ is the radius of the potential core. The upper limit is infinite to account for the assumed exponential nature of the velocity profile.

It is assumed that

$$U = U_m \, e^{-\eta^2/2} \tag{A2}$$

and

$$T_T = T_o + (T_{m_T} - T_o) \, e^{-\eta^2/2.5} \tag{A3}$$

(see text) where the subscripts T, m, and o denote total, centerline and ambient conditions, respectively.

Putting $t = T_{m_T}/T_o$ we can write

$$T_T/T_o = 1 + (t - 1) \, e^{-\eta^2/2.5} \tag{A4}$$

Now, for a perfect gas $\rho_T = \rho_o \cdot T_o/T_T$ and for an isentropic compression

$$\rho/\rho_T = \left[ 1 - \frac{\gamma - 1}{2} \left( \frac{U}{a_T} \right)^2 \right]^{1/\gamma - 1} \tag{A5}$$

and $a_T$ = the total speed of sound

$$a_T = a_o \sqrt{T_T/T_o} \tag{A6}$$

Combining equations (A2), (A4), and (A5)

$$\left(\frac{U}{a_T}\right)^2 = \frac{U_m^2 \; e^{-\eta^2}}{a_o^2 \left[1 + (t-1)\, e^{-\eta^2/2.5}\right]} \tag{A7}$$

But, $U_m^2 = M_m^2 \; a_m^2$ and again for an adiabatic process in a perfect gas

$$a_m = a_{m_T} \left(1 + \frac{\gamma - 1}{2} M_m^2\right)^{-1/2} \tag{A8}$$

Now,

$$a_{m_T} = a_o \sqrt{\frac{T_{m_T}}{T_o}} = a_o \sqrt{t}$$

and therefore,

$$U_m^2 = a_o^2 \; t \; M_m^2 \left(1 + \frac{\gamma - 1}{2} M_m^2\right)^{-1}$$

Substituting into equations (A7), gives

$$\left(\frac{U}{a_T}\right)^2 = \frac{t\, M_m \left(1 + \frac{\gamma - 1}{2} M_m^2\right)^{-1} e^{-\eta^2}}{1 + (t-1)\, e^{-\eta^2/2.5}} \tag{A9}$$

Finally, equations (A1), (A2), (A5), and (A9) can be combined to yield

$$m_M = 2\pi \rho_o U_m^2 \int_{r=a r_E}^{\infty} \left[1 + \frac{\gamma - 1}{2} \left\{ \frac{t\, M_m \left(1 + \frac{\gamma - 1}{2} M_m^2\right)^{-1} e^{-\eta^2}}{1 + (t-1)\, e^{-\eta^2/2.5}} \right\} \right]^{1/\gamma - 1} \times \tag{A10}$$

$$\times \quad \frac{e^{-\eta^2}\, r}{1 + (t-1)\, e^{-\eta^2/2.5}} \cdot dr \qquad \text{(A10) Cont.}$$

where $a \cdot r_E$ = radius of potential core.

In the downstream region $a = 0$ and this equation can be written

$$m_M = 2\pi \rho_o U_M^2 b^2 \int_o^\infty \left[ 1 + \frac{\gamma - 1}{2} \left\{ \frac{t M_m \left(1 + \frac{\gamma - 1}{2} M_m^2\right)^{-1} e^{-\eta^2}}{1 + (t-1)\, e^{-\eta^2/2.5}} \right\} \right]^{1/\gamma - 1} \times \qquad \text{(A11)}$$

$$\times \quad \frac{e^{-\eta^2}\, \eta}{1 + (t-1)\, e^{-\eta^2/2.5}} \cdot d\eta$$

The radial profile of flow Mach number can be obtained from the perfect gas relationship

$$M^2 = \left(\frac{U}{a_T}\right)^2 \left[ 1 - \frac{\gamma - 1}{2} \left(\frac{U}{a_T}\right)^2 \right]^{-1}$$

which, upon substitution of equation (A9) becomes

$$M^2(\eta) = \frac{t M_m \left(1 + \frac{\gamma - 1}{2} M_m^2\right)^{-1} e^{-\eta^2}}{1 + (t-1)\, e^{-\eta^2/2.5}} \times \qquad \text{(A12)}$$

$$\times \left[ 1 - \frac{\gamma - 1}{2} \left\{ \frac{t M_m \left(1 + \frac{\gamma - 1}{2} M_m^2\right)^{-1} e^{-\eta^2}}{1 + (t-1)\, e^{-\eta^2/2.5}} \right\}^2 \right]^{-1}$$

a function of $M_m$, $t$ only.

Profiles of this expression have been calculated for various values of $t$ and are presented in Figure 20.

It should be noted that an increase of temperature, which implies an increase in velocity for a given Mach number moves the sonic boundary outwards toward the jet boundary.

## APPENDIX B

## DERIVATION OF THE SOUND FIELD OF CONVECTED LATERAL QUADRUPOLES IN TERMS OF TOTAL SOUND POWER

Franz gives (equation 91 of Reference 15) the following expression for the sound field of a region of lateral quadrupoles, aligned with the $x_1$ and $x_3$ axes, and convected along the $x_3$ axis at the convection Mach number, $\overline{M}_c$

$$\overline{p^2} = \frac{1}{16\pi^2 a_o^4} \iint \left\langle \frac{4 \sin^2\theta \cos^2\phi}{r^2 (1 - \overline{M}_c \cos\theta)^6} \left\{ \cos^2\theta \; \overline{\ddot{T}_{13} \; \ddot{T}_{13}'} \right.\right.$$

$$+ \frac{a_o^2}{r} \left[ \frac{3 (1 - \overline{M}_c^2)^2 \cos^2\theta}{(1 - \overline{M}_c \cos\theta)^2} - \frac{6 M_c (1 - \overline{M}_c^2) \cos\theta}{1 - \overline{M}_c \cos\theta} + 4 \overline{M}_c^2 \right] \overline{\dot{T}_{13} \; \dot{T}_{13}'}$$

(B1)

$$+ \frac{a_o^4}{r^4} \left[ \frac{9 (1 - \overline{M}_c^2)^4 \cos^2\theta}{(1 - \overline{M}_c \cos\theta)^4} - \frac{18 \overline{M}_c (1 - M_c^2)^3 \cos\theta}{(1 - \overline{M}_c \cos\theta)^3} \right.$$

$$\left.\left. + \frac{9 \overline{M}_c^2 (1 - \overline{M}_c^2)^2}{(1 - \overline{M}_c \cos\theta)^2} \right] \overline{T_{13} \; T_{13}'} \right\} \Big\rangle \, d\underset{\sim}{\eta} \, d\underset{\sim}{\eta}'$$

where $\underset{\sim}{\eta} = \underset{\sim}{y} + \underset{\sim}{M} \cdot r$, and $T_{13} = \dot{T}_{13} \; (\gamma, \; t - r/a_o)$. The brackets $\langle \; \rangle$ denote evaluation at the retarded time $t - r/a_o$. However this equation is subject to the correction, made by Ffowcs Williams (Reference 35) to Lighthill's original result (Reference 1), namely that a multiplicative factor $(1 - \overline{M}_c \cos\theta)$ must be introduced to account for the increased volume of the region of sources whose sound reaches the field point simultaneously. This reduces the exponent of $(1 - M_c \cos\theta)$ in the common denominator from 6 to 5.

Following Lighthill (Reference 1, equations 21 and 34b) the total sound power generated by the same volume of turbulence is, since the near field components integrate to zero,

$$P = \frac{1}{60\,\rho_o\,a_o^5} \iint \left\langle \frac{(1+5\,\bar{M}_c^2)}{(1-\bar{M}_c^2)^4} \quad 2\,\overline{\ddot{T}_{13}\;\ddot{T}_{13}'} \right\rangle d\underset{\sim}{y}\;\; d\underset{\sim}{y}' \qquad \text{(B2)}$$

Now if the volume of interest is small, such that r lies outside its geometric near field, i.e., at distances large compared with a typical eddy dimension, equations (B1) and (B2) can be simplified, for then the integration can be applied to the terms in $T_{13}$ and its derivatives alone. For the narrow band of frequencies centered on $\omega$, $\ddot{T} \approx \omega^2 T$, and $\dot{T} \approx \omega T$. Making these substitutions, and combining (B1) and (B2) leads to:

$$T_{13}^2 = 30 \quad \frac{\pi\,\rho_o\,a_o^5 \quad P(\omega)}{V_c\,\omega^4} \quad \frac{(1-\bar{M}_c^2)^4}{1+5\,\bar{M}_c^2} \qquad \text{(B3)}$$

(where $V_e$ is the eddy volume and $P(\omega)$ is the total power in the given frequency band) and then:

$$\begin{aligned}
\overline{p^2}(\omega) = {} & \frac{15\,\rho_o\,a_o\,P(\omega)}{2\pi r^2} \quad \frac{(1-\bar{M}_c^2)^4}{(1+5\,\bar{M}_c^2)} \quad \frac{\sin^2\theta\cos^2\phi}{(1-\bar{M}_c\cos\theta)^5} \left[ \cos^2\theta \right. \\
& + \frac{a_o^2}{r^2\omega^2}\left\{ \frac{3(1-\bar{M}_c^2)^2\cos^2\theta}{(1-\bar{M}_c\cos\theta)^2} - \frac{6\,\bar{M}_c(1-\bar{M}_c^2)\cos\theta}{1-\bar{M}_c\cos\theta} + 4\,\bar{M}_c^2 \right\} \\
& + \frac{a_o^4}{r^4\omega^4}\left\{ \frac{9(1-\bar{M}_c^2)^4\cos^2\theta}{(1-\bar{M}_c\cos\theta)^4} - \frac{18\,\bar{M}_c(1\,\bar{M}_c^2)^3\cos\theta}{(1-\bar{M}_c\cos\theta)^3} \right. \\
& \left. \left. + \frac{9\,\bar{M}_c^2(1-\bar{M}_c^2)^2}{(1-\bar{M}_c\cos\theta)^2} \right\} \right]
\end{aligned} \qquad \text{(B4)}$$

# APPENDIX C

## INITIAL EXPERIMENTS TO MEASURE THE NEAR NOISE FIELD OF A SUPERSONIC JET

Section 4.0 of the main text describes the theory behind the method for a determination of the unknown coefficients in the near field sound pressure prediction equation (4.10), which is

$$p_j^2 (r, \theta) = \sum_i^N \frac{\rho_o a_o P_{ij}}{r_i^2} \left[ F_{ij} (\theta_i) + \frac{G_{ij} (\theta_i)}{(k_j r_i)^2} + \frac{H_{ij} (\theta_i)}{(k_j r_i)^4} \right] \qquad (4.10)$$

The experimental procedure involves the following steps:

- Measure the flow properties
- Define the locations of the N sources along the jet axis from boundary pressure correlations
- Determine $P_{ij}$, $F_{ij} (\theta_i)$, $G_{ij} (\theta_i)$, and $H_{ij} (\theta_i)$ for all i, j, and $\theta_i$ by sound pressure correlation techniques, where i denotes the i-th source, j the j-th frequency band and $\theta_i$ is the angle from the jet axis
- Using the calculated coefficients, compute the sound pressure level contours according to equation (4.10), and compare with measurements to check results. If necessary, redefine source locations and repeat Item 3.

Of these steps, the third is the most extensive and Figure 31 shows a sketch of the proposed instrumentation layout for acquisition of the sound pressure signals required for correlation. A particular source location is shown on the jet axis and a series of microphones mounted upon a boom are aligned with the source in the horizontal plane. The boom can be rotated, in the horizontal plane, about an axis through the source. The angle between the boom and the jet axis defines the angle $\theta_i$.

The signals from all microphones are to be recorded simultaneously and the number of microphones is, therefore, governed by the number of data channels available. However, a minimum of six is recommended and provision should be made to attach them at arbitrary positions on the boom up to a maximum of 30 diameters from its pivot. It is further recommended that the boom is provided with a constant speed drive motor to rotate it through the full range of $\theta_i$, within the duration of one jet run. If the angular position $\theta_i$ is also recorded on a further channel of information and the rotation is sufficiently slow, a specified

record sample can be regarded as applying to a fixed value of $\theta_i$, only. This provision will considerably expedite the experimental procedure.

As shown in Figure 31, the boom pivot is mounted on a saddle, which is free to travel on the rail running below, and parallel to the jet axis. If this slide is suitably scaled, the boom pivot can be accurately located at any point under the jet axis. However, the boom rail should have latitude in the horizontal plane so that it can be aligned with the jet boundary. Then, if the boom is arranged to lock at the 90-degree position, an auxiliary traverse can be mounted upon it, which holds one fixed and one traveling microphone. This equipment may then also be used to perform the space correlations parallel to the jet boundary which are required to aid the specification of the source distribution.

It is recognized that this system could cause serious sound reflection problems and, after installation of the facility, it will be essential to investigate and minimize these reflections. It is suggested that all surfaces in the immediate vicinity of the rig, including the boom, traversing gear, and microphone bodies, be covered, or wrapped, in sound absorbent material such as cotton blanketing. A loudspeaker should then be installed in the approximate vicinity of the jet nozzle to generate discrete frequency sound of constant level, scanning the frequency range of interest. For various boom positions, the output levels from each of the microphones can be compared with that from a reference microphone near the speaker. Reflections will manifest themselves by continuously modifying the sound level at the affected microphone as the frequency changes, and steps can then be taken to find and remove the source of the reflection.

Since the signals from all microphones are to be correlated, it is of course essential that all microphones and their associated recording channels are phase matched throughout.

When the facility is checked out, the measurement program can proceed, and the following sequence is proposed.

1) Install a small, ideally expanded Mach 3.0 nozzle and run, at the design pressure ratio, at a temperature which will give an exhaust velocity around 4 times the ambient speed of sound. Check that the flow is shock free by taking shadowgraphs. Ensure repeatability by installing a monitoring static pressure transducer in the nozzle expansion chamber wall close to the exit plane.

2) Measure radial velocity and temperature profiles at several stations along the jet axis in order to define the dimensions of the laminar core, the supersonic core and the jet boundary. This information can be used to align the boom rail parallel to the jet boundary.

3) Traverse the jet boundary, with the microphone located as near to it as possible, recording the sound pressure level. This signal may then be analyzed in octave or third-octave bandwidths to determine the approximate distribution of the sound flow along the jet in each frequency band. This will indicate suitable source locations for each frequency band.

4) Using a fixed microphone at a selected station along the boundary, cross correlate its output with that of a second microphone spaced at a number of intervals along the auxiliary traverse, parallel to the jet boundary. Cross correlations in the required frequency band will indicate the extent of an equivalent correlated source region. Repetition of this procedure at various stations along the jet will enable the source spacings to be optimized and an approximate filter band spectrum allocated to each. It is recommended that the source spacings be regular, or in the form of a convenient mathematical progression, in order to simplify the analysis and the later use of the prediction method.

5) Align the boom rail parallel to the jet axis as determined by 2). For each source, a suitable microphone spacing along the boom can be determined from its approximate spectrum. The near field in each frequency band can be expected to extend for a few wavelengths and the outboard microphone should be outside the near field of the lowest expected frequency component. The inboard microphone should be located to avoid impact with the jet flow at the smallest boom angle envisaged. It may prove necessary to adjust the microphone positions at the extreme boom angles to avoid this occurrence. It is recommended that $\theta_i$ be traversed in the range of 25 degrees through 155 degrees to the jet axis. The intermediate microphones should be arranged to give a reasonable coverage between those at the two ends, being more closely spaced towards the inboard end.

The boom is now rotated through the range of $\theta_i$ at a steady rate, simultaneously recording the signals from all microphones. The signal from the inboard microphone is then cross correlated with that from each of the other microphones in turn, for a number of discrete values of $\theta_i$ (assuming that a certain duration of the signal can be extracted, which approximates the values for a fixed value of $\theta_i$), and at various time delays. These correlations are used to determine the source coefficients $P_{ij}$, $F_{ij}(\theta_i)$, $G_{ij}(\theta_i)$, and $H_{ij}(\theta_i)$ according to the methods of Section 4.0 of the main text.

The actual microphone spacings along the boom and the filter bandwidths can only be determined by experience. The microphone spacing must be chosen to meet the requirement defined in Section 4.0 of the text. Firstly, the "boundaries" of the near field must be known before the outboard microphones can be mounted in the far field. Secondly, it may be necessary to adjust the position of the outer microphone to acquire further data, if the near and far

fields are found to be substantially correlated. Thirdly, the spacings of the intermediate microphones may need adjustment to provide satisfactory points for the curve fitting processes involved in the extraction of $G_{ij}(\theta_i)$ and $H_{ij}(\theta_i)$. The filter bandwidth should be as broad as possible, preferably octave band, but third octave analysis may prove necessary to achieve the required degree of resolution of the cross-covariagram. In this case, it will quite probably be satisfactory to perform analyses in alternate, or every third band, estimating intermediate results by interpolation.

The entire procedure must, of course, be repeated for each source location.

6) Use the calculated values of the coefficients to compute the frequency band noise contours for comparison with measurements. Prior to this, some degree of smoothing of the coefficients could prove advantageous to ensure that, for example, $F_{ij}(\theta_i)$, $G_{ij}(\theta_i)$, and $H_{ij}(\theta_i)$ are continuous functions of $\theta_i$.

If the agreement between measured and computed SPL's is deficient, then reasons for the deficiencies must be analyzed. This may lead to definition of an improved source distribution, in which case, operation (5) and (6) must be repeated.

7) Replace the ideally expanded nozzle by a conical nozzle of the same area ratio and run at the previous values of the pressure ratio and total temperature. The flow will now contain the cellular shock structure which is characteristic of supersonic jets but in other respects the flow should remain basically the same as that from the ideal nozzle.

Take shadowgraphs of the flow to determine the location of the visible shocks and extrapolate the results to the region where they are masked by the surrounding turbulence.

8) Measure velocity and temperature profiles at various stations, taking due account of the possible effects of the shocks. Determine the sonic point as accurately as possible by traversing the probe along the jet axis towards the nozzle until the critical pressure ratio is measured.

9) Check that the likely shock noise sources coincide with or fall close to source locations in the previously determined distribution. If not, it may be necessary to make some adjustments or insert additional sources.

10) Repeat the procedure defined by steps (3) through (6).

Figure 1. Shadowgraph Photograph of the Mach Wave Field of a Supersonic Jet, from Unpublished Work at NASA Langley Research Center.

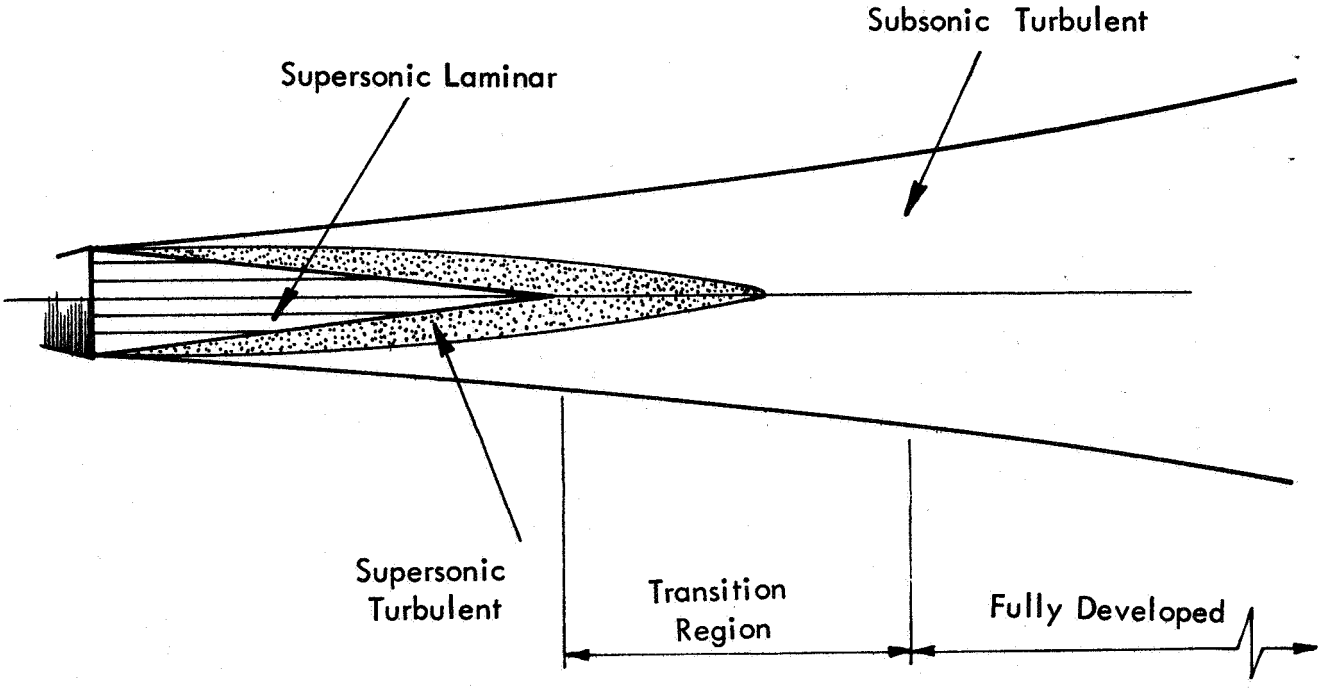


Figure 2. Shock Free Supersonic Flow

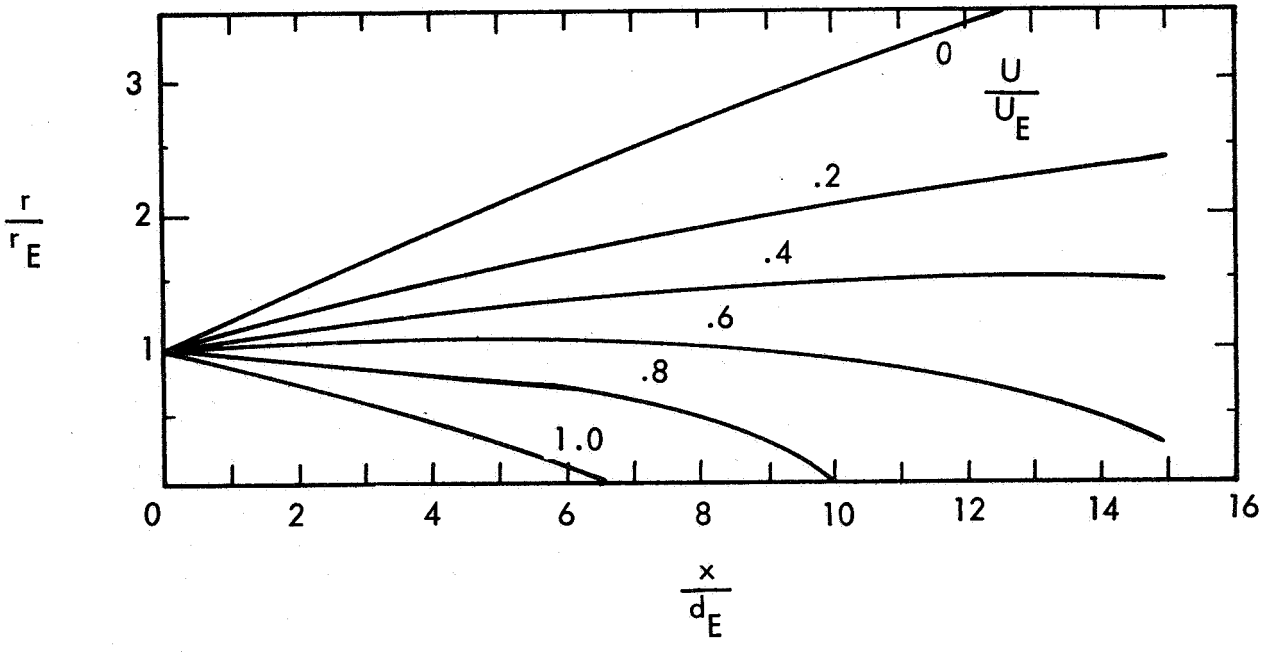


Figure 3. Calculated Flow Contours for Constant Density Axisymmetric Jet. From Reference 17.

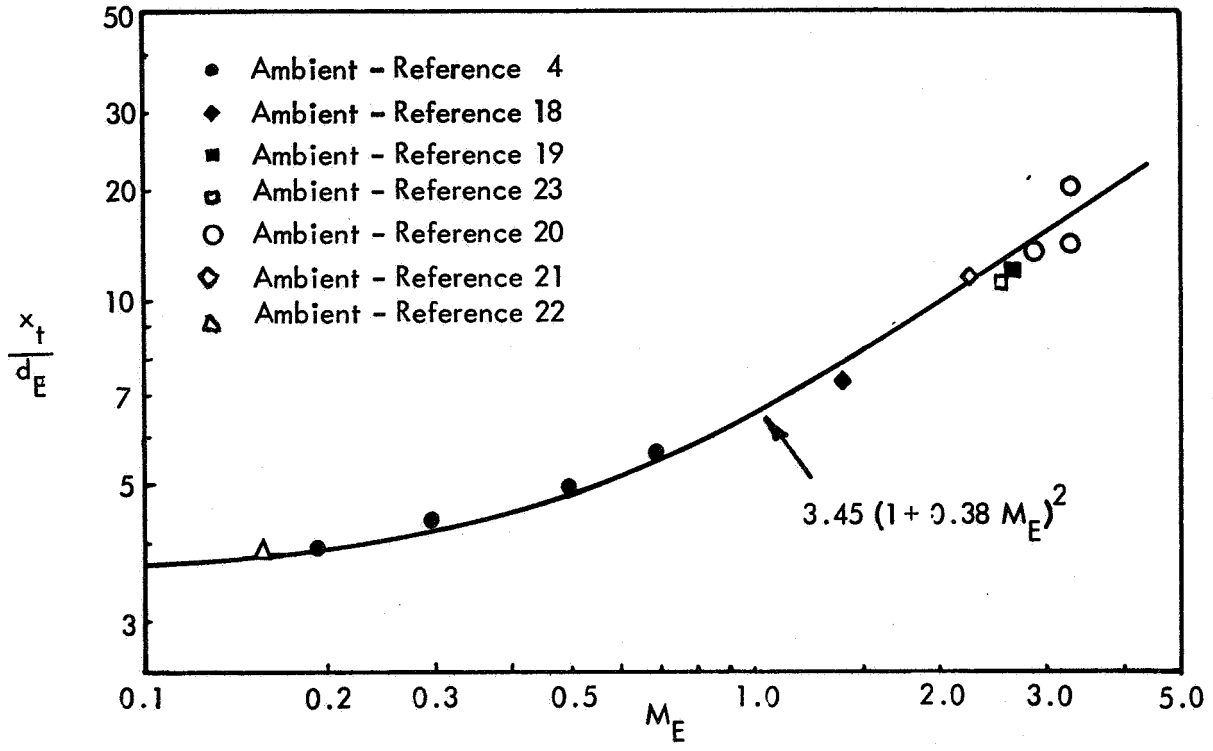


Figure 4. Variation of Core Length with Exit Mach Number. (After Eldred et al. Reference 17.)

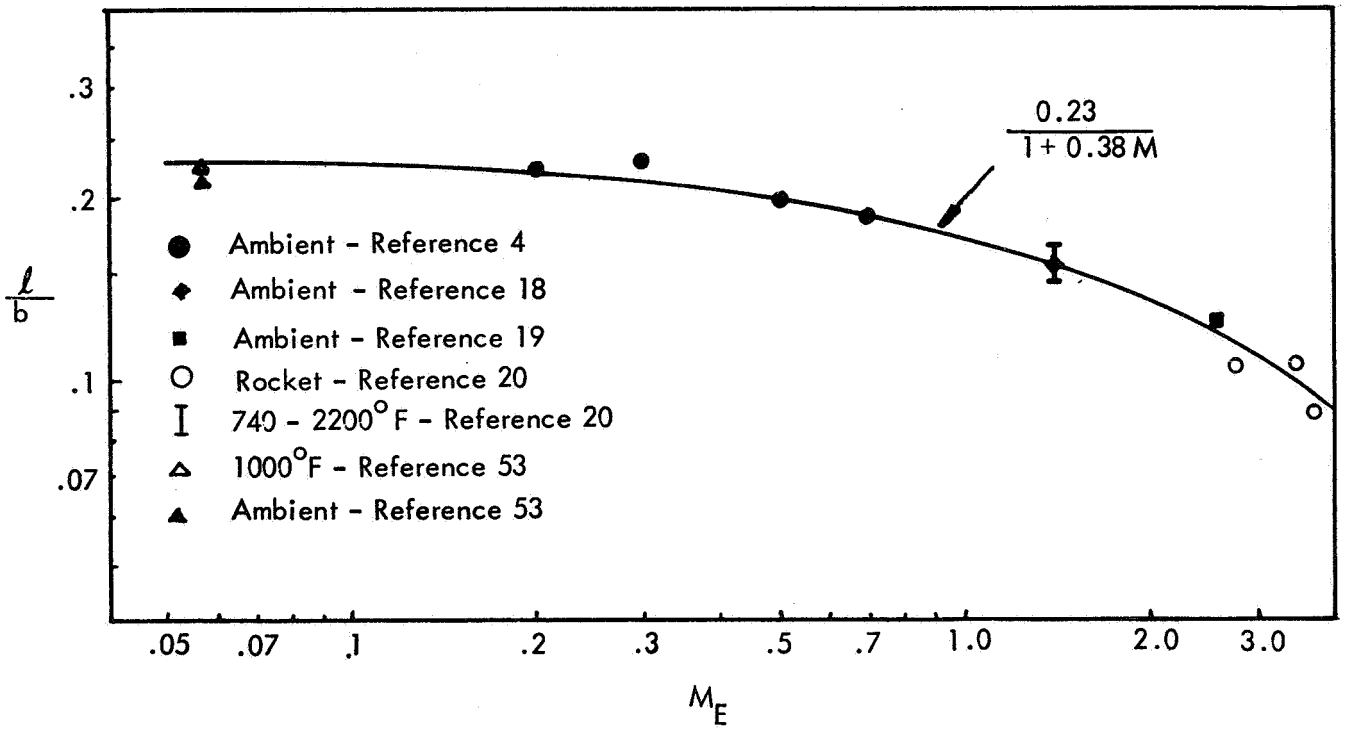


Figure 5. Variation of $\ell/b$ with Exit Mach Number (From Eldred et al. Reference 17.)

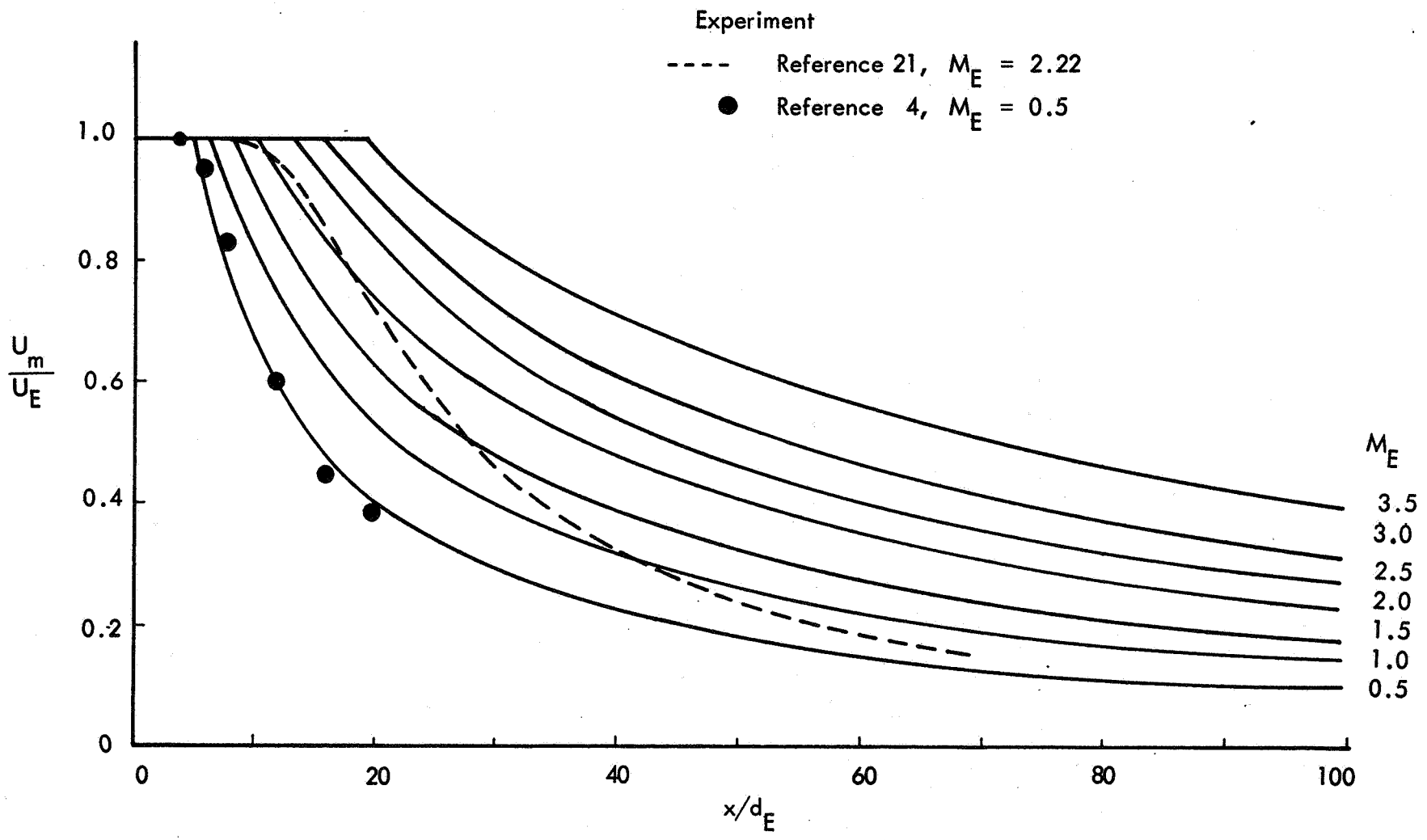


Figure 6. Axial Velocity Decay for Various Exit Mach Numbers Calculated by Method of Reference 17.

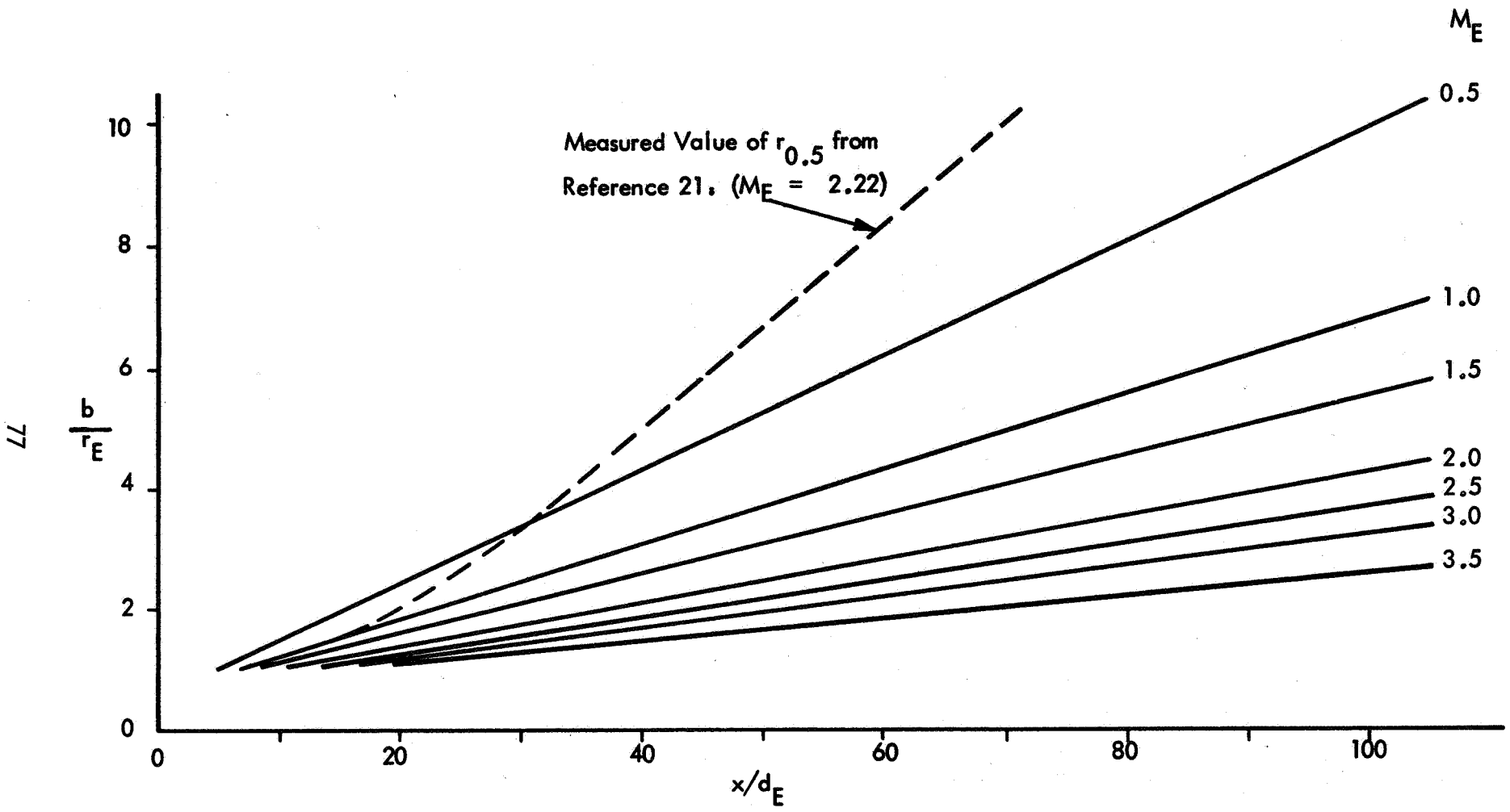


Figure 7. Jet Spreading Curve Corresponding to Figure 6.

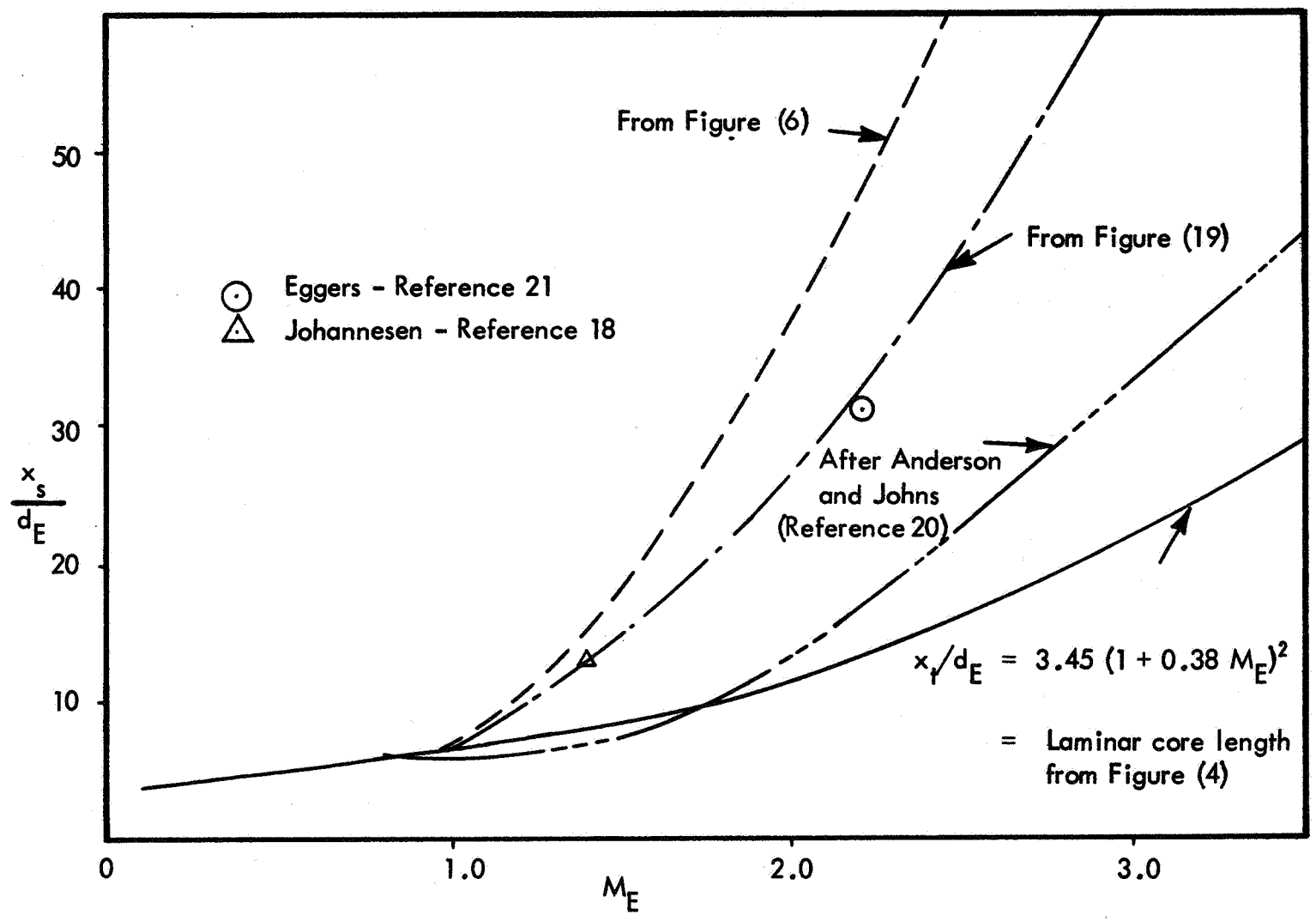


Figure 8. Length of Supersonic Core Versus Exit Mach Number

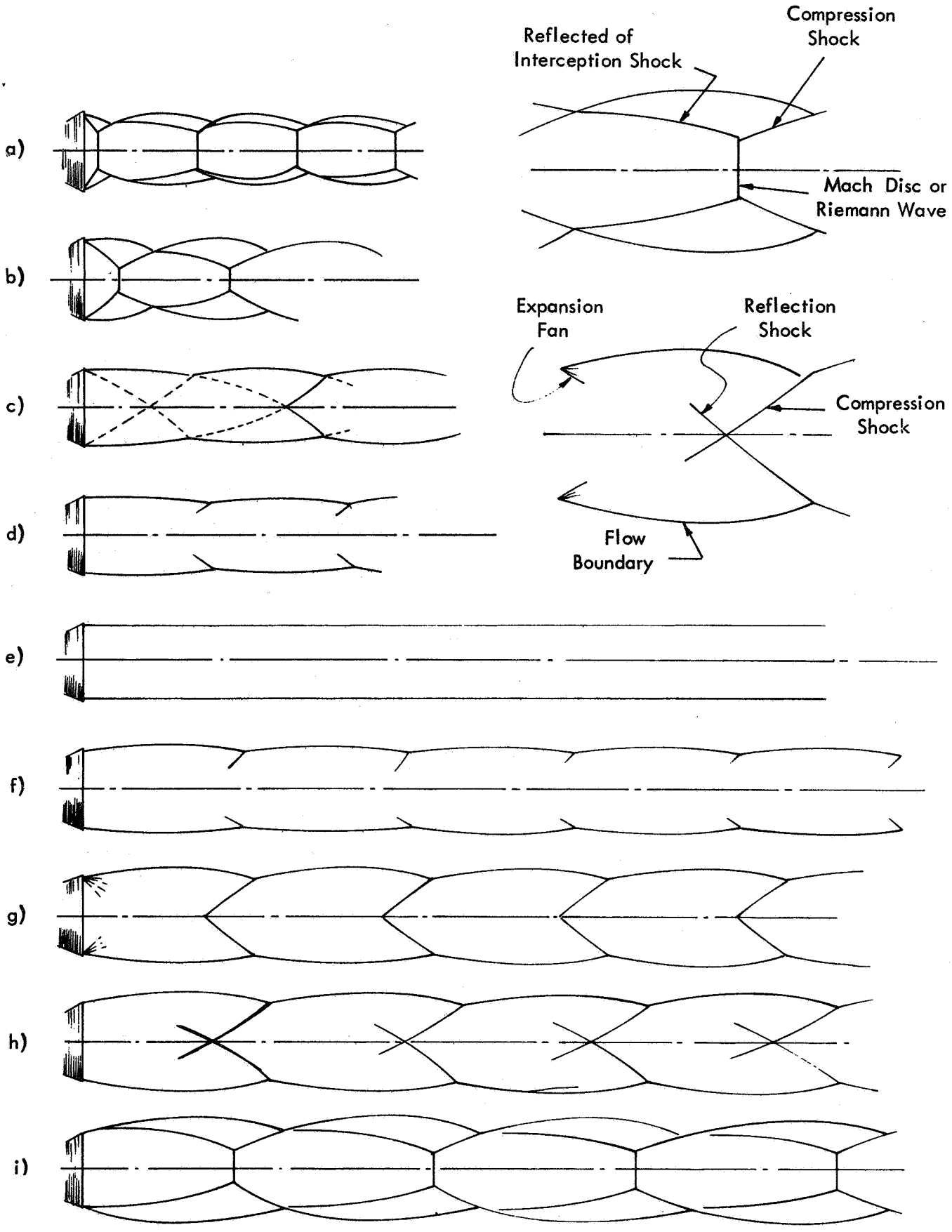


Figure 9. Development of Shock Patterns.

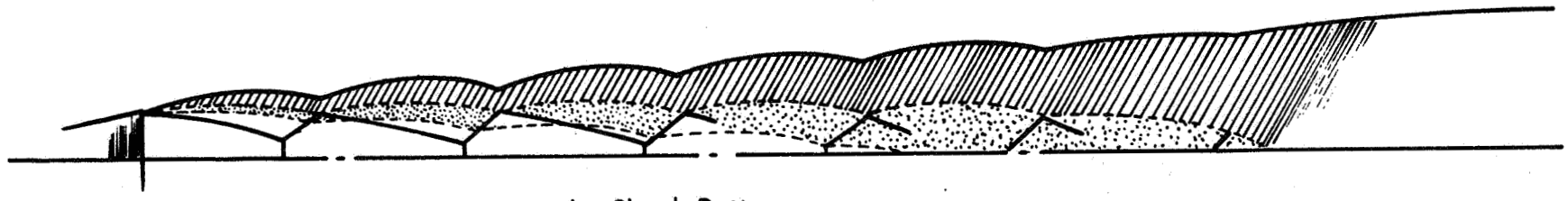

(a) Distortion of Regional Boundaries by Shock Pattern.

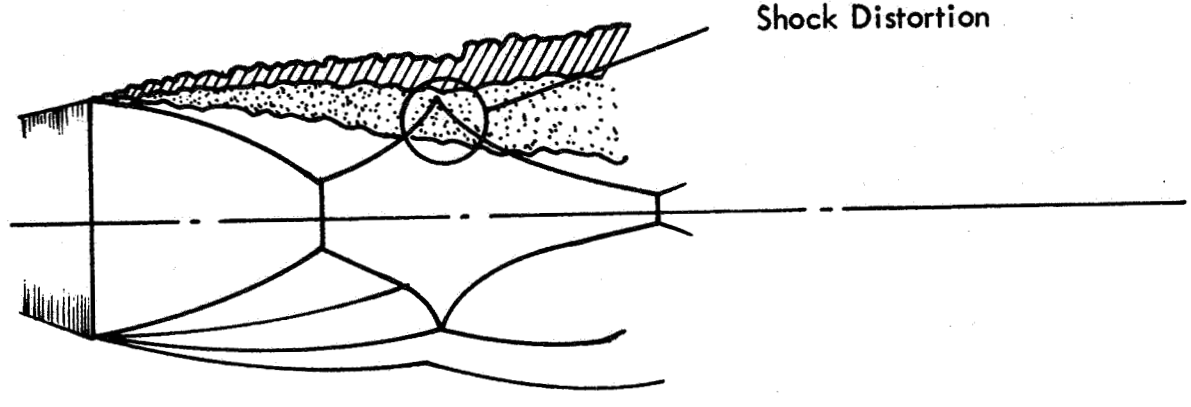


(b) Radial Scale Exaggerated To Illustrate Shock Front Distortion in Shear Layer.

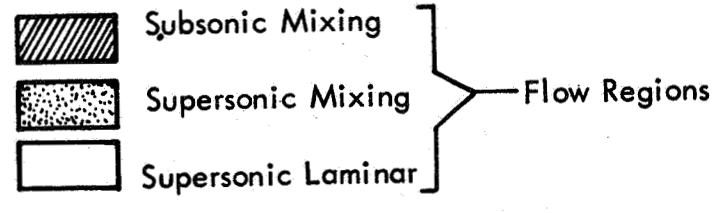


Figure 10. Badly Expanded Supersonic Jet Flow.

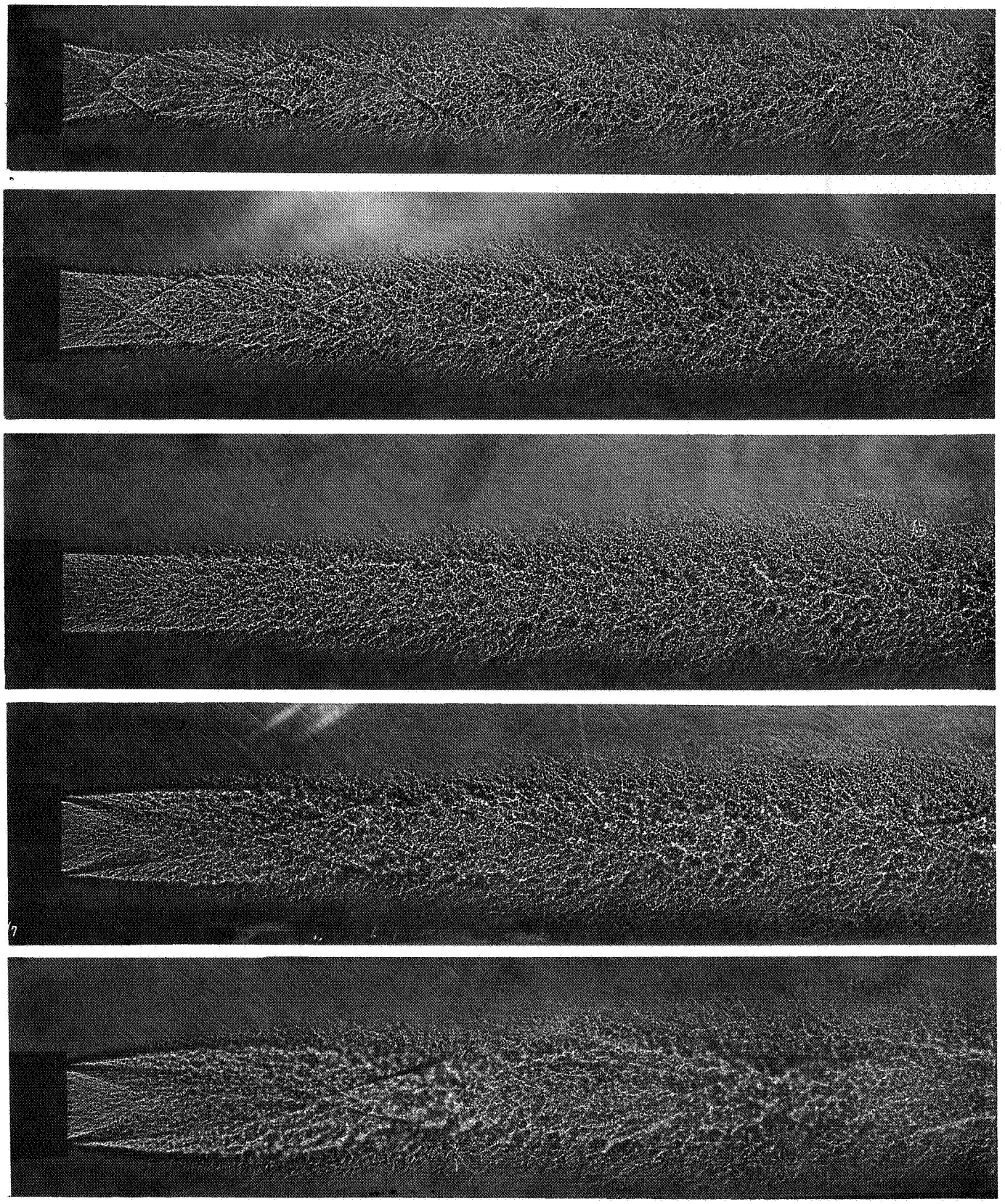

Figure 11. Development of Shock Pattern with Nozzle Exit Pressure, Design Mach Number = 2.47. From top to bottom; $p_E/p_o$ = 0.497, 0.747, 1.0, 1.53, 1.98.

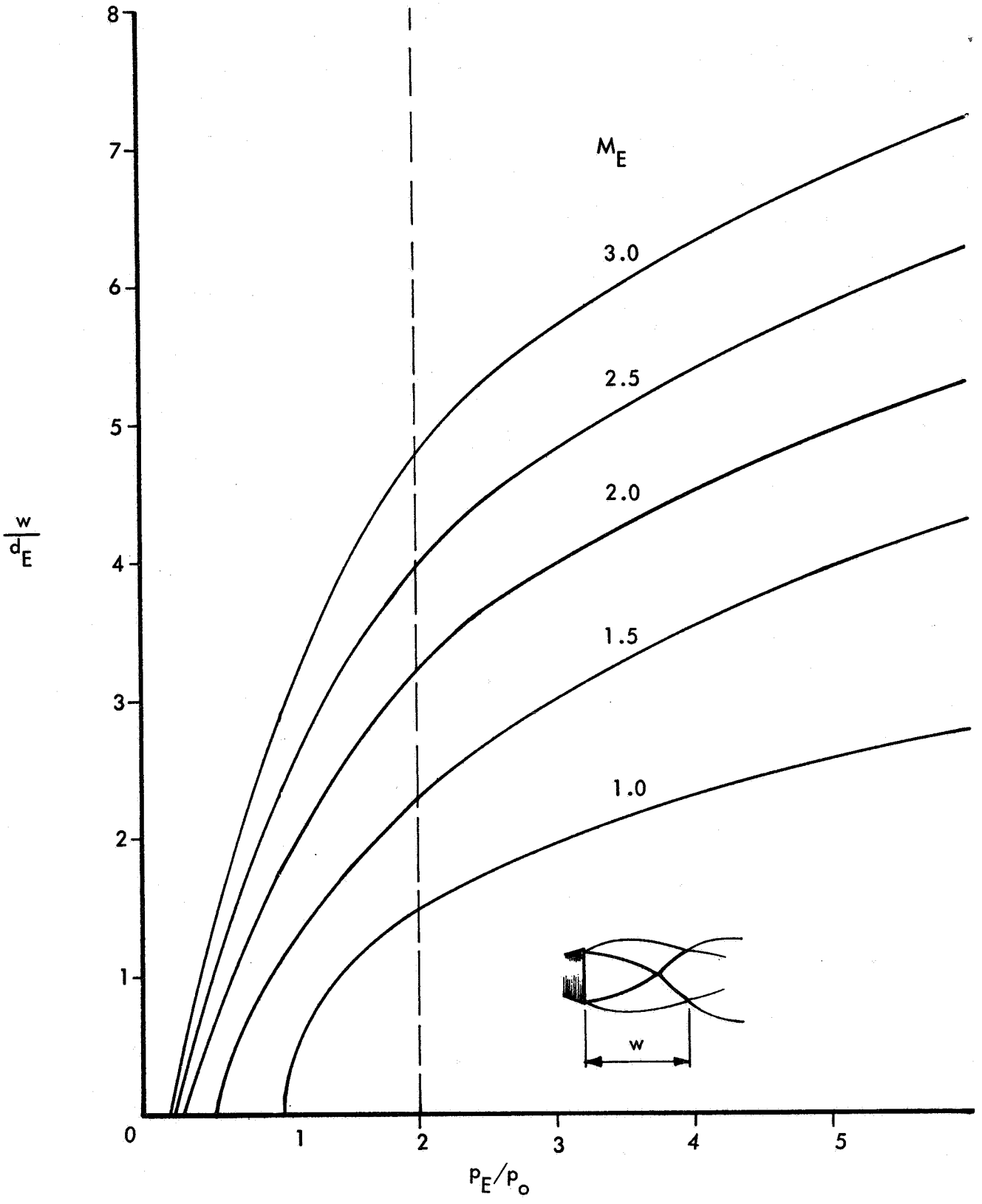


Figure 12. Width of Primary Cell; Empirical Relationships from Love et al. (Reference 31)

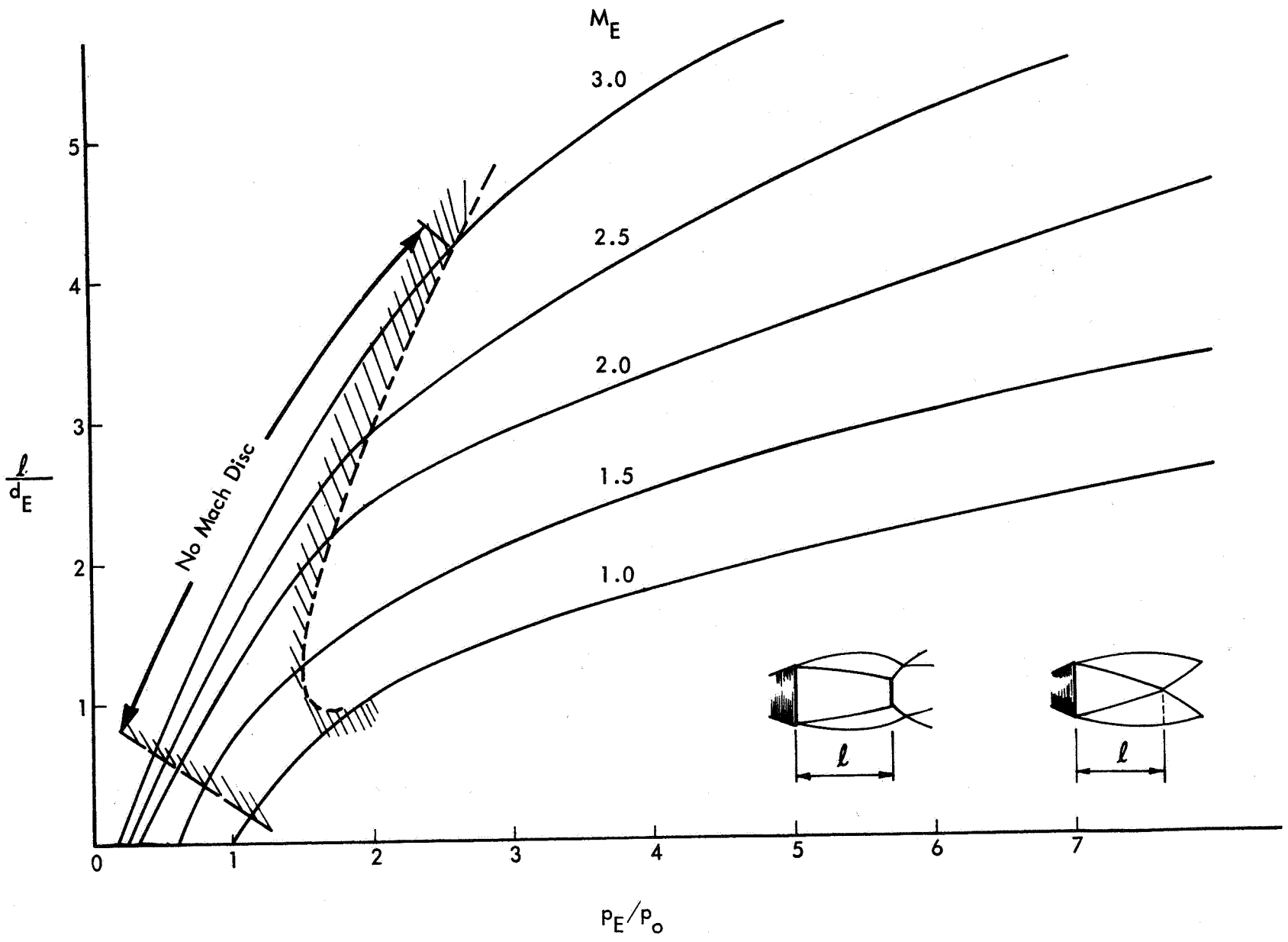


Figure 13. Effect of Pressure Ratio on Distance to First Mach Disc or Intersection Point for Ideally Expanded Jet, From Love et al. (Reference 31).

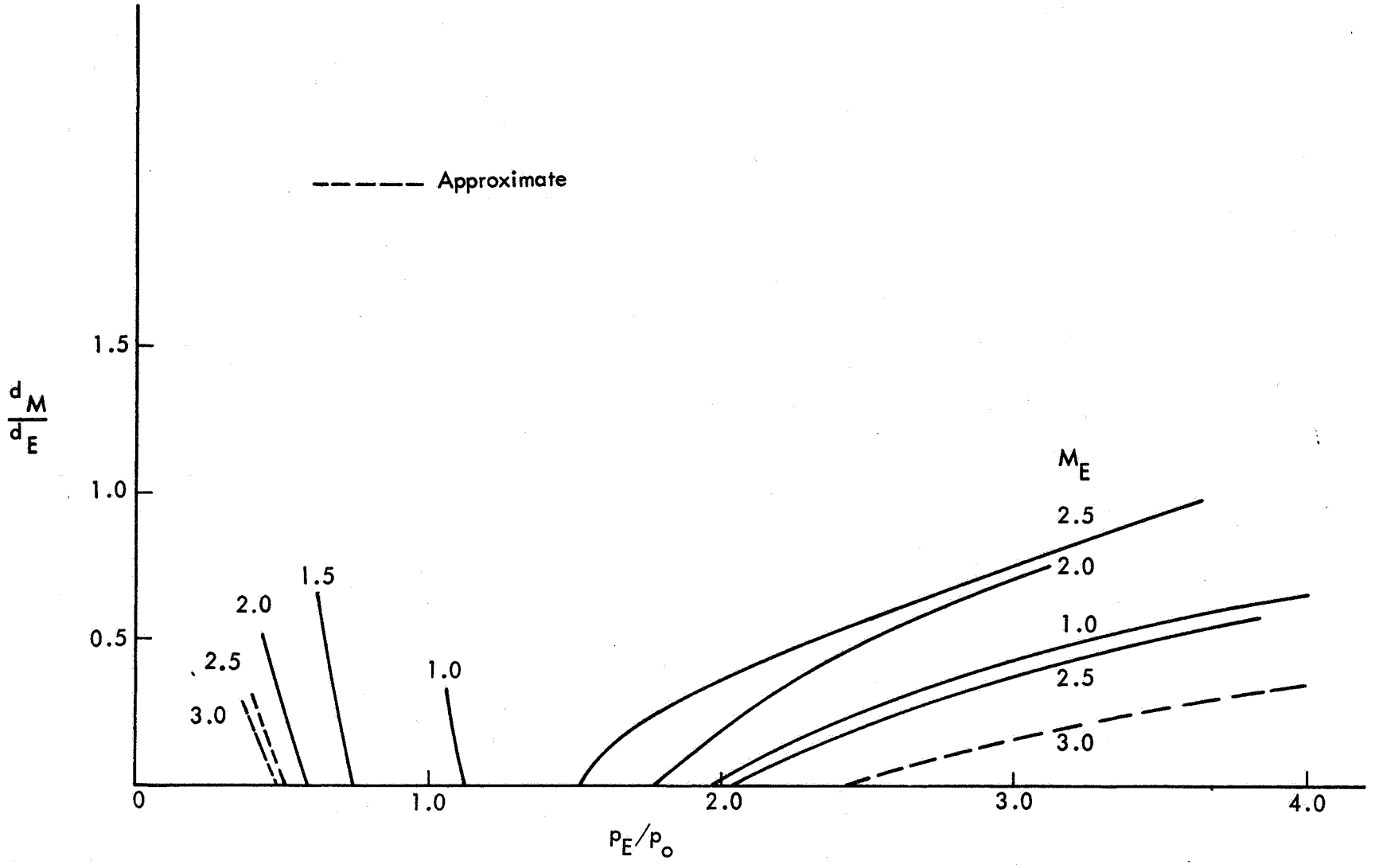


Figure 14. Variation of Mach Disc Diameter With Pressure Ratio and Design Mach Number for for Ideally Expanded Nozzle, From Love et al. (Reference 31).

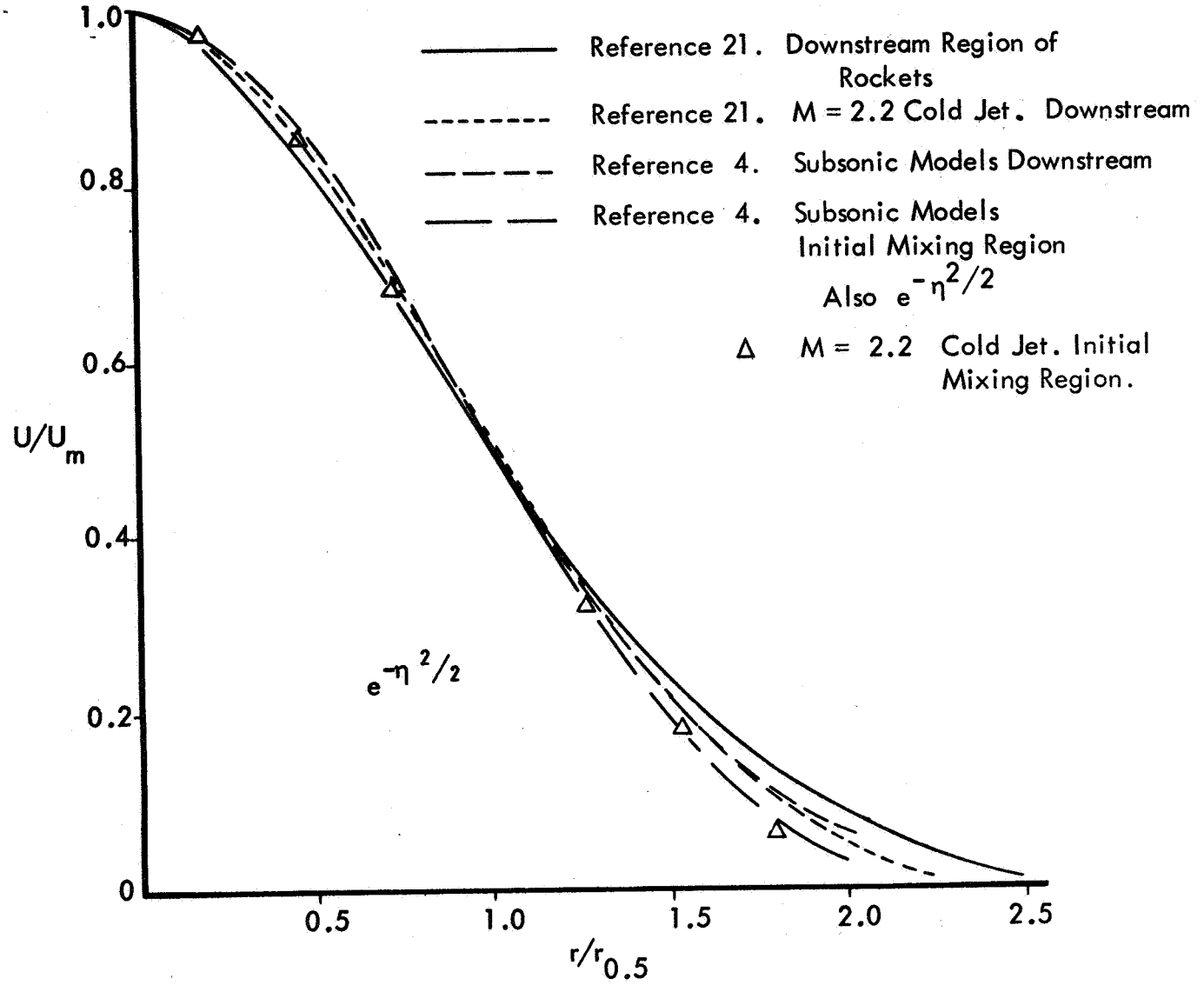


Figure 15. Similarity of Radial Velocity Profiles in Jet Mixing Region

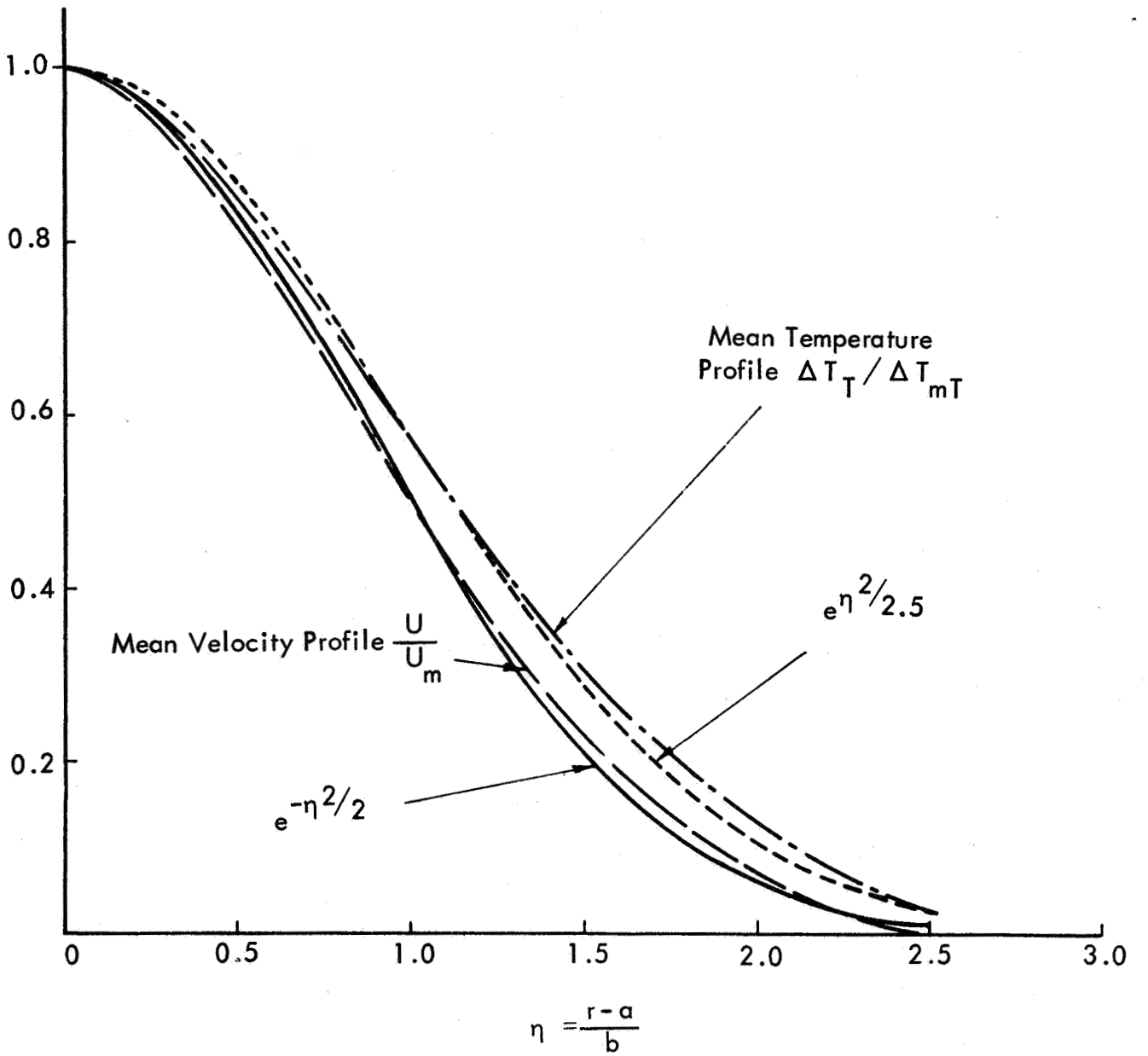


Figure 16. Similarity of Radial Velocity and Temperature Profiles in Subsonic Flow of Rocket Exhaust. After Anderson and Johns. (Reference 20)

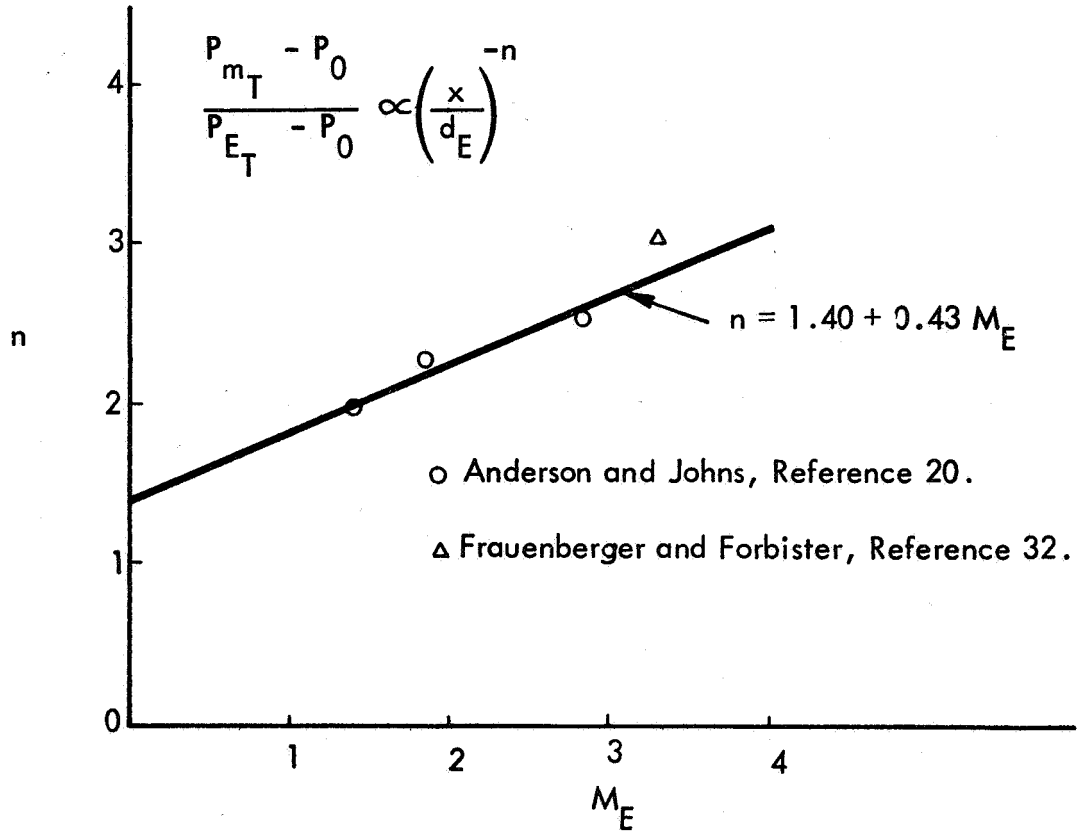


Figure 17. Exponent of Downstream Centerline Pressure Decay.

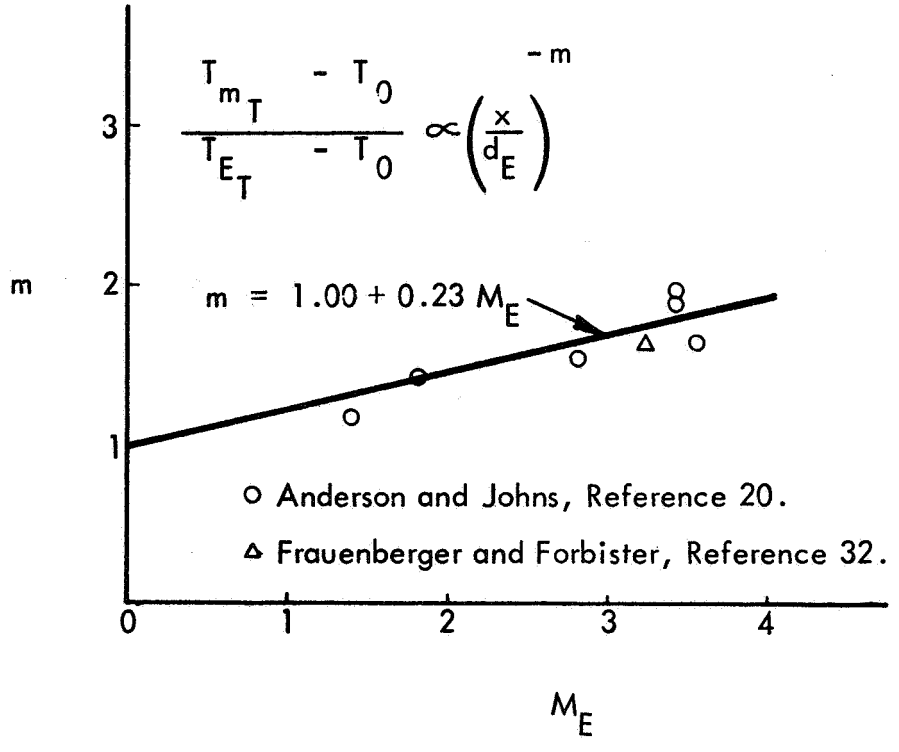


Figure 18. Exponent of Downstream Centerline Temperature Decay.

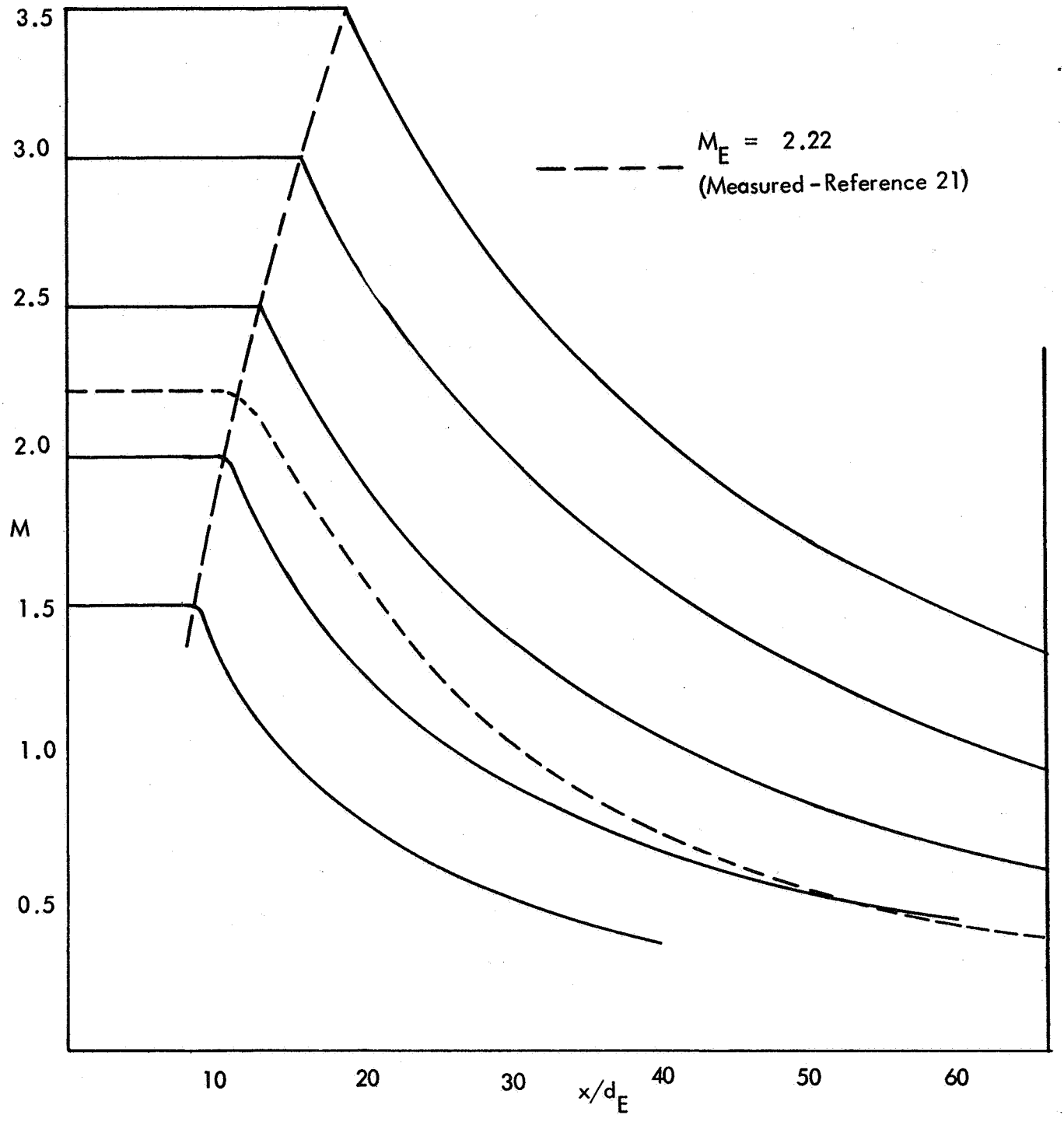


Figure 19. Calculated Centerline Mach Number Decay

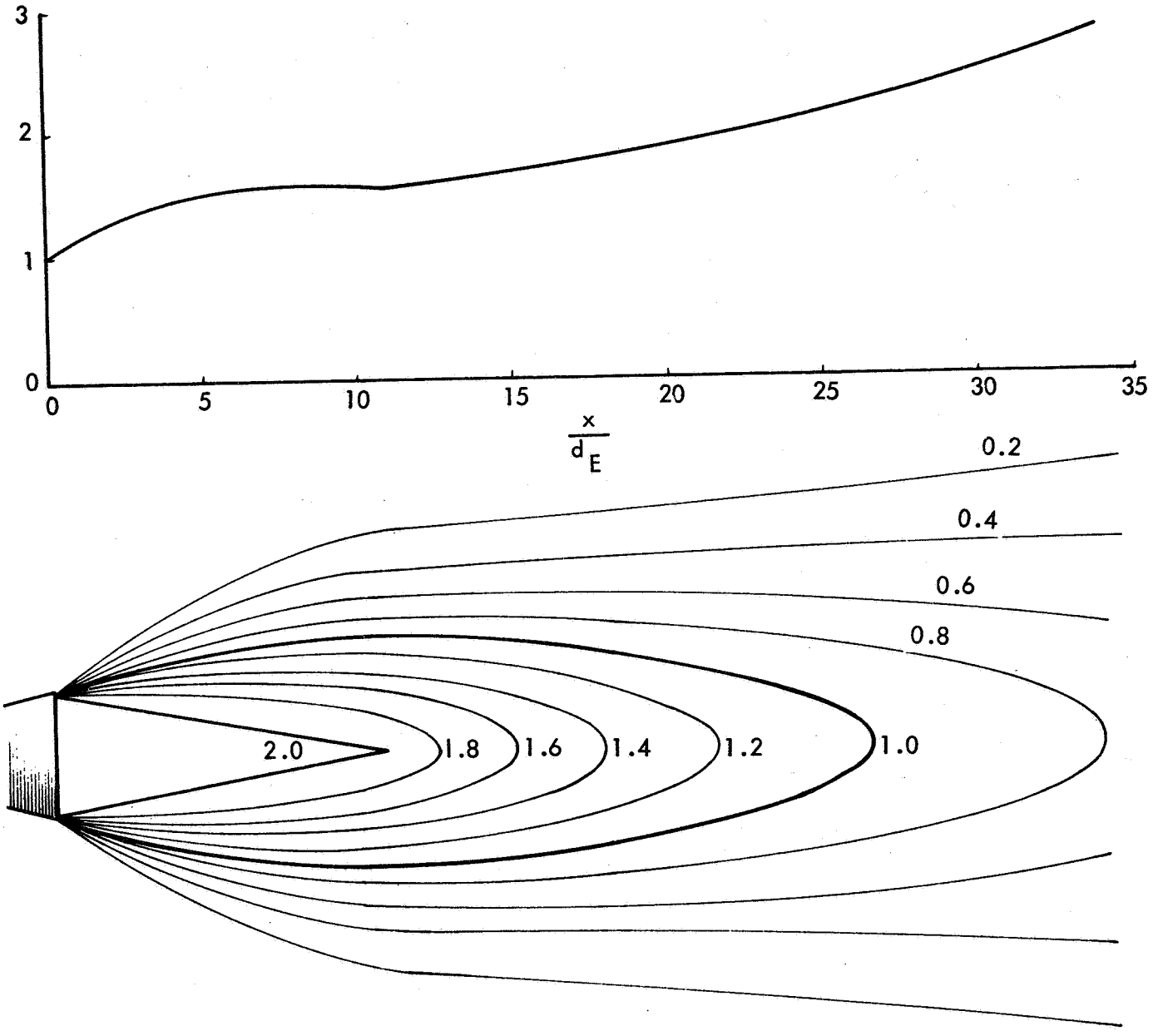


Figure 20. Axial Variation of $b/r_E$ and Mach Number Profiles for $M_E = 2.0$, t = 5 Jet.

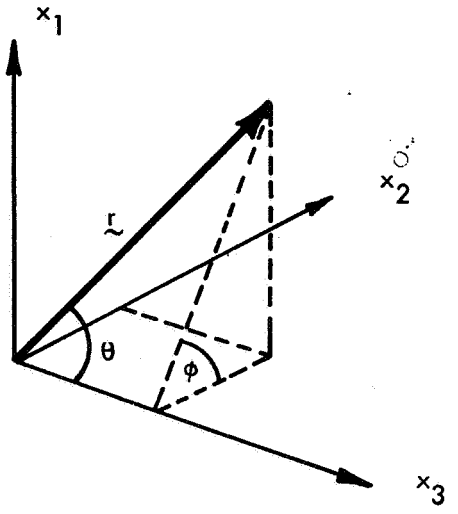


Figure 21a. Relationship Between Cartesian and Polar Coordinates.

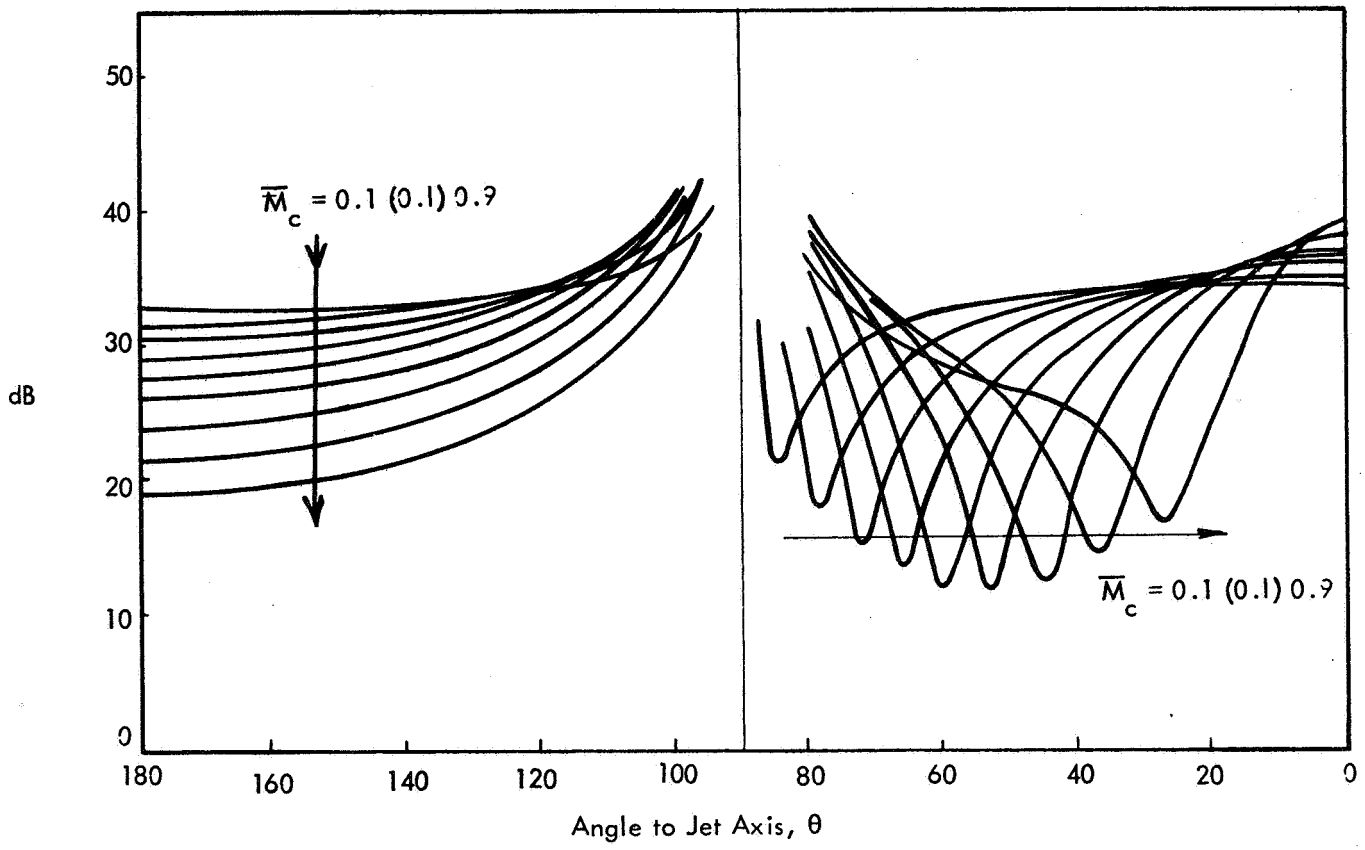


Figure 21b. Near Field Amplification due to $x_1$, $x_3$ Lateral Quadrupoles ($k\,r = 0.25$).

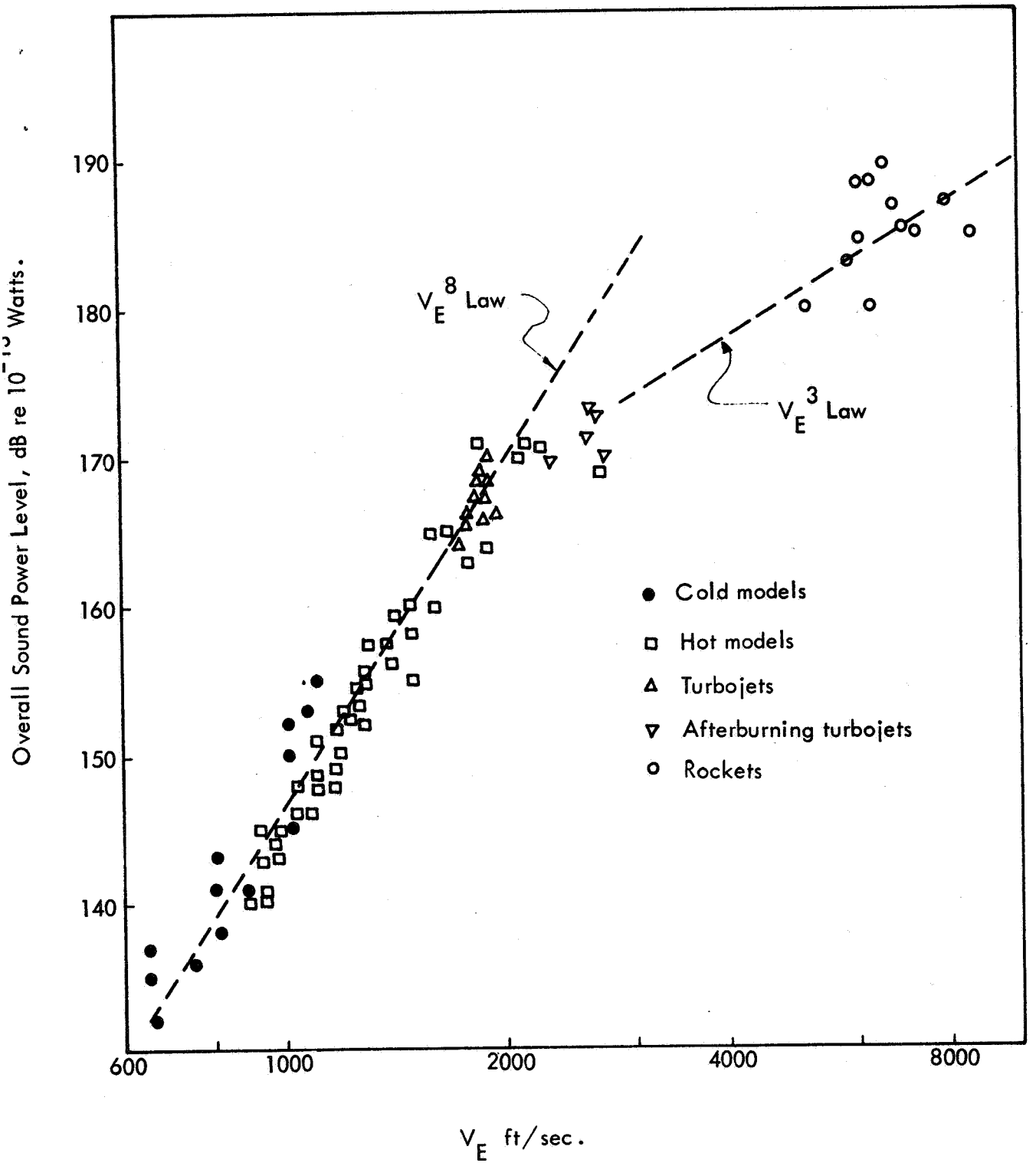


Figure 22. Overall Jet Sound Power Per Unit Nozzle Area Versus Exhaust Velocity, From Reference 37.

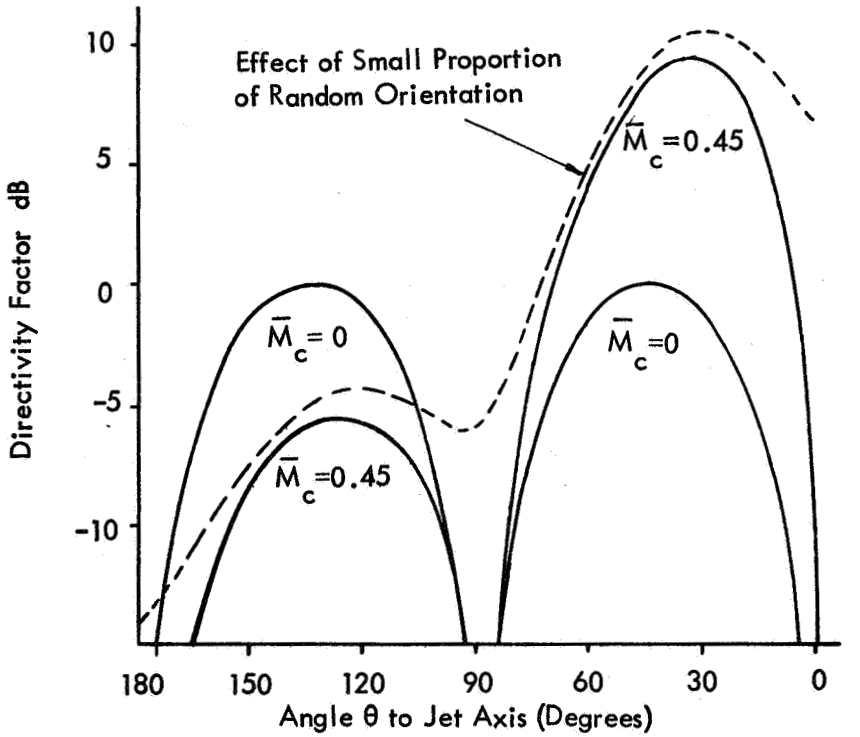


(a) Directivity of Lateral Quadrupoles in Shear Region.

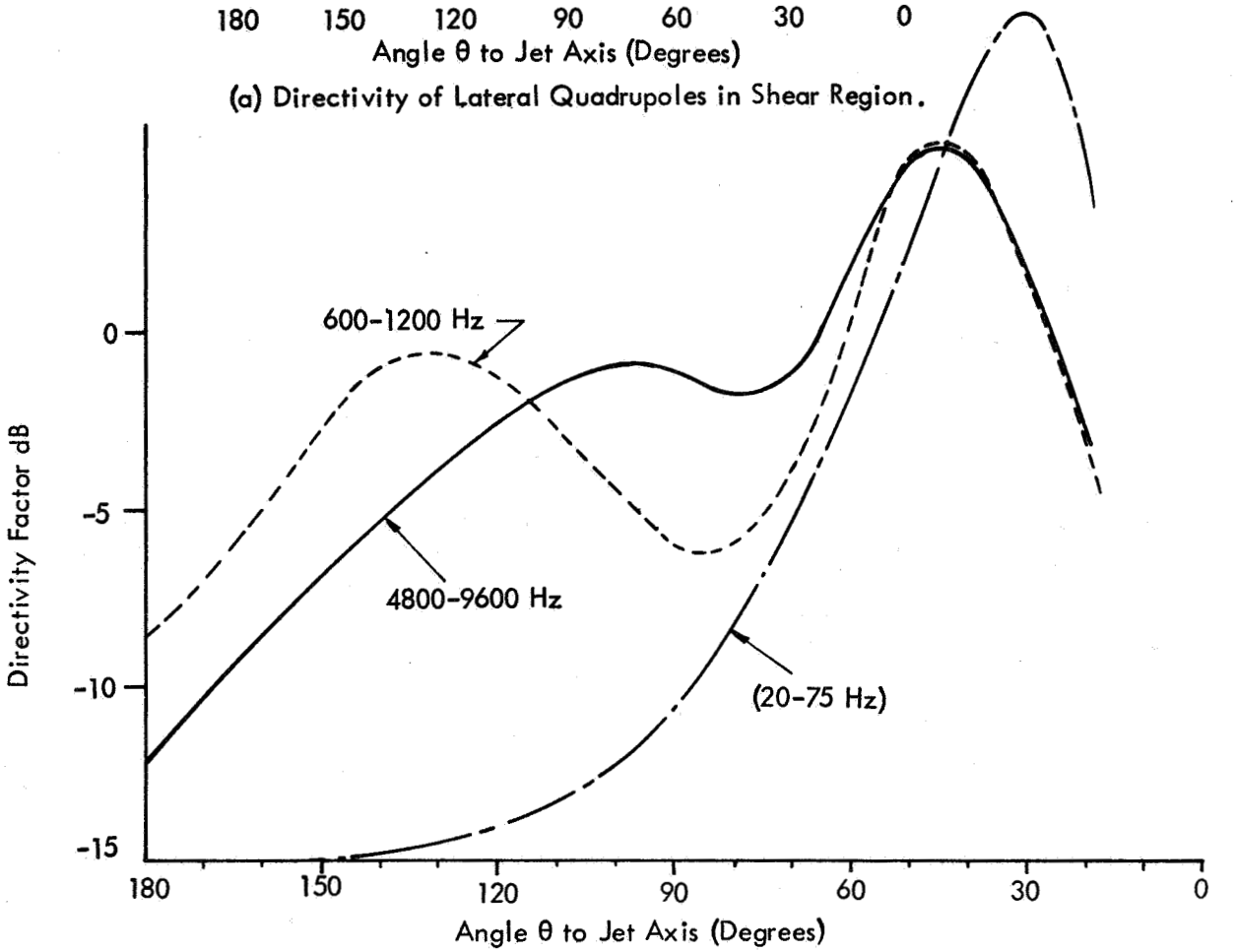


(b) Measured Directivity in Selected Octave Bands (From Lee et al).

Figure 23. Jet Noise Directivity

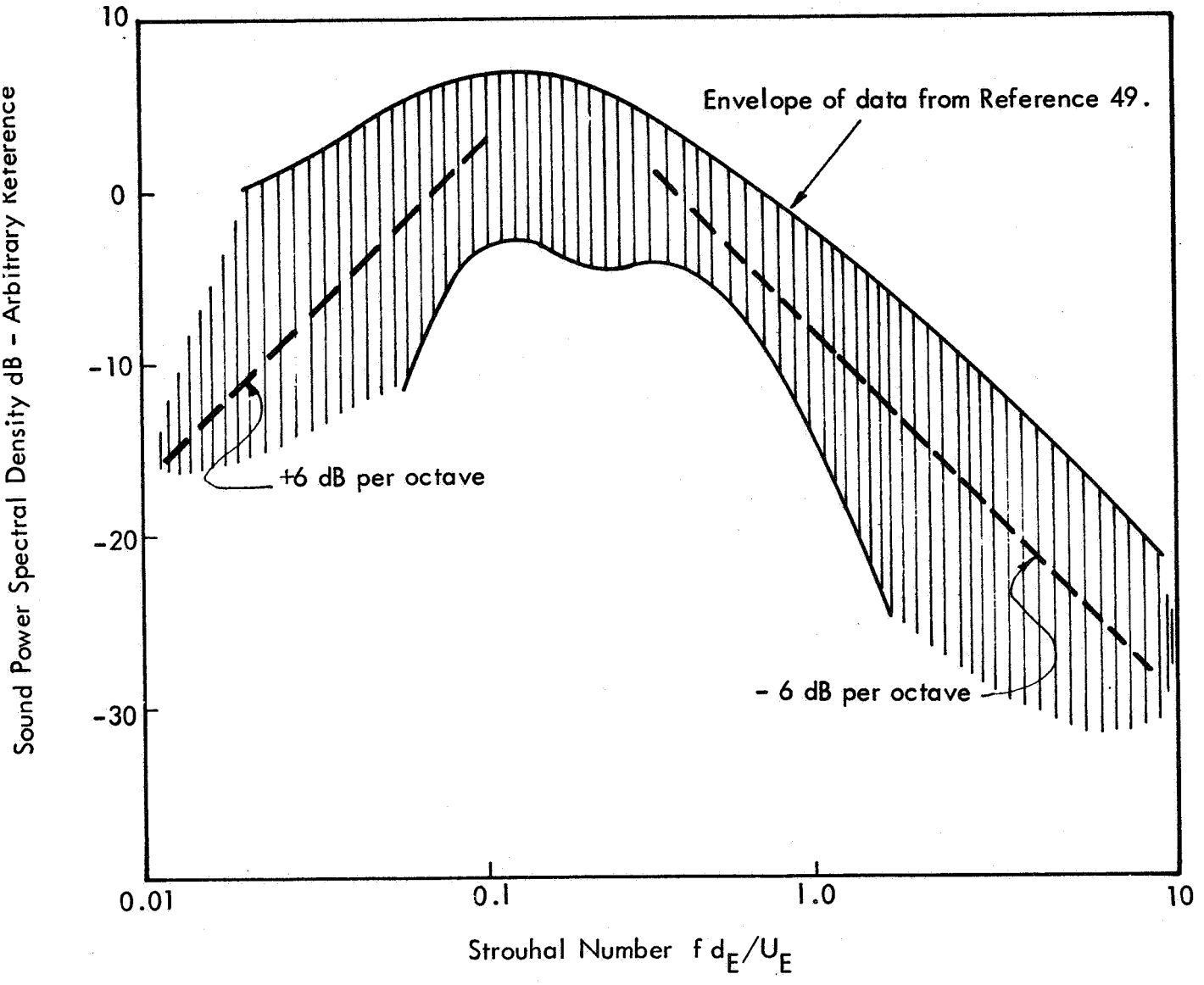


Figure 24. Power Spectral Density of Jet Noise.

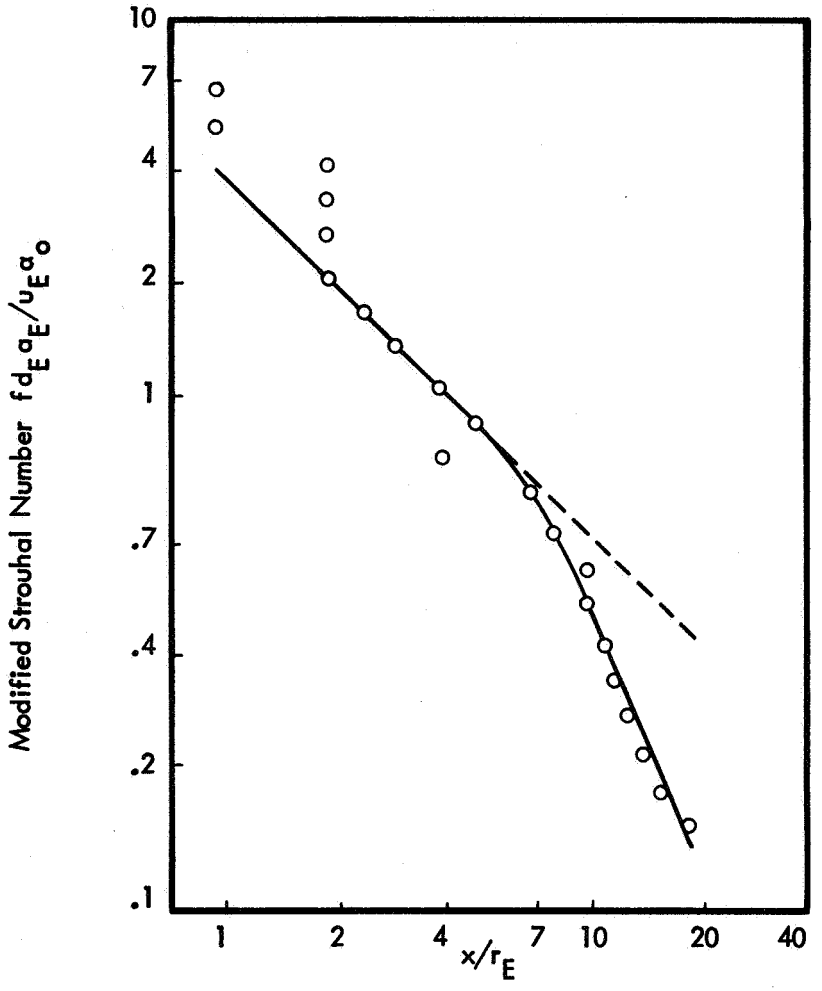


Figure 25. Location of Maximum Sound Pressure Level in 1/3 Octave Frequency Bands as Function of Modified Strouhal Number, From Reference 17.

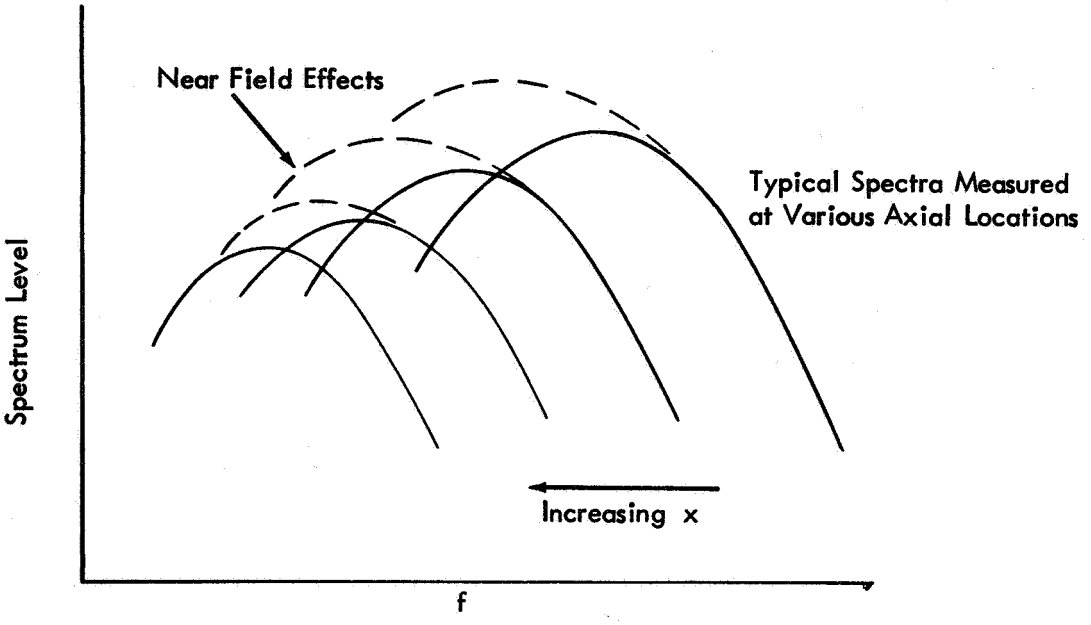


Figure 26. Modification of Apparent Spectrum by Near Field Effects.

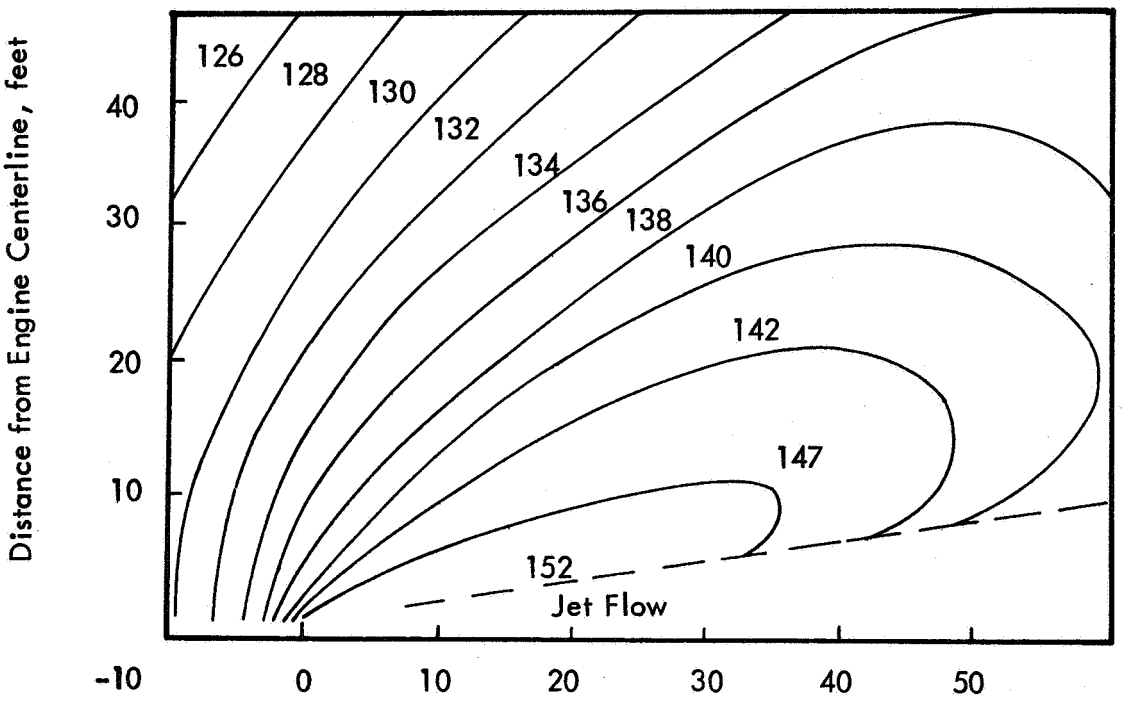


J 57 Turbojet

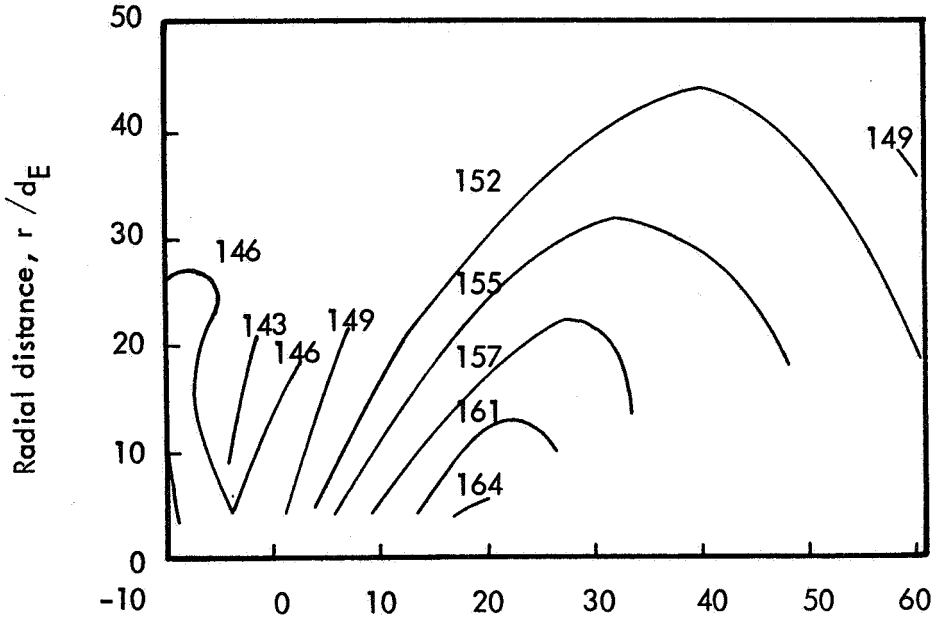


Small Rocket - Nozzle F of Reference 10

Figure 27: Near Field Noise Pattern of a Jet and a Rocket, SPL in Decibels re: 0.0002 dynes/cm $^2$

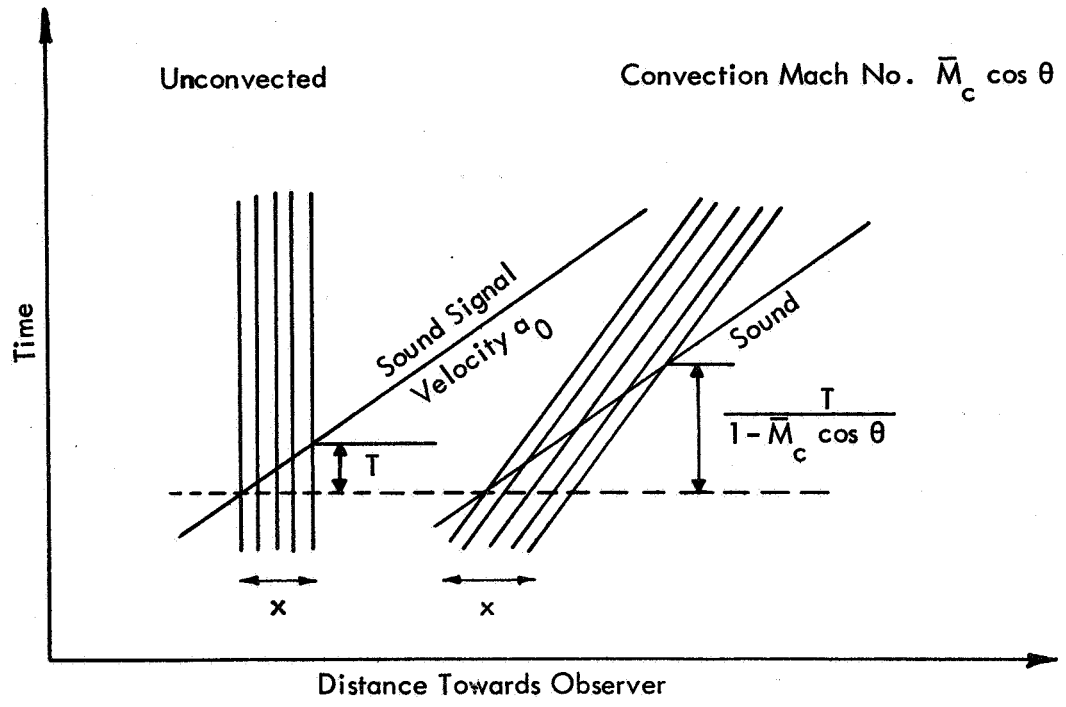


(a) Non-Decaying Eddy.

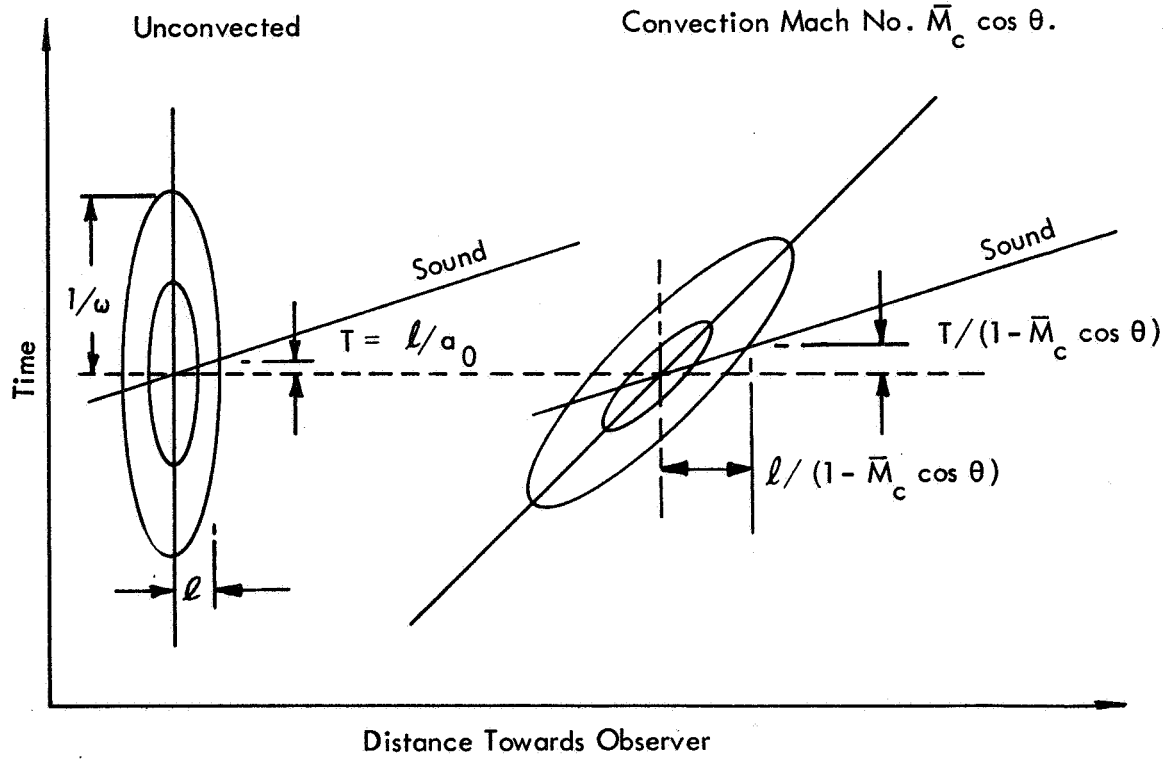


(b) Finite Eddy.

Figure 28. Effects of Eddy Convection on Emission Volume and Emission Time Differences. (Reference 36)

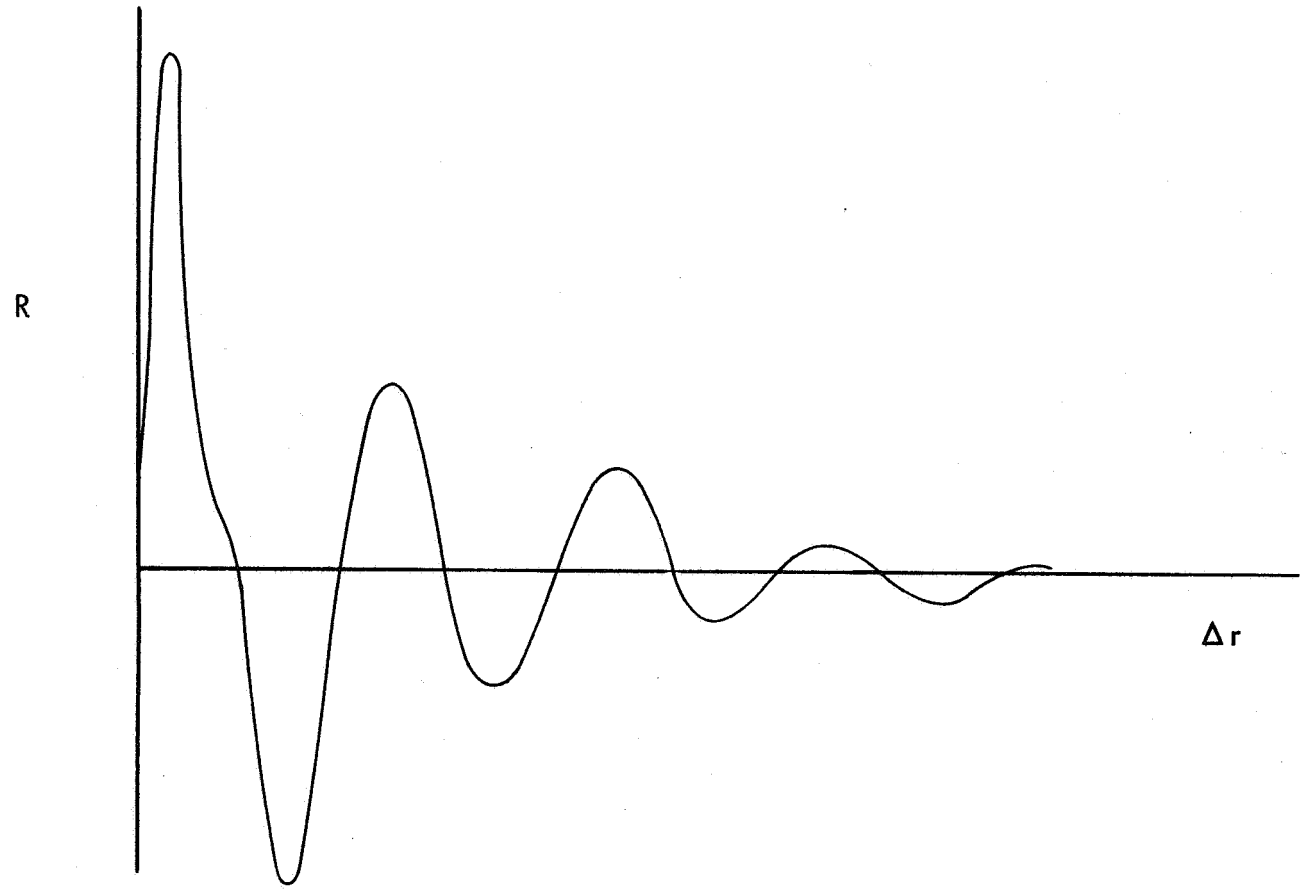


Figure 29. Typical Cross-Covariance given by Equation 4.5

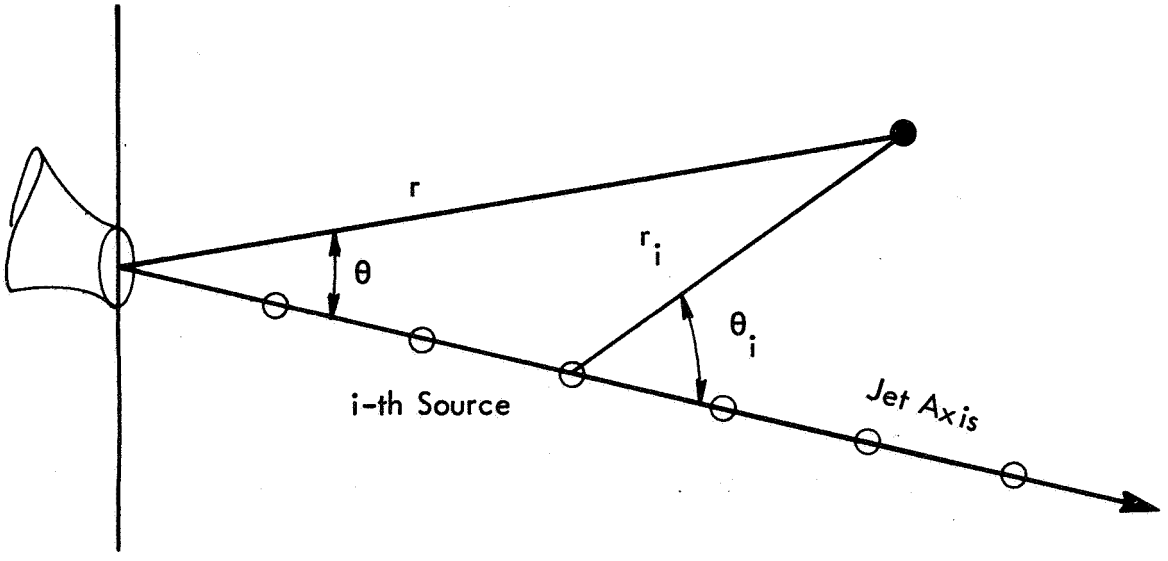


Figure 30. Coordinate System for Discrete Source Acoustic Model of Jet Stream

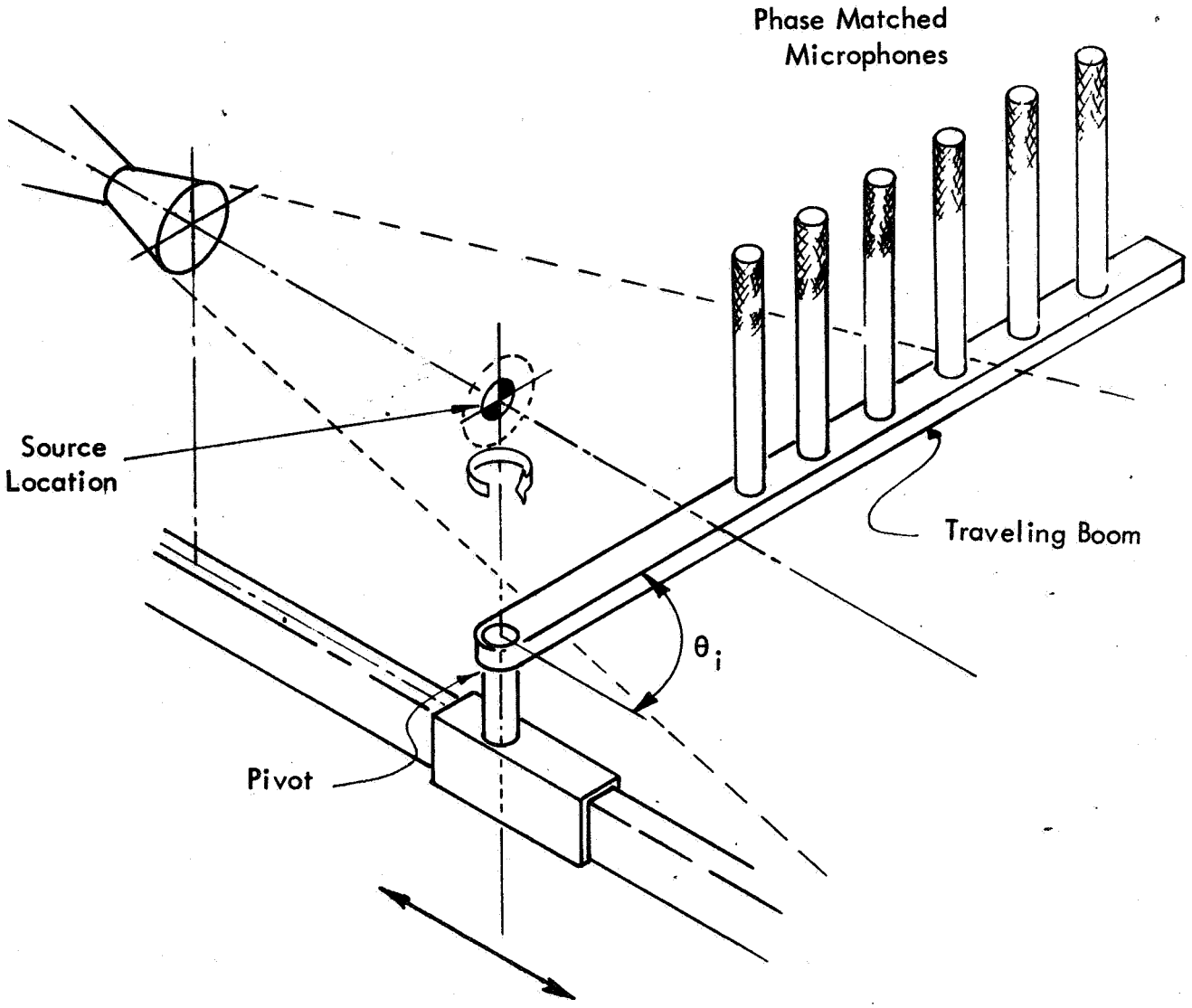


Figure 31. Schematic of Proposed rig for Near Field Correlation Experiments.



NASA-Langley, 1967 —— 23 CR-857